The role of ICT1 during MYC-deregulated fast-onset mouse plasmacytomagenesis

by

Amy Kathleen Dahl

A Thesis submitted to the Faculty of Graduate Studies of

The University of Manitoba

in partial fulfilment of the requirements of the degree of

MASTER OF SCIENCE

Department of Physiology and Pathophysiology

University of Manitoba

Winnipeg

Abstract

Murine plasmacytoma models human cancers that involve deregulation of MYC. Overexpression and duplication of the immature colon carcinoma transcript 1 gene, *Ict1,* along with MYC deregulation may contribute to the aggressive mechanism for disease development in fast-onset mouse plasmacytomas. This study looks at *Ict1* and *c-MYC* overexpression in mouse PreB^{mycER} cells that serve as a cell culture model for MYC-dependent plasmacytomagenesis. An *Ict1* inducible vector was transfected into the mouse PreB^{mycER} cell line that contains inducible *c-MYC.* This allowed us to examine the effect of overexpression of ICT1 and c-MYC proteins simultaneously or each separately, on selected hallmark cancer cell traits such as increased proliferation, evasion of apoptosis and increased genomic instability. An increase in the number of cells in the S-phase was observed by 15 % and up to 20 % at 24 and 36 hours respectively, and cell doubling time shortened by almost 2 hours at 24 hours during peak ICT1 and c-MYC overexpression. Although, no noticeable change in apoptosis levels, or large scale genomic alterations were detected up to 96 hours post-ICT1 and c-MYC peak-overexpression, genomic instability was observed when MYC protein was overexpressed with or without ICT1 protein overexpression. Extrachromosomal elements increased in number and size during conditional MYC deregulation, and most of these elements (25 %) classified as Chromosome 11. These findings support *Ict1* as a candidate gene that is selected for by MYC-deregulation during plasmacytomagenesis, and show promise that the experimental model of induced MYC and ICT1 overexpression in mouse PreB cells, deserves further investigation, specifically with *in vivo* studies.

Acknowledgements

There are many people who have helped me along this journey, from all the way back in high school, up until the final days of edits. I would like to start by thanking my supervisor, Dr. Sabine Mai. Thank you for taking me on as a graduate student. The knowledge I gained through this experience is invaluable. I extend this thanks to the other members of my committee, Dr. Hao Ding for his challenging questions, Dr. Peter Cattini for getting me to look at the bigger picture, and Dr. Kirk McManus for your patience and ability to guide me when I needed support.

A special thank-you to the entire Mai Lab, especially Cheryl Taylor-Kashton, whose laughter, friendship and help motivated me. The support I received from the Genomic Centre for Cancer Research and Diagnosis (GCCRD) was immense, as this facility supported my entire project. I must thank Ludger Klewes the manager of the GCCRD, as he provided much support and comedic relief. I also thank the Research Institute in Oncology and Hematology (formerly, the Manitoba Institute of Cell Biology); the people who work there, and the students, who are part of such an important mission. Specifically, I thank Brent Guppy for essentially being my "student" mentor. I greatly appreciate your complete willingness to help me.

I would like to thank my entire family for their support, which included excited phone calls asking me about what I was doing. These are the moments that motivated me, even when my experiments were not working so well. To my husband John, I would like to say thank you for your understanding and willingness to support me while I continued in my studies. I look forward to achieving further personal and professional growth with you. I have

countless amazing friends who have been some of my biggest fans as I pursued my Master's degree, especially Coreen Panteluk, Paulette Brenner, Laxmi Mehta, Mylène Chicoine, Gillian Storsley, Christey Allen, Dana Kowalski and Jennifer Genest. I want to thank the entire Range family, for putting the idea into my head that I should pursue post-secondary studies. Thank you to Teresa Cabral who showed me how to "lab", and helped me in my decision to enter into graduate studies.

I must express my gratitude to Manitoba Health Research Council and to the Canadian Institutes of Health Research, as without their funding, my project would not have been possible.

Dedication

To my sister Julie Nadeau for everything you do for me, especially your help editing.

Table of Contents

List of Tables

List of Figures

List of Abbreviations

2° Ab	Secondary antibody
3D	Three dimensional
4HT	4 hydroxytamoxifen
Ab	Antibody
A-MulV	Abelson murine leukemia virus
Aspscr1	*Alveolar soft part sarcoma chromosome region, candidate 1*
BALB/c	Bagg Albino (inbred research mouse strain)
bcr	*Breakpoint cluster region*
BL	Burkitt Lymphoma
BSA	Bovine serum albumin
c-MYC	*Cellular Myelocytomatosis*
Chr	Chromosome
CPTS	Copper phthalocyanine 3,4',4'',4'''-tetrasulfonic acid tetrasodium salt
DAPI	4'6-diamidino-2 pheylindole
DHFR	*Dihydrofolate reductase*
DNA	Deoxyribonucleic acid
dsDNA	Double stranded deoxyribonucleic acid
EdU	5-ethynyl-2'-deoxyuridine
EE	Extrachromosomal element
FBS	Fetal bovine serum
FITC	Fluorescein isothiocyanate
Foxk2	*Forkhead box K2*
Ict1	*Immature colon carcinoma transcript 1*
Ig	*Immunoglobulin gene*
IgH	*Immunolglobulin heavy chain*
Igκ	*Immunolglobulin light chain (κ)*
Igλ	*Immunolglobulin light chain (λ)*
Il-6	Interleukin-6
IP	Intraperitoneal
Kcnj2	*Potassium inwardly-rectifying channel subunit 2*
mBAND	Multicolour banding
MM	Multiple myeloma
MOPC	Mineral oil induced mouse plasmacytoma

mPCT	Mouse/murine plasmacytoma
mRNA	Messenger ribonucleic acid
MYC	Myelocytomatosis protein
MycER	MYC-estrogen receptor fusion protein
MYCN	Myelocytomatosis protein (Neuroblastoma)
NHEJ	non-homologous end joining
NI	Non-induced
PARP	Poly(ADP-ribose) polymerase
PBS	Phosphate-buffered saline
PVDF	polyvinylidene difluoride
RIPA	Radioimmunoprecipitation assay
RFU	Relative Fluorescent Units
ROS	Reactive oxygen species
RPMI	Roswell park memorial institute
SCID	Severe combined immunodeficiency
SDS-PAGE	sodium dodecyl sulfate-polyacrylamide gel electrophoresis
Sec14l1	*Sec14-like1*
SKY	Spectral Karyotype
SSC	Saline-sodium citrate
TAE	Tris base, acetic acid and EDTA
Tbcd	*Tubulin folding cofactors D*
TBST	Tris-buffered saline (pH 7.4) containing 0.1 % Tween-20
TC	Transfection control
TF	Transfected
TUNEL	TdT-mediated dUTP nick end labeling
UT	Untransfected
v-Abl	*Abelson murine leukemia viral oncogene*
σ	Standard Deviation

1 INTRODUCTION

Cancer cells are characterized by genetic alterations, however, not all changes advance cells to a tumorigenic state, but specific changes are essential drivers (1-3). Neoplastic transformation occurs as a multi-step process, with successive accumulation of genetic and epigenetic changes (4). The genetic mutations found in cancer cells can be as tiny as a single nucleotide substitution or as large as whole chromosome aberrations (5). These mutations, if tumorigenic drivers, promote resistance to cell controls that in normal cells regulate immune response, cell growth, division, apoptosis or senescence. The development of Hallmark cancer cell traits include resistance to apoptosis, increased proliferation, altered metabolism, cellular immortalization, and the ability to ignore cell cycle checkpoints (6,7). Epigenetic alterations such as DNA methylation and histone modifications can also help a cell to adopt these tumorigenic traits (8). Altogether, these various mutation types in cancer demonstrate that genomic stability is compromised, and so it is not surprising that research attention has commonly been directed toward oncogenes that alter genomic integrity.

The *c-MYC* oncogene has been associated with the induction of genomic instability, where its protein product, MYC, deregulation presents with large-scale genomic changes. MYC deregulation leads to altered chromosome and telomere positions, illegitimate chromosomal recombination, long range chromosomal rearrangements which ultimately lead to translocations, deletions and insertions, but surprisingly no point mutations (9, 10). Louis *et al*. (2005) found conditional MYC deregulated nuclear changes in chromosome and telomere positions to always precede dynamic chromosomal rearrangements (9). Conditional

MYC deregulation can also be followed by altered copy numbers for specific genes (11-14). These amplifications can exist intrachromosomally, or on extrachromosomal elements (EEs) (11, 13, 15, 16). When these genetic alterations follow MYC deregulation, they may help to promote dynamic rearrangements and the onset of tumorigenesis (17). Therefore, recurrent genetic changes need to be explored for their contribution to the mechanism of pathogenesis for cancers in addition to increased MYC activity.

Deregulation of MYC occurs in more than 70 % of cancers (18), and can occur by multiple mechanisms, including enhanced transcription (19), chromosomal rearrangements (20), and resistance of the MYC protein to ubiquitin-mediated proteolysis (21). These different mechanisms for deregulation of MYC argue that its increased levels are a necessary driver of tumorigenesis (22, 23). The involvement of MYC in so many different cancers demonstrates how oncogenes that obliterate genomic stability may play a major role that leads to the accumulation of additional genetic alterations necessary for disease development.

Slow-onset mouse plasmacytoma (mPCT) carries a MYC activating translocation, which brings the murine *c-Myc* gene under the control of one of the *Immunoglobulin* (*Ig*) gene enhancers (22). Normally, *c-Myc* is under strict control from transcription through to modulation of protein activities, but this *c-Myc/Ig* juxtaposition results in increased expression of MYC as well as mPCT development. There are different experimental models to induce mPCT, and in the model that generates fast-onset plasmacytomas an additional alteration is always observed in 100 % of mPCT cells, duplication of chromosome 11 at subcytoband E2 (11E2) (23). There are six genes within this region found amplified that have

increased copy number, and are found overexpressed (S. Mai, University of Manitoba, Winnipeg Manitoba; unpublished results). Immature colon carcinoma transcript 1 (*Ict1*) is one of the candidate genes, and this thesis focuses on increased ICT1 protein levels during conditional MYC deregulation in mouse PreB lymphocytes. Recent research has identified the proliferative potential for ICT1 in lung cancer (24) glioblastoma (25), and prostate cancer (26). MYC is well established as an oncogene involved in the initiation and progression for these abovementioned cancers, and is involved in > 70 % of human cancers (18, 27-29). As such, the tumor initiating MYC deregulation may pair with amplification of 11E2 in order to recruit the activity of genes, such as *Ict1*, that have a potential to promote accelerated disease onset and/or progression for mPCT.

Deregulation of *c-MYC* has been directly related to neoplastic development in a variety of human blood cancers. Increased MYC levels occur during the transition of myelodysplastic syndrome to acute myeloid leukemia, the development of multiple myeloma, and Burkitt Lymphoma (BL) (30, 31). The development of mPCT models BL, where they are cytogenetically identical and their mechanisms for disease progression involve MYC deregulation by the classical *c-MYC/Ig* translocation (32). In fast-onset mPCT, increased MYC protein levels precede duplication of 11E2 (23), and the 11E2 homology region is evolutionarily conserved across several species, including rat (10q32) and humans (17q25) (33, 34). These regions are involved in amplification, duplication, or translocation events in several tumor types in all three species (35-40). The human synteny region 17q25 is implicated in human malignancies such as acute myeloid leukemia, chronic myeloid leukemia, breast, ovarian, thyroid and neuroblastoma (18, 20, 34, 41, 42). The conservation of this region demonstrates an evolutionary importance for the genes within this region, and

their involvement in several tumor types suggests that 11E2 harbors genes, such as *Ict1*, that may have a fundamental role in tumor development and/or progression. Characterization of candidate genes within the 11E2 duplicated region may elucidate new targets for therapeutic development for human cancers where MYC has been shown to play a role, but the downstream mechanism has yet to be uncovered. A great number of oncogenes have been identified from studying genes within amplified regions common to many cancers (43). Therefore, gene amplifications downstream from MYC deregulation, like *Ict1* amplification within 11E2, may help the mechanism for development and progression for cancers with increased MYC levels.

2 BACKGROUND

2.1 *MYC* in Cancer

The *MYC* gene family includes *c-MYC, N-MYC, L-MYC, S-MYC,* and *B-MYC,* where all but *B-MYC* have been identified as oncogenes (44-47). Although these members of this family of proteins have similar functions, they display notable differences in expression patterns that are tissue specific. *c-MYC* is overexpressed in most human blood-borne and solid tumors, where *N-MYC* is found overexpressed in solid cancers of the neural tissue, and *L-MYC* is overexpressed in lung carcinomas (44, 45). The gene *c-MYC* encodes the multifunctional protein MYC that regulates many cellular processes such as transcription (44), translation (48), replication (14, 49), chromatin structure (50), and ribosome biogenesis (51). Normally, *c-MYC* is under strict transcriptional control because its normal very important host of functions are utilized for development and differentiation (52). *MYC* is found altered in > 70 % of all cancers (18) and can be altered by several mechanisms that increase expression of the gene, mRNA, or protein level. At the gene level, amplifications or enhancing translocations, or alternatively, an increase in MYC protein activity is achieved by stabilizing the protein or mRNA (53). Of medical importance, the dysregulated *MYC* gene and/or MYC protein is associated with aggressive tumor development and poor prognosis (18, 20, 42). There is much research effort to elucidate the role of *MYC,* and its downstream products, on tumor initiation and propagation (54, 55. MYC deregulation occurs in so many cancers and can be related to prognosis.

The MYC transcription factor contains conserved elements associated with the various functions. It contains a DNA binding basic helix-loop-helix motif and a leucine

zipper domain that allows dimerization to its partner transcription factor MAX (56). MYC acts as either a transcriptional activator or repressor depending on the proteins it recruits. MYC has highly conserved regions that altogether contribute to the many functions it can play (56). The abovementioned domains are required for full transformation of primary and immortal cells. The Myc box I element is required for the transactivation and repression of its many target genes (57), whereas, the Myc box II element is crucial for transcription-independent functions of MYC (58). These conserved regions contribute to the quintessential biological functions that allow deregulated MYC to contribute to tumorigenesis.

2.1.1 *c-MYC*-Dependent Tumorigenesis

The *c-MYC* gene has a long history of involvement in cancer as an oncogene. Firstly, it was originally identified in Burkitt lymphoma patients, where chromosomal translocations involving chromosome 8 were frequently observed (59, 60). Cloning the break-point of the translocation chromosome revealed *c-MYC* to be the cellular homologue of the avian myelocytomatosis retroviral oncogene, *v-Myc* (61). Bursal lymphomas induced by an avian retrovirus were first reported in 1908 (62). This led to sequence analysis for a host of avian retroviruses that revealed *c-MYC* (63-67). Since its discovery, MYC has been identified as a multifunctional protein, involved in many cellular processes with critical roles in regulating the cell cycle, apoptosis and cellular transformation (68-70). Therefore, it is not surprising to find its broad set of activities, including generation of genomic instability, high-jacked during the development of different cancers. It is debatable whether a large number of genetic changes are required for malignancy to occur from an integrated effort, or whether a single oncogene may be responsible for the downstream events that lead to tumor progression. Spontaneous lymphomas and lung tumors are linked to increased rates of aneuploidy in older

animals (71). MYC, as a potent modulator of the transcriptome during normal cell growth and proliferation (68-70), fits the profile of being one such candidate protein with dire downstream consequences. The fact that MYC has such a broad set of activities means that the downstream events may be due to recruitment of other proteins whose expressions are modulated by MYC activity.

2.1.2 *c-MYC*-Induced Genomic Instability

Deregulation of MYC is well known to directly induce genomic instability, where MYC remodels nuclear architecture in a variety of ways in order to promote neoplastic transformation (11-13, 17). Genomic instability can be broadly classified as either non-random or random genetic changes. Non-random genomic instability is a recurring genomic change such as the 11E2 duplication in fast-onset mPCT, or even the *c-MYC/Ig* translocation in BL and slow-onset mPCT (32). A well-known example of a common recurring genomic change in cancer is the Philadelphia chromosome *BCR/ABL* of chronic myeloid leukemia (72). Non-random genomic alterations are used for diagnosis and studied to understand disease progression. In contrast, random genomic instability can include any number of changes within the genome where no common alteration occurs. Such random genomic changes can occur due to breakage-fusion bridge cycles and altered centrosomes as observed in Hodgkin's lymphoma Reed-Sternberg cells (73).

Deregulated MYC promotes genomic instability in such a way that propagates additional genetic alterations and ultimately leads to dynamic and ongoing genomic destabilizing events (74, 75). Elevated MYC levels cause telomeric aggregates and

chromosome end-to-end fusions, and as a result either create dicentric chromosomes or Robertsonian fusions (76). A Robertsonian fusion is a type of translocation that involves two centromerically fused chromosomes with a short or non-existent p arm, also called whole-arm translocations (77). Dicentric chromosomes form anaphase bridges that break upon cell division, and the DNA is unevenly distributed to daughter cells where one daughter cell will receive the unbalanced translocation chromosome and the other cell receives the corresponding terminally deleted chromosome. The broken chromosome ends then activate double stranded DNA break repair mechanisms (78). Either homologous repair activation results in deletions at the terminal ends of chromosomes, or non-homologous end joining leads to more end-to-end fusions, which initiates the above breakage-fusion-bridge cycle all over again (79). These cycles repeat and generate chromosomal breaks, translocations, ring formation, aneuploidy, fusions, deletions and double minute chromosomes (10, 17, 80-82). Multiple cycles can generate even more complex rearrangements where multiple chromosome partners are involved to give multi-chromosomal rearrangements. Important studies found Myc box II to be the functional element required for the nuclear remodeling activity of MYC that leads to telomeric aggregate formation, which shows how MYC activity is directly involved in causing genomic instability (82, 83). MYC mutants with a defective MYC box II lost their transforming activity in cell lines, and were unable to induce tumors (83). Telomeric aggregates were not observed, and required the functional Myc box II. In mouse PreB cell lines and *in vivo* experiments of the mouse model of plasmacytoma, MYC deregulation has been shown to precede the onset of genomic instability that enables cellular transformation, and in mPCT development, MYC deregulation precedes 11E2 duplication (76, 23).

Increased levels of MYC induce BFB cycles and endo-reduplication events that increased the potential for amplifications. High levels of MYC have been shown to increase the copy number for certain genes, such as *dihydrofolate reductase (DHFR), ribonucleotide reductase 2, carbamyl-phosphate synthetase, aspartate transcarbanylase, dihydro-orotase, ornithine decarboxylase, cyclin B1* and *cyclin D2* (84- 90). MYC driven *DHFR* amplification occurs intrachromosomally as well as extrachromosomally on EEs (11, 15, 16). *DHFR* encodes an enzyme that regulates the tetrahydrofolate levels that are important DNA synthesis and, subsequently, cell proliferation and growth (90). It is not surprising that *DHFR* has become a target for chemotherapeutics due to its role in generation of precursors for DNA synthesis (92). *Ribonucleotide reductase 2* is a key regulator of dNTP biosynthesis in mammals that impacts cancer susceptibility (93). *Carbamyl-phosphate-synthetase,* which catalyzes pyrimidine biosynthesis, shows increased activity in many cancer cells (94). *Ornithine decarboxylase* is a target for MYC transcription activation, and is found upregulated in many human cancers (95). The *Cyclin* family are involved in cell cycle control, and are overexpressed in many human cancers (96). These are just a few examples of MYC affected genes and their roles that contribute to tumorigenesis.

Increased MYC levels have been associated with increased copy number for *Ict1* and the other five 11E2 genes in mPCT. Genes that can increase metabolism for the cell will support an increased proliferative potential. MYC, being involved in so many tumor types, must recruit genes that provide an advantage for tumorigenic potential.

Increased MYC levels remodel the organization of the nuclear contents in three dimensional (3D) space (74, 75). The nuclear periphery has been shown to mostly contain genes that are transcriptionally repressed, where the more central nuclear space typically

contains genes at are transcriptionally active (99, 100). To further support these spatio-functional nuclear regions, even gene rich chromosomes are found more centrally, whereas gene poor chromosomes are found closer to the periphery (101, 102). This large-scale organization of chromosomes within the nucleus into different chromosome territories, may act to enable a global level of gene expression regulation (97, 98).

In mPCT, Chromosome 11 (Chr 11) is positioned more centrally compared to control cells (103). This led the Mai to lab investigate if deregulated *c-MYC* drives Chr 11 nuclear repositioning in mouse plasmacytoma. Altered positions for Chr 11 have been observed with movement from the periphery to a more central position in mouse PreB cells (103, 104). These findings support a relationship between MYC deregulation and Chr 11 that may help to explain why the 11E2 region becomes an additional genetic abnormality in the fast-onset mPCT model. The positions of genes within the nucleus has been linked to transcriptional activity, and so alteration of chromosome positions by MYC could lead to changes in their transcriptional status (104). The functional consequence of chromosomal movement due to increased MYC activity levels can therefore lead to repositioning of genes into incorrect transcriptional activity spaces with an increased potential for amplification events and increased protein levels. If these amplified regions harbor genes with tumorigenic potential, then the mechanisms for disease progression is accelerated with the activity of these recruited genes protein products. Relocating genes by chromosomes repositioning is another way deregulated MYC disorganizes the genome that could lead to increased tumorigenic potential.

Altered chromosome positions within the nuclear 3D space has an additional consequence, where genes that are normally not juxtaposed to each other are now in close proximity, and can now be translocating partners. Louis *et al*. (2005) showed that post-MYC deregulation, chromosome rearranging partners move toward each other within 96 hours (9). Translocation partner proximities were examined in plasmacytoma cells compared to normal B cells, and the more frequently translocating partners were found in closer proximity than the less common translocating partner chromosomes (22). The hallmark translocation in mPCT juxtaposes *c-MYC* to one of 3 *Ig* loci, with the immunoglobulin heavy chain (*IgH)* of Chr 12 being the most frequently observed translocation partner, T12;15. The mouse *IgH* locus is on Chromosome 12, and similar to BL the most frequent translocation involves the *c-MYC* gene, in 90 % of tumors, and less frequently the light chain *Igκ* and *Igλ* on chromosomes 6 and 16 respectively (22). In BALB/cRb6.15 mice with the Robertsonian Chromosome 6 and 15 centromerically fused, now the *Ig* locus from Chromosome 6 was found in close proximity to the *c-MYC* locus, and T6;15 was observed at the same frequency as the dominant translocation in this model (74, 105). These findings suggest that chromosome proximity drives translocations. In human multiple myeloma, for all patient samples, the translocation-prone gene loci display an intermediate position in the nucleus that is more transcriptionally active relative to control B lymphocytes from healthy donors (103). Conversely, in non-malignant B-cells from the same patients, these genes are found more centrally, and in closer spatial proximity. This demonstrates that gene positioning differs in all patient B-cells compared to healthy control cells, potentially contributing to translocation probability in patient cells and suggesting that proximity drives translocations (103). Additional studies have further shown how spatial proximity of chromosomes influences translocation probability for *in vitro* model systems, as well as for chronic myeloid leukemia

Chr 9 and 22 translocation partners (106, 107). These recurrent translocations are useful as diagnostic tools, and help us to understand the mechanism of disease development. The classic example being the Philadelphia chromosome found in chronic myeloid leukemia (106). MYC has the potential to rearrange chromosome positions that may help to recruit accomplice tumorigenic genes.

In mouse plasmacytoma, MYC deregulation pairs with 11E2 duplication as the aggressiveness of the disease increases (23). In the fast onset model of mouse plasmacytoma, the cytoband 11E2 is always found duplicated (23). In order to understand the downstream effects of 11E2 during MYC-deregulation there is a need to understand the contributions of genes located on 11E2, such as *Ict1* that are overexpressed, to the mechanism disease development.

2.1.3 Burkitt Lymphoma Harbours the *c-Myc* Translocation

Burkitt Lymphoma (BL) is a neoplasia of germinal center B lymphocytes (59). BL is a blood cancer that is the most common non-Hodgkin lymphoma in children and adolescents (31). The Epstein-Barr Virus (EBV) associated BL is especially prevalent in equatorial Africa, as opposed to sporadic non-EBV BL found more commonly in immunocompromised patients in Western countries, with high risk of development especially post-transplant patients (31). The non-EBV associated form of BL is also found in patients without compromised immune systems, where in Western Europe and the United States sporadic BL affects 3 out of a million people each year (31, 108). Current treatments have improved prognosis by an increase in the 5 year event-free survival from 40 % to 85-90 % (31). Treatment requires chemotherapy for less than 6 months rather than previously prescribed combined chemotherapy with radiation therapy. Although treatment options have improved to some extent, prognosis is still poor, especially in older patients (109). *c-MYC* is consistently altered in BL by balanced chromosomal translocations. This is the most common mechanism of *c-MYC* deregulation, with the gene *c-MYC* juxtaposed to any of the three enhancing immunoglobulin gene (*Ig*) promoters (heavy-chain *IgH*, or light-chain *Igκ*, *Igλ*) (22). A better understanding of the underlying mechanism of BL development and the downstream effect of *c-MYC* deregulation is imperative to improve treatment options and prognosis.

2.2 Plasma Cell Tumors

Plasmacytomas are defined as immunoglobulin-secreting neoplastic plasma cell tumors growing within soft tissue (110). They arise from a megaclonal expansion of a single plasma cell that arises from a specific B cell clone. B lymphocytes express unique surface antibodies that interact with a specific antigen that triggers the B cell to differentiate into a plasma cell (111). Normally, these plasma cells die within several days from activation, whereas transformed plasmactyoma cells continue to grow and divide indefinitely within human bone marrow, or the peritoneal cavity in mice. Additionally, these tumors secrete large amounts of monoclonal immunoglobulins increasing blood protein levels causing the blood to become highly viscous, termed paraproteinemia (112). Mouse plasmacytoma of BALB/c mice is cytogenetically similar to multiple myeloma (MM), but lacks bone changes and subsequent hypercalcemia characteristic in MM (110). MYC is paired with superenhancers in MM, not necessarily the *Ig* enhancing loci, but MYC still becomes deregulated (104). Burkitt Lymphoma involves the *c-MYC* oncogene as a translocation partner with the 14q32/*IgH* in up to 93 % of cases, and less frequently the light chain *Igκ* and *Igλ* on chromosomes 6 and 16 respectively (22). These plasma cell tumors have cytogenetic similarities, and mPCT is especially a good model to study to give mechanistic insights into BL development.

2.3 Chronic Inflammation and Increased Cancer Risk

There is substantial evidence that chronic inflammation is a causative factor for various cancers. Epidemiological studies have been key in uncovering inflammation as a risk factor for development of certain cancers arising from the tissue of inflammatory incidence (114). The best understood links to chronic inflammation for human cancers are esophageal adenocarcinoma, liver cancer, stomach cancer, bladder and colon carcinomas (114). Animal models have been instrumental to demonstrate that chronic inflammation can cause cancer to develop in the tissue directly affected by the inflammation. This includes the mPCT model, where inflammation is caused by introduction of mineral oils or plastic objects into genetically susceptible BALB/c or NZB mice (115). The tumors in the animal models develop in the inflammatory tissue, which suggests that local mediators from the inflammation are involved in tumor development. Local inflammatory mediators may be responsible for some cases, but there exists evidence that genetic susceptibility is also a requirement. This is true for again for the mPCT model, where not all mouse strains are susceptible, but mPCT development has been shown to depend on the BALB/c or NZB genetic background (116, 22).

The inbreeding of laboratory mice has led to strains that are either resistant or susceptible to certain pathogens, such as susceptibility to mineral oil induced mPCT (117). Alternatively, diseases can be induced in immuno-compromised mice, but these models miss mechanistic insights considering the natural microenvironment, with a fully functioning immune system. The susceptible inbred laboratory mouse strains, such as BALB/c or NZB, allow the study of diseases within the context of a functioning immune system. Even the

BALB/c mouse sub-strains vary in their susceptibility to mPCT development when subjected to mineral oil intraperitoneal injection (22). Plasmacytomas can also be induced in the NZB mouse strain, however these mice demonstrate longer latency periods for disease onset, with lower paraprotein levels (22, 118). This difference in disease progression may be because the NZB and BALB/c have a different pool of variable heavy chain gene determinants for generation of immunoglobulin classes (112, 118).

Animal models have also provided evidence for some inflammation-mediating agents likely to promote tumorigenesis. Non-steroidal anti-inflammatory drugs have been shown to inhibit formation and/or progression of experimentally induced tumors (119). Interleukin-6 (IL-6) is a main paracrine growth factor important in inflammation and immune response which has been demonstrated to be a necessary factor required for mPCT development (112, 114, 120). The oil granuloma macrophages serve as the source for IL-6 (121). An IL-6 transgenic cell line was created and introduced into C57BL/6 fertilized egg donors, which wasn't susceptible to mPCT until the BALB/c genetic background was introduced (121). The plasmacytomas these mice developed carried the T12;15 *c-MYC* carrying translocation. To further support the role of IL-6 in mPCT development, IL-6 deficient mice developed plasmacytomas only at a frequency lower than wild type mice, and their tumors showed defective ability to proliferate (120). These findings support that IL-6 plays a crucial role in mPCT progression and not necessarily disease onset.

2.4 Mouse Plasmacytoma Develops From Induced Chronic Inflammation

Mouse plasmacytoma (mPCT) is a well-known model to study MYC-induced tumorigenesis in human cancers (112). The genesis of mPCT, like human BL, involves the hallmark *c-MYC/IgH* chromosomal translocation that brings the *c-MYC* gene under the control of the *Ig* enhancer. mPCT is experimentally induced in genetically susceptible mice by intraperitoneal (IP) injection with agents that cause chronic inflammation, such as plastic particles or mineral oils (22). BALB/c and NZB mice are known for their genetic susceptibility to mPCT from mineral oil IP injections (122), and the most common inflammatory oil used is pristane (2,6,10,14-tetra-methyl-pentadecane). The invading oil, macrophages and neutrophils collect together to form oil granulomas (123). Moreover, large amounts of reactive oxygen species (ROS) are released as the immune cells try to clear the foreign substance. Increased ROS production may foster gene amplifications or illegitimate recombination by inducing DNA double strand breaks (124, 125). The peritoneal oil granuloma tissue provides a source of essential factors that includes IL-6 which is a macrophage-derived soluble factor that functions to support tumor growth and survival (126). This environment fosters chromosomal rearrangements such as the *c-MYC/Ig* translocation which is a crucial initiating event for plasmacytomagenesis.

Pristane-induced mPCT has a long mean latency for disease onset that ranges from 210-220 days (22). The mean latency period shortens to 88 days when pristane injection is followed by infection with the Abelson Murine Leukemia Virus (A-MuLV). The *v-abl* oncogene expressed by A-MuLV has transforming activity increasing *c-MYC* expression for Pre B lymphocytes and other hematopoietic cell lineages (127). Plasmacytomas that develop

from this method display *c-MYC/Ig* translocation > 95 % of the time. Of experimental importance, the mean latency period shortens even more to 45 days when pristane treatment is followed by infection with a helper-free retrovirus that carries the *v-abl/c-MYC* vector. Here, the retroviral vector carries *c-MYC* with constitutive expression which bypasses the need for the hallmark *c-MYC/Ig* translocation that acts to elevate MYC protein levels (22). Plasmacytoma incidence increases to 100 % with fast-onset models (128), compared to slow models where incidence of 20-60 % is dependent upon the amount of oil injected into the mouse, genetic susceptibility of the mouse strain and housing conditions (22). Interestingly, housing conditions may expose the PreB cell precursors to antigenic agents that aid susceptibility to the immune response that seems to aid plasmacytomagenesis (112). These methods of slow-, intermediate- and fast-onset mPCT all achieve elevated MYC levels necessary for plasmacytomagenesis. Ohno *et al*. (1999) show that mPCTs carrying the *c-MYC* translocations develop from immature B-cells and not from differentiated plasma cells (129). Conclusively, the clonal origin for these tumors and the more aggressive onset in *c-MYC/v-abl* induced mPCTS argue that along with increased MYC levels, additional genetic alterations may be required for full development of the disease (130).

2.5 Chr 11 Duplication is Associated with Accelerated mPCT Development

As mean latency periods shorten for experimentally induced mPCT development, another genetic aberration increases in frequency, duplication of Chromosome 11 (Chr 11) at the subcytoband E2 (11E2) (23). When slow-onset mPCT develops from pristane treatment alone, 11E2 duplication occurs only at a frequency of 7.1 % (131), but rises to 61.1 % when intermediate-onset mPCT is induced with pristane treatment followed by infection with the

transforming virus, A-MuLV. The incidence of trisomy 11 reaches 100 % in fast-onset *v-abl/c-MYC* experimentally induced mPCTs (Table 1). Increased frequency of this Chr 11 aberration, as the mean latency period decreases, suggests that this non-random duplicated region may harbor genes that contribute to the accelerated mechanism of plasmacytomagenesis.

Table 1 Chromosome 11 aberrations occurence in mPCT development.

Method of Induction	***c-myc*/*Ig***	**Latency (days)**	**Chr 11 Aberrations**	**Onset**
Pristane	Yes	180-300	7.1%	Slow
Pristane + A-MuLV	Yes	88	61.1%	Intermediate
Pristane + *v-abl/c-MYC*	No	45	100%	Fast

The 11E2 duplication harbors candidate genes identified by the Mai group with comparative genomic hybridization and functional genetic analysis of *v-abl/c-MYC* induced mPCTs. The genes *Aspscr1*, *Ict1*, *Kcnj2*, *Foxk2*, *Sec14l1* and *Tbcd* (Table 2) were found consistently amplified with increased copy number and overexpression (Mai, unpublished results). All of these genes play a role in various cellular processes that likely contribute to the development of hallmark cancer cell traits. Although MYC is the driving force for mPCT development, these 11E2 genes were consistently upregulated in fast-onset mPCTs compared to slow-onset mPCT cells, suggesting that they contribute to a more aggressive mechanism of disease progression.

Table 2 Candidate genes located on mouse Chromosome 11E2 with increased expression in mouse plasmacytoma.

Gene		Expression Value (fold increase)
Aspscr1	*Alveolar soft part sarcoma chromosome region, candidate 1*	10.5-10.7
FoxK2	*Forkhead box K2*	10.1
Ict1	*Immature colon carcinoma transcription 1*	10.5
Kcnj2	*Potassium inwardly-rectifying channel subunit 2*	9.6
Sec14l1	*Sec14-like1*	10.4-11.2
Tbcd	*Tubulin folding cofactors D*	10.8

2.6 11E2 Candidate Genes

Alveolar soft part sarcoma chromosome region, candidate 1 (*Aspscr1),* as the name suggests, is a candidate gene for alveolar soft part sarcoma (132), and is located on the 11E2 human synteny region 17q25. This gene is found fused with transcription factor TFE3 gene in alveolar soft part sarcoma, and renal cell carcinomas (133, 134). *Forkhead box K2 (Foxk2)* encodes a protein that belongs to the *Fox* family of proteins, which are evolutionarily conserved transcriptional regulators for a wide range of cellular processes, including DNA repair (135). The *Fox* family members are often found deregulated in cancer (136). *Potassium inwardly-rectifying channel subunit 2 (Kcnj2)* encodes a potassium channel that helps to maintain the cell membrane potential for a variety of cells, and its activity is linked to mitochondrial function (137). *Sec14l1* is poorly characterized, and the protein product is suspected to regulate phospholipid distribution in the membrane (138, 139). *Tubulin folding cofactors D (Tbcd)* encodes a chaperone protein that helps to correctly fold beta-tubulin by

capturing and stabilizing its intermediate structure conformations, which ultimately aids at various stages within the cell cycle program (140).

2.7 Immature Colon Carcinoma Transcript 1 in Cancer

Immature colon carcinoma transcript 1 (*Ict1*) within 11E2 was discovered during colon carcinoma cell lines transcriptomic screening, where *Ict1* mRNA was significantly down-regulated in differentiated HT29-D4 and Caco-2 cells (141, 142). Undifferentiated tumors tend to have higher proliferative potential and are often more aggressive than differentiated tumors, which makes characterization of markers from differentiation pathways in normal and neoplastic colon epithelial cells valuable (141). Subsequent research by Handa *et al*. (2010) demonstrated ICT1 protein function is important for cell viability and mitochondrial function by knockdown of *Ict1* in HeLa cells (143). Reduced ICT1 levels resulted in increased apoptosis, decreased mitochondrial membrane potential, reduced mitochondrial mass, and altered cytochrome c oxidase activity. Recent research suggests a role for *Ict1* in lung cancer progression where network analysis of gene-expression profiles identified *Ict1* as a hub gene, defined as a network of interacting genes centralized around *Ict1*, and a potential biomarker in three different types of lung cancers (24). More recently, knockdown of *Ict1* inhibited proliferation in glioblastoma and prostate cancer cell lines (25, 26). Moreover, the *Ict1* silenced prostate cancer cells also showed an increase in apoptosis. The emerging role for *Ict1* in various cancer cells is strong rationale to explore the role of ICT1 overexpression during MYC deregulated mPCT.

There is emerging research that supports a role *Ict1* may play in tumorigenesis. There has been increasing evidence for participation of translation release factors in cancer development, especially ones that have lost codon specificity, such as ICT1 (143). Translation release factors normally only activate release of protein from the ribosome when the mRNA feeds a stop codon to the ribosome. Loss of codon specificity affords these general translation release factors the ability to rescue stalled ribosomes and allow release of truncated proteins in a case where mutations have propagated into the mRNA sequence bypassing the requirement for a stop codon (143). Mitoribosomal protein recruitment in tumor progression would provide an advantage when the altered cellular metabolism cancer hallmark is considered. The increased energy demand of the developing cancer cell would require recruitment of machinery, specifically mitochondria, to support the increased metabolism (6, 7). Also, the role *c-MYC* plays in cellular processes that would require recruitment of mitoribosomal proteins, such as translation (48), and ribosome biogenesis (51). It is well established that dysregulated *c-MYC* is involved in early initiating events for mPCT onset, but that additional genomic alterations are necessary for the full progression of mPCT. These events would likely include recruitment of a partner able to help with increased metabolic demand that allows accelerated transformation such as *Ict1*. In addition, recent studies have found connections between increased *Ict1* in human cancers, such as lung (24), glioblastoma (25), and prostate cancer (26), where *c-MYC* also is involved in the mechanism of tumorigenesis (27-29).

2.8 Rationale

There is a great demand to uncover contributions from downstream genetic alterations that result from increases in MYC. Mouse lymphoma models have been successful for extrapolation to human cancers (144), and so there is great importance to understand the underlying mechanism for development of mouse plasma-cell neoplasms. Mouse model relevance depends entirely on their biological similarities to human lymphomas, and mPCT and BL share the *c-MYC* deregulating translocation and are cytogenetically identical (32). The focus of this thesis is to mimic conditions of accelerated transformation by staging MYC deregulation, and overexpression of the 11E2 duplicated gene, *Ict1* in cell lines in order to understand the potential role of overexpressed ICT1. Here, the role of ICT1 overexpression is explored during MYC deregulation, or on its own to try to understand ICT1 contributions to shortened latency for mPCT development. To achieve this goal, six conditions were explored (Table 3), which include MYC overexpression, both ICT1 and MYC overexpression together, and only ICT1 overexpression. Three negative control conditions were explored, where neither MYC nor ICT1 were induced for overexpression (Non-Induced), cells not transfected with the *Ict1* carrying vector (Untransfected), and cells treated by the same transfection conditions, except, with no vector (Transfection Control). We expect when ICT1 protein expression is induced in transfected cells, accelerated tumorigenic traits will occur, such as increased proliferation, evasion of apoptosis, and maybe the occurrence of an abnormal karyotype, which are all hallmark traits of tumorigenic potential (6,7).

Table 3 Experimental conditions to study ICT1 and/or MYC overexpression.

Condition	*c-MYC* Induction	*Ict1* Induction	Expected Result
MYC	+	-	Slow tumorigenic traits
ICT1+MYC	+	+	Accelerated tumorigenic traits
ICT1	-	+	Intermediate tumorigenic traits
Non-Induced	-	-	No tumorigenic traits
Untransfected	-	-	No tumorigenic traits
Transfection Control	-	-	No tumorigenic traits

2.9 Hypothesis

It is hypothesized that ICT1 overexpression resulting from MYC deregulation is required for increased tumor progression and affects pathways that result in accelerated mPCT development. In the PreB^{mycER} mouse cell line that models mPCT development, the downstream effects of overexpression of ICT1 will increase tumorigenic traits such as increased proliferation, evasion of apoptosis, and/or cause an altered karyotype.

2.10 Aims

To study the effects of *immature colon carcinoma transcript 1* overexpression during MYC-deregulation in PreB^{mycER} cells in order to determine if *Ict1* plays a role in acceleration of disease progression by altering the following selected hallmark cancer cell traits: increased proliferation, evasion of apoptosis, and genomic instability.

Aim 1. Induce ICT1 overexpression with and without MYC overexpression in mouse PreB^{mycER} cells.

Aim 2. Measure proliferation levels after ICT1 and/or MYC overexpression by looking at EdU incorporation during S-phase, and growth rates by cell growth curves.

Aim 3. Determine if there are changes in the level of apoptosis during ICT1 and/or MYC overexpression with a TUNEL assay to detect DNA strand breaks.

Aim 4. Use spectral karyotyping (SKY) experiments to observe if genomic instability is induced when ICT1 and/or MYC are overexpressed.

3 MATERIALS AND METHODS

3.1 Cell Culture

Mouse PreB^{mycER} lymphocytes, with the pVgRXR regulatory vector stably introduced (PreB^{mycER}) into the genome (clone 22), were grown in Roswell Park Memorial Institute (RPMI) 1640 media supplemented with 10 % (v/v) fetal bovine serum (FBS), 1 % L-glutamine, 1 % sodium pyruvate, 1 % penicillin-streptomycin, and 0.1 % β-mercaptoethanol (all reagents from Gibco, Burlington ON, Canada) and 7.5 μL of Zeocin (ant/zn-5; InvitrogenTM, Carlsbad CA, USA) per mL of media. Mineral oil induced mouse plasmacytoma cell line (MOPC 460D, a gift from Dr. J. F. Mushinski, National Institutes of Health, Laboratory of Cancer Biology and Genetics, Bethesda MD, USA) were cultured in RPMI 1640 media supplemented as above, with 100 μL of IL-6 hybridoma supernatant per 10 mL media. Both cell lines were incubated at 37 °C, 5 % CO_2 in a humidified atmosphere and maintained at a cell density of 10^5-10^6 cells/mL.

3.2 Immunofluorescence

PreB^{mycER} cells or MOPC 460D cells (10^5 suspended in 100 μL RPMI 1640) were centrifuged 290 x g onto a glass slide (Type K102; Kindler GmbH & Co., Freiburg Baden-Württemberg, Germany) by cytospin (Shandon Cytocentrifuge; Thermo Fisher Scientific, Rockford IL, USA). Supernatant was absorbed onto filter cards (Shandon Filter Cards; Fisher Scientific, Rockford IL, USA). Cells were fixed in fresh 3.7 % formaldehyde/1x phosphate-buffered saline (PBS) containing 50 mM $MgCl_2$ for 10 minutes, then washed three times in 1x PBS/50 mM $MgCl_2$. The fixed cells were permeabilized in 0.2 % TritonX-100 for 12

minutes at room temperature, then washed three times in 1x PBS/50 mM $MgCl_2$. Blocking was achieved with 3 % bovine serum albumin (BSA) in 4x saline-sodium citrate (SSC) for 30 minutes at room temperature (80 µL/slide with 24x60 mm coverslip). After blocking, the coverslips were removed and primary antibody applied to the slides (20 µL/slide, and 24x24 mm coverslip), polyclonal anti-*c-MYC* (N262; Santa Cruz Biotechnology, Dallas TX, USA) 1/200 and anti-*Ict1* (H00003396-B01P; Abnova, Walnut CA, USA) 1/100. After 1 hour incubation at 37 °C, the slides were washed 3 x 5 minutes with 1x PBS/50 mM $MgCl_2$. Secondary antibodies were applied (20 µL/slide and 24x24 mm coverslip), goat-anti-rabbit IgG fluorescein isothiocyanate (FITC) (A-1108; Life Technologies Inc., Burlington ON, Canada) 1/10000, and goat-anti-mouse Alexa Fluor488® (A-11006 Molecular Probes; Thermo Fisher Scientific, Rockford IL, USA) 1/1000, and incubated at room temperature for 45 minutes, then washed three times with 1x PBS/50 mM $MgCl_2$. The slides were dehydrated in an ethanol series, 70 %, 90 % and 100 % for 2 minutes each, then 4'6-diamidino-2 phenylindole (DAPI) was applied to each slide to counterstain the DNA and incubated 5 minutes in the dark. DAPI was washed off with distilled water, and Vectashield (Vector Laboratories, Burlington, ON, Canada) to prevent photobleaching was applied and a 24x24 mm coverslip. Fluorescent images were taken with AxioImager Z2 microscope (Carl Zeiss, Toronto, ON, Canada) an AxioCam MRm charged coupled device (Carl Zeiss), equipped with a HXP 120C light source, with a 63x1.4 oil objective lens (Carl Zeiss), and DAPI and FITC filters (Carl Zeiss). Exposure times were first measured and optimized, then kept constant at 800-1000 milliseconds throughout acquisition to allow comparison of quantitative immunofluorescence analysis.

3.3 Restriction Enzyme Digestion

To a 1.5 mL tube, 1 µL of DNA (1µg/µL), 10 enzyme units of restriction enzyme (New England BioLabs, Ipswich MA, USA) of each *XbaI* (R0145M) and *HindIII* (R0104S), 3 µL of enzyme digestion buffer, 3 µL of BSA and 21 µL of double distilled H_2O to obtain a final volume of 30 µL. The tube was incubated at 37 °C in a waterbath for 4 hours. Digested samples were analysed on a 0.8 % agarose gel in TAE buffer (Tris base, acetic acid and EDTA, pH 8) for 45 minutes at 15 V/cm, with undigested vector run on the same gel. 1 kb DNA ladder (M1182; Fermentas Canada Inc, Burlington ON, CA) was run in lane 1 of the gel, and Gel Loading Dye, Blue 6x (B7021S; New England Biolabs, Ipswich MA, USA) was added to digested and undigested samples before loading onto the gel. 7 µL (approximately 230 ng digested DNA) of reaction mixture, and 500 ng of undigested vector were loaded onto the gel.

3.4 Western blot

A Western blot was performed on MOPC 460D positive control cell line. MOPC 460D cells were seeded at 2 x 10^5 cells/mL in 2 mL of RPMI 1640 supplemented media with IL-6 (100-200 µL), and incubated at 37 °C, 5 % CO_2. $PreB^{mycER}$ cells transfected with pIND/Hygro-*Ict1* were induced for *Ict1* expression, and 24 hours later cells were harvested during peak ICT1 expression. Approximately 1 x 10^6 cells for each MOPC 460D and transfected $PreB^{mycER}$ cells were lysed 24 hours later with Radioimmunoprecipitation assay (RIPA) buffer (147) containing protease inhibitor, and sonicated on ice. Cellular debris was removed by centrifugation. Protein concentration was measured using Bradford Reagent. Equivalent protein amounts (100 µg) were resolved by sodium dodecyl sulfate-

polyacrylamide gel electrophoresis (SDS-PAGE) with a 4-20 % gradient. Resolved protein was transferred to a 0.45 µm polyvinylidene difluoride (PVDF) membrane (ImmunoBlot, Bio-Rad, Montréal QC, Canada) in transfer buffer (48 mM Tris-base, 39 mM glycine, 0.04 % SDS, and 20 % methanol) at 100 V for 1 hr. Equivalent protein amounts were confirmed by copper phthalocyanine 3,4',4'',4'''-tetrasulfonic acid tetrasodium salt (CPTS) staining (148). The membrane was then washed two times in 1x PBS to remove CPTS dye and then blocked in 5 % skim milk in Tris-buffered saline (pH 7.4) containing 0.1 % Tween-20 (TBST) for 1 hr at room temperature. The membrane was blotted overnight at 4 ºC with anti-*Ict1* (H00003396-B01P; Abnova, Walnut CA, USA) in a dilution of 1/1000, and anti-α Tubulin (ab7291; Abcam Inc, Toronto ON, Canada) as a loading control diluted 1/1000 in 5 % skim milk containing 0.1 % Tween 20. After three ten minute washes in TBST each time for 10 minutes, the membrane was incubated at room temperature for 1 hr with horseradish peroxidise-conjugated anti-mouse secondary antibody (115-035-146; Jackson ImmunoResearch Laboratories, West Grove PA, USA) 1/10,000 in 5 % skim milk in TBST. The membrane was again washed as described above, and then incubated for 5 minutes with Western blotting luminescence detection reagent (GE Healthcare, Saskatoon SK, Canada). The blots were imaged and the bands were visualized using a MycECL Imager (Thermo Scientific, Rockford IL, USA) using standard chemiluminescence.

3.5 Transfection of PreB^{mycER} Cells

Transfections of PreB^{mycER} cells were performed by electroporation (Amaxa Nucleofector Transfection System, Lonza, Allendale NJ, USA), Kit V, Program Z-01. RPMI 1640 (Gibco, Burlington ON, Canada o) was supplemented as above but without penicillin-

streptomycin. For transfection of *Ict1* into PreB^{mycER} pVgRXR containing cells, the Ecdysone-Inducible Mammalian Expression System was used (No, 1996). PreB^{mycER} cells were split 24 hours prior to transfection. 5 x 10^6 cells (passage 11-13) were transfected with 1 μg of pIND/Hygro-*Ict1* and transferred to 2 mL media in a 6 well plate, incubated for 4-6 hours at 37 °C 5 % CO_2. After recovery incubation, the 2 mL media containing transfected cells were added to 8 mL pre-warmed media in 10 mL plates. To ensure selection of pVgRXR containing cells, 75 μL of Zeocin (ant/zn-5; Invitrogen, Carlsbad CA, USA) was added to the plate and then the cells were incubated for 20 hours at 37 °C, 5 % CO_2. After 24 hours of recovery from transfection, the live cells were sorted from dead cells by Flow Cytometry Live/Dead cell sorting using DAPI staining as the exclusion criteria. Viability was determined by adding 10 μL vital stain Trypan blue (Invitrogen, Carlsbad CA, USA) to 10 μL of cell suspension, and counts determined with a hemocytometer. Viability at 4 hours was between 40-50 %, and at 24 hours 60-70 %. A transfection control was included, that went through the same experimental conditions, minus inclusion of any vector. The non-induced negative control contained the vector, but was never induced for MYC or ICT1 expression. A third negative control was included which was untransfected cells from the same plate the transfected PreB^{mycER} cells came from.

3.6 Flow Cytometry Live/Dead Cell Sorting

PreB^{mycER} cells were collected (approximately 5 x 10^6) 24 hours after transfection, centrifuged at 129 x g for 10 minutes. They were washed with sterile filtered 1 x PBS (5 mL) and re-suspended in fresh sterile 1 x PBS (500 μL) containing 1 % FBS and 5 units of DNAse (RQ1; Promega, Madison WI, USA). DAPI was added 0.5 μL of 1 mg/mL to sort

live from dead cells. Cells were sorted in an AriaIII system housed in a ClassII Type A2 biosafety cabinet to ensure sterile conditions. DAPI stained dead cells were excluded. Cells were sorted using a 85 micron nozzle. Cells were collected into RPMI 1640 that contained 20 % FBS. Sorted live cells were centrifuged 129 x g for 10 minutes, and re-suspended in RPMI media (supplemented with 10 % (v/v) FBS, 1 % L-glutamine, 1 % sodium pyruvate, 1 % penicillin-streptomycin, and 0.1 % β-mercaptoethanol (all reagents from Gibco, Burlington ON, Canada). Cells were allowed to recover 12 hours before induction.

3.7 Induction of ICT1 and/or MYC Expression

ICT1 was induced with Ponasterone A (P3490-1MG; Sigma-Aldrich, Oakville, ON, Canada) to a final concentration of 10 µM in 10^5 transfected and flow sorted PreB^{mycER} cells/mL. Induction of ICT1 was confirmed by immunofluorescence. A slide was prepared by cytospin for 0, 24, and 36 hours after *Ict1* induction for each of 5 conditions. In sorted PreB^{mycER} cells, MYC was activated by 4-hydroxytamoxifen (4HT; Sigma-Aldrich, Oakville, ON, Canada) at a final concentration of 100 nM in 10^5 cells/mL (9). Induction of *c-MYC* was confirmed by immunofluorescence as described in Section 3.2 (Immunofluorescence). A slide was prepared by cytospin for 0, 6 and 12 hours after MYC induction for each of 5 conditions (Table 3). Slides prepared for immunofluorescence included a negative non-induced control condition at the same time points treated with ethanol, a transfection control that never received the vector or inducing agents, and a positive control of MYC/ICT1 overexpressing mPCT cells MOPC 460D.

3.8 ClickIt ® EdU Cell Proliferation Assay (Invitrogen)

PreB^{mycER} pVgRXR cells were split to 2 x 10^4 cells/mL and induced with Ponasterone A (P3490-1MG; Sigma-Aldrich, Oakville, ON, Canada) and/or 4HT (4HT; Sigma-Aldrich, Oakville, ON, Canada). 5 x 10^5 cells were collected for time 0, and again at 12, 24, 36, 48, 72, 96 hours. Cells were induced to have peak expression of ICT1 and/or MYC occur simultaneously at 24 hours after ICT1 induction. Cells were centrifuged at 129 x g for 10 minutes, supernatant was discarded, and the cell pellet re-suspended in 1 mL of RPMI 1640. 1 mL of 2x 5-ethynyl-2'-deoxyuridine (EdU) solution was mixed to make a final concentration of 10 μM of EdU, and the cells were incubated for 20 minutes at room temperature. Slides were prepared by cytospin from this cell suspension, and were fixed in 3.7 % formaldehyde in 1x PBS for 10 minutes at room temperature. Fixative solution was removed from slides with three washes in 1x PBS. The cells were permeabilized in 0.5 % TritonX-100 in 1x PBS for 12 minutes. After permeabilization, slides were washed two times in 1x PBS. Freshly made Click-iT reaction cocktail (Click-iT® EdU Alexa647® HCS Assay, Invitrogen, Carlsbad CA, USA) was added, 60 μL/slide 24x60 mm coverslip, and incubated in a humidified chamber for 30 minutes at room temperature in the dark. After incubation, slides were washed three times in 1x PBS, and nuclear DNA counterstained with DAPI. Antifade/Vectashield was applied and then slides were imaged using an Axio Imager.Z1 microscope (Carl Zeiss, Toronto, ON, Canada) equipped with an AxioCam HRm camera and EXFOx-Cite 120 light source. Images were acquired with a 63x Plan-Apochromat 1.4 oil objective with DAPI and Texas Red filters, and analyzed with AxioVision 4.8 software. Exposure times were first measured and optimized, then kept constant throughout acquisition to allow comparison of quantitative fluorescence analysis of EdU incorporation between each

experimental condition, for each experimental trial. The slides were imaged to count 100 cells per condition, in 3 independent experiments.

3.9 In Situ Cell Death Detection Kit, Fluorescein (Roche)

PreB^{mycER} pVgRXR cells were split to 2 x 10^4 cells/mL and induced with Ponasterone A and/or 4HT. Cells were collected (5 x 10^5) for time 0, and again at 12, 24, 36, 48, 72, 96 hours. Cells were induced to have peak expression of ICT1 and/or MYC to occur simultaneously at 24 hours. Cells were centrifuged at 129 x g for 10 minutes, the supernatant was discarded, and the cell pellet was re-suspended in 1 mL of RPMI 1640 and slides were prepared by cytospin as above. TdT-mediated dUTP nick end labeling (TUNEL) reaction mixture (*In Situ* Cell Death Detection Kit, Fluorescein, Sigma-Aldrich Canada Co., Oakville, ON, Canada) was added to the slides (60 µL/slide and 24x60 mm coverslip) and incubated for 1 hour at 37 °C in a dark humidified chamber. After incubation the slides were washed three times in 1x PBS. The nuclei were counterstained with DAPI, and Vectashield applied with a 24x24 coverslip. Exposure times were first measured and optimized, then kept constant throughout acquisition to allow comparison of quantitative fluorescence analysis of Fluorescein incorporation between each experimental condition, for each experimental trial. The slides were imaged to count 100 cells per condition, in 3 independent experiments.

3.10 Spectral karyotype analysis (Applied Spectral Imaging (ASI))

Spectral karyotype (SKY) analysis was performed using the ASI (Applied Spectral Imaging, Vista, CA, USA) kit for mice in accordance with the supplier's hybridization protocols. At 48 hours post-ICT1 and/or MYC peak expression approximately 10^7 cells were centrifuged at 800 RPM (129 x g) for 10 minutes, re-suspended under hypotonic conditions in 0.075 M KCl for 30 minutes at room temperature. The cells were centrifuged again at 800 RPM, 10 minutes and supernatant removed. The cell pellet was fixed by drop fixation (145) with fresh fixative 3:1 methanol:acetic acid. Fixation solution was added drop by drop. First 5 X 1 drop with 1 minute wait between each drop was added to the cell pellet by 9" Pasteur pipette (Thermo Fisher Scientific, Rockford IL, USA). Then 2, 5, 7, 10, 15, 20, 30, and 60 drops with 2 minute wait following each set of drops. The cell pellet was re-suspended and left to incubate 10 minutes at room temperature. The cells were centrifuged at 129 x g for 10 minutes, supernatant removed, and re-suspended in 5 mL fixative to incubate for 20 minutes, then again centrifuged and again re-suspended with 5 mL fixative to incubate for 30 minutes. After centrifuging fixed cells were re-suspended in 5 mL fixative and stored at – 20 ºC.

Metaphase spreads were prepared by re-suspending fixed cells in fresh 1 mL of fixative, and 30 µL dropped approximately 1 meter onto glass microscope slides (Type K102, Kindler GmbH & Co., Kindler GmbH & Co., Freiburg Baden-Württemberg, Germany) pre-chilled on dry ice until fog appeared on the surface, approximately 5 seconds, and held at a 45º angle. Slides were immediately warmed on a 37 °C hot plate for 4 seconds, then submerged briefly into 50 % acetic acid (Thermo Fisher Scientific, Rockford IL, USA) and returned to the hot plate to dry. Dried slides were incubated for 2 minutes in 10 %

Giemsa (Gibco, Burlington ON, Canada) solution in 0.15 M K_2HPO_4/KH_2PO_4 phosphate buffer (pH 8.0), rinsed under distilled water, air dried, then viewed with a light microscope. Slides with at least 20 high quality metaphase spreads in roughly an 18x18 area with no overlapping chromosomes were selected.

Slides were equilibrated in 2x SSC for 10 minutes, then treated with RNaseA (6 µg/mL in 2x SSC, and 24x60 mm coverslip) and incubated for 1 hour at 37 ºC. Slides were washed three times in 2x SSC and treated with 40 µg/mL pepsin in 0.01 M HCl (pH 2.0) for 12 minutes at 37 ºC. After pepsin treatment, slides were washed two times in 1x PBS, then once in 1x PBS/50 mM $MgCl_2$, and fixed in fresh 3.7 % formaldehyde/1x PBS/50 mM $MgCl_2$ for 10 minutes. Fixed slides were washed in 1x PBS, dehydrated 2 minutes each in 70 %, 90 %, and 100 % ethanol (Fluka-02855; Sigma-Aldrich Canada Co., Oakville, ON, Canada), and air dried. The slides were incubated in 70 ºC oven for 5 minutes, then transferred immediately into 70 ºC denaturing solution 70 % formamide/2x SSC (pH 7.0) for 2 minutes. Denatured slides were dehydrated 2 minutes each 70 %, 90 %, and 100 % ethanol (Fluka, USA) pre-chilled to -20 °C, then air dried. Mouse SKYPaint™ (Applied Spectral Imaging, Vista CA, USA), previously denatured for 5 minutes at 85 ºC and incubated at 37 ºC for 30 minutes, was added to each slide (9 µL) on the selected metaphase area, and then a coverslip (24x24 mm) was applied and sealed with rubber cement. Slides were incubated for 36 hours in a humidified chamber at 37 ºC, 5 % CO_2. At 36 hours, rubber cement and coverslips were removed, and the slides were washed three times in 50 % formamide/2x SSC at 45 ºC, followed by two washes in 4x SSC/0.1 % Tween 20 at 45 ºC, then in 1x SSC at 45 ºC. Blocking reagent (Applied Spectral Imaging, Vista CA, USA) was added to each slide (80 µL/slide, and 24x60 mm coverslip) and incubated 30 minutes at 37 ºC. Mouse anti-

digoxigenin (mouse IgG, D8156, Sigma-Aldrich Canada Co., Oakville, ON, Canada) stock (1 mg/mL) was diluted 100 times in 4 % BSA/4x SSC and added to the slides (80 µL/slide with 24x60 mm coverslip) and incubated 45 minutes at 37 °C. Slides were washed 3 X 5 minutes in 4x SSC/0.1 % Tween 20 at 45º C. Goat anti-mouse IgG conjugated to Cy5.5 (610-113-121, Rockland, USA), and biotin conjugated to Cy5 (S000-06, Rockland, USA) were prepared together by diluting stocks (1 mg/mL) 100x in 4 % BSA/4x SSC, and added to slides (80 µL/slide, 24x60 mm coverslip). After incubation for 45 minutes at 37 °C, slides were washed three times for 5 minutes in 4x SSC/0.1 % Tween 20 at 45º C. DNA was counterstained and photo-bleaching minimized with DAPI/anti-bleach (Applied Spectral Imaging, Vista, CA) added to each slide (10 µL/slide, with 24x24 mm coverslip).

Slides were imaged under oil immersion (63x/1.4 objective, Zeiss Axioplan 2 microscope equipped with a SpectraCube SD-300, Applied Spectral Imaging, Vista, CA) and VDS COOL-1200QS CCD camera (VDS Vosskühler GmbH, Freiburg Baden-Württemberg, Germany), using a PC with Spectral Imaging Case Data Manager 6.0.0.16 software (Applied Spectral Imaging, Vista CA, USA). Spectral karyotypes from at least 20 cells per condition were analyzed in three independent experiments.

3.11 Statistical Analysis

Mean with standard deviation (σ) were calculated to show the consistency within replicates for each experimental condition. The standard deviation quantifies the amount of variation or dispersion of a set of data values. The differences between experimental groups were analyzed with the χ^2 test for independence and the Fisher's exact test to compare variation in proliferation, apoptotic levels and the occurrence of EEs. $P < 0.05$ was considered significant. Calculations performed in Excel were verified manually with a calculator.

4 RESULTS

4.1 Determined Peak Expression Levels for ICT1 and MYC

The level of ICT1 overexpression was measured by immunofluorescence, first to determine when peak ICT1 expression occurs. MOPC 460D cell line was used as the positive expression control for ICT1 and MYC as this is a mineral oil induced mouse plasmacytoma cell line that has the enhancing *c-MYC* translocation. Deregulated MYC results in higher levels for these genes, the level of ICT1 expression peaked at 24 hours post-induction with Ponasterone A (Figure 1). Protein levels were determined based on measured relative fluorescent intensity, and ICT1 levels compared to negative controls achieved a 3-4 fold increase in expression, close to the plasmacytoma MOPC 460 D positive cell line control ICT1 protein levels. When both *c-MYC* and *Ict1* were induced, ICT1 protein levels were measured at 3580 RFU (σ = 199), similar to the MOPC 460D ICT1 positive expression control cells with ICT1 levels measured at 3232 RFU (σ = 163). Separate induction of *Ict1* gave increased fluorescent intensity at 2507 RFU (σ = 210). When *c-Myc* alone was induced,

ICT1 levels only increased to 1372 RFU (σ = 178). Non-induced controls showed ICT1 levels (mean = 1162 RFU, σ = 142) similar to untransfected cells (mean = 902 RFU, σ = 13) and transfection control cells (mean = 1028, σ = 52) and secondary antibody controls showed even lower expression levels (2° Ab mean = 681 RFU, σ =20). As fluorescent levels increased, the differences between cell expression showed greater variance in intensity levels, seen by the increased standard deviations for high ICT1 expressing conditions relative to low level ICT1 expressing conditions with smaller deviations.

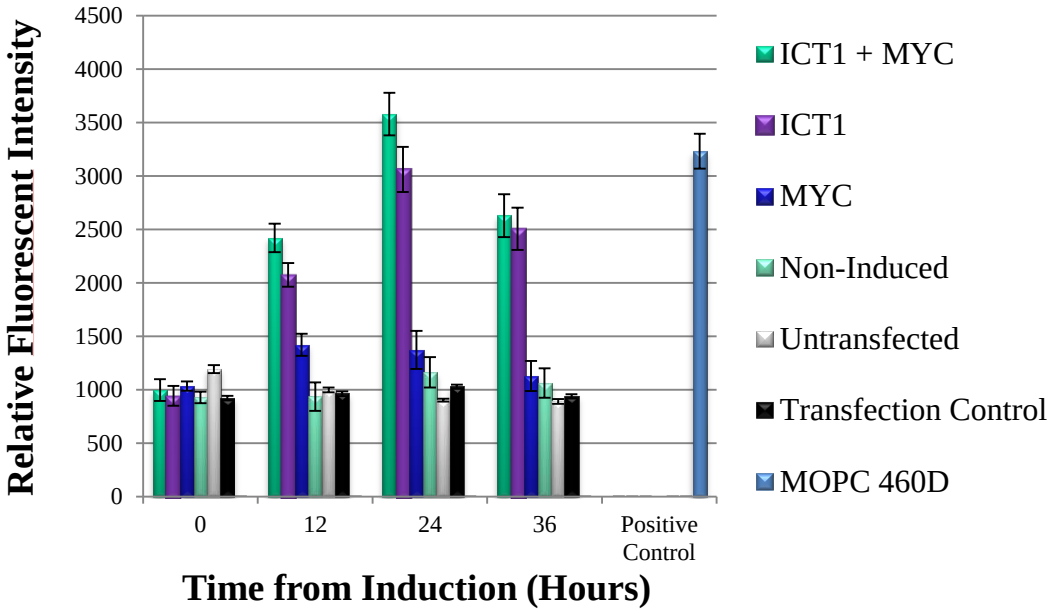

Figure 1 Mean relative fluorescent intensity measurements to determine ICT1 peak expression levels in transfected PreB^{mycER} cells.

Transfected cells with both *Ict1* + *c-MYC* induced, *Ict1* only induced, *c-Myc* only induced, and negative controls: Non-Induced, Untransfected, and Secondary Antibody Control (2° Ab controls), and the Positive Control for ICT1 expression: MOPC 460D. Relative fluorescent intensity was determined in 3 independent experiments. Error bars show one standard deviation of uncertainty.

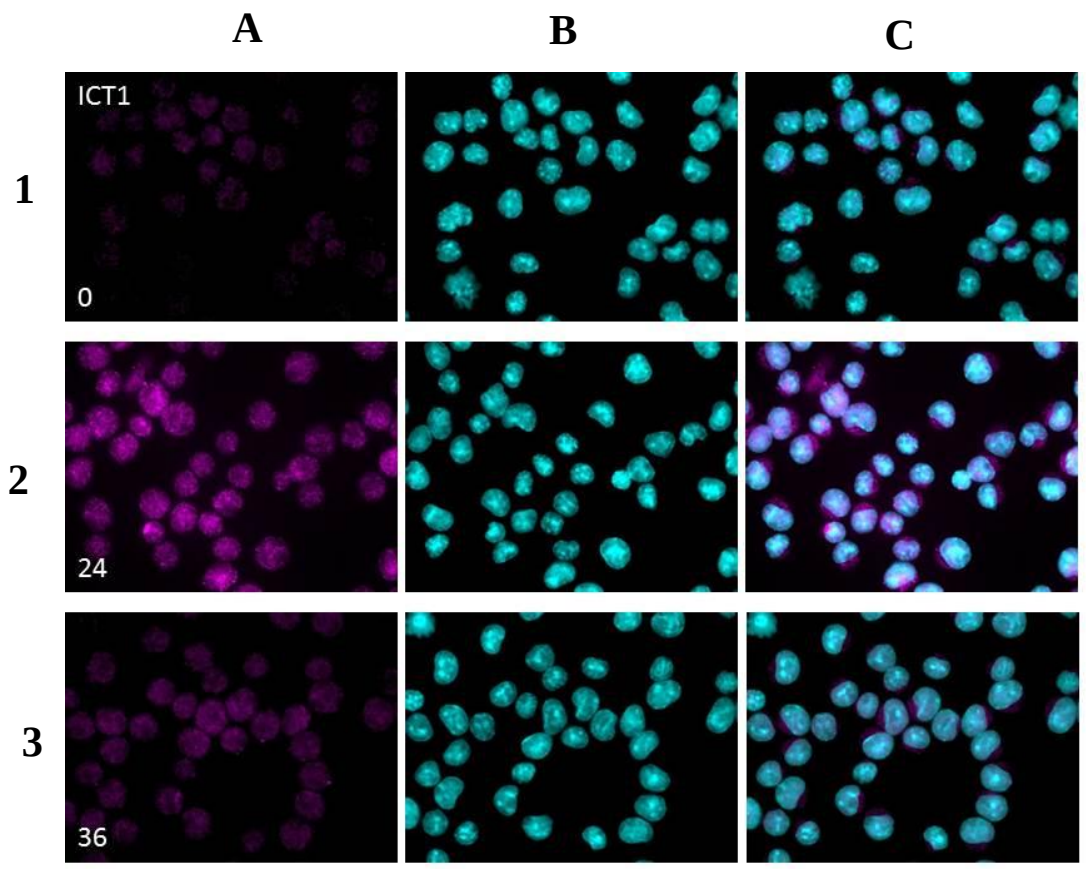

Figure 2 Immunofluorescent detection of peak ICT1 expression levels in transfected PreB^{myER} cells.

ICT1 (magenta) is shown in panels A1-3, nuclear DNA is counterstained with DAPI (cyan) in B1-3 and both are shown merged in panels C1-3. ICT1 expression at 0 hours is low (mean = 998 RFU, σ = 102; panels A1 and C1), but peak at 24 hours (mean = 3433 RFU, σ = 193; panels A2 and C2), and are shown declining at 36 hours (mean = 730 RFU, σ = 201; panels A3 and C3) during transient *Ict1* induction with Ponasterone A. To confirm peak MYC expression levels, 4HT induced PreB^{mycER} cells were monitored at 0, 2, 4, 6, 8, 12 and 24 hours. They showed peak expression at 6 hours (Figure 3), and the signal was localized in the nucleus where MYC exerts it effects as a transcription factor.

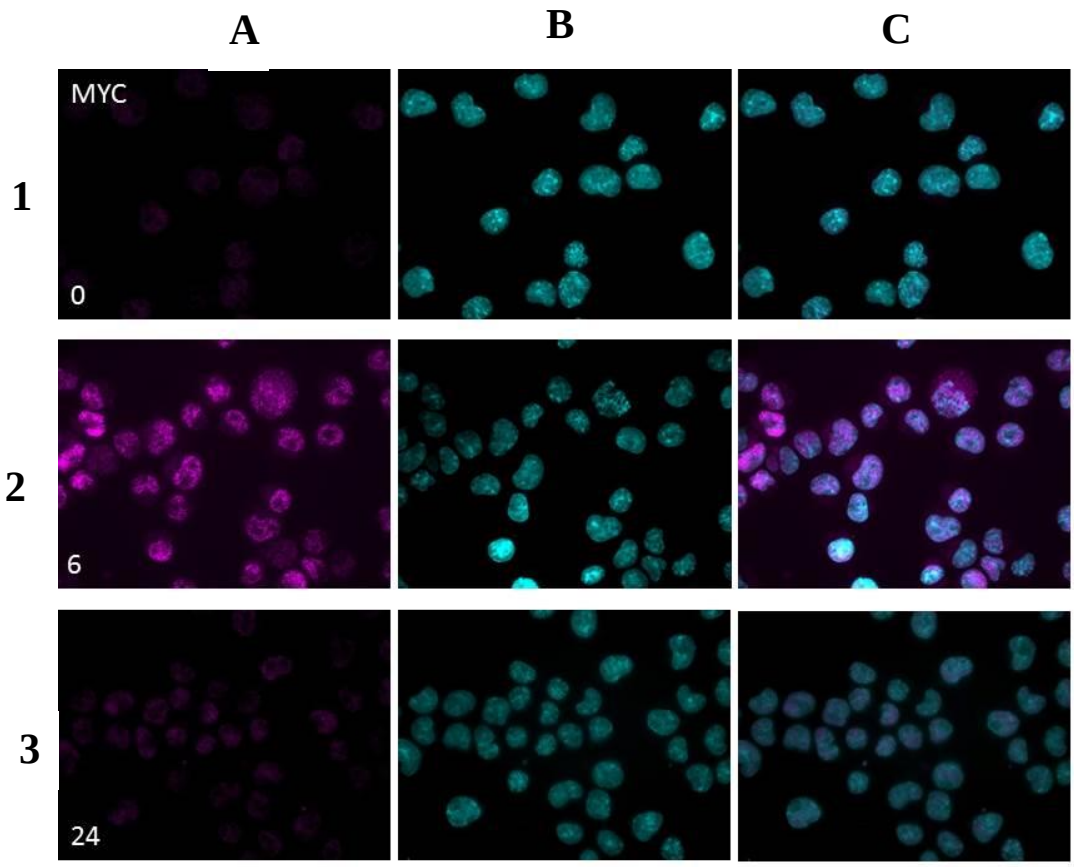

Figure 3 Immunofluorescent detection of peak MYC expression levels in the nuclei of PreB^{mycER} cells.

MYC (magenta) is shown in panels A1-3, nuclear DNA is counterstained with DAPI (cyan) in B1-3 and both are shown merged in panels C1-3. At 0 hours post-4HT induction MYC expression is low (mean = 892 RFU, σ = 52; panels A1 and C1), MYC levels peak at 6 hours with concentrated localization in the nucleus (mean = 3027 RFU, σ = 172; panels A2 and C2), and have declined at 24 hours (mean = 1429 RFU, σ = 348; panels A3 and C3) during transient *c-MYC* induction with 4-HT.

4.2 Vector and Antibody Validation

Digestion with restriction enzymes to cut out the *Ict1* sequence was performed to confirm the integrity of the vector (previously prepared and sequenced by the Mai lab; Appendix 1, Figure 17). Digestion resulted in a 627 kb fragment (Figure 4, Panel A), the same size as observed after sequencing the vector to also confirm correct orientation of *Ict1* into the pIND/Hygro vector. A Western blot was performed in order to compare MOPC 460D ICT1 protein levels with untransfected PreB^{mycER} cells with PreB^{mycER} cells transfected with the pIND/Hygro-*Ict1* vector (Figure 4, Panel B) to ensure the anti-ICT1 antibody was in fact detecting the ICT1 protein. Untransfected cells showed lower levels of ICT1 expression. Ponasterone A levels were titrated to reach physiologically relevant levels of ICT1 expression as in the plasmacytoma ICT1-overexpressing MOPC 460D cell line.

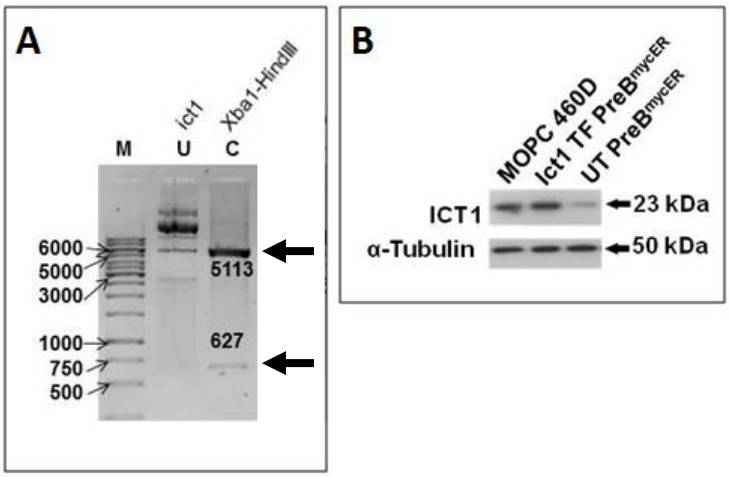

Figure 4 Vector validation for pIND/Hygro-*Ict1* and anti-ICT1 antibody validation.

A restriction enzyme digest (Panel A) was done on the pIND/Hygro-*Ict1* vector to confirm the gene insert was *Ict1*. Expected fragments appeared at 627 bp and 5113 bp. Western blot (Panel B) showed the ICT1 protein levels at 23 kDa from positive control cells (MOPC

460D), and PreB cells transfected with *Ict1* (*Ict1* TF PreB^{mycER}) were compared to untransfected PreB cells (UT PreB^{mycER}).

4.3 Proliferation Levels during ICT1 and/or MYC Overexpression in PreB^{mycER} Cells

Induction of *Ict1* and *c-MYC* were confirmed for each set of experiments at expected peak expression time-points. At 24 hours post-Ponasterone A induction, ICT1 expression was observed in transfected PreB^{mycER} cells. At 6 hours post-4HT induction, MYC expression was observed and found to be localized in the nucleus in transfected PreB^{mycER} cells (Figure 5).

Proliferation levels were measured by EdU incorporation into newly synthesized DNA. The average % proliferative cells (Figure 6, Figure 7) show that when ICT1 and MYC are overexpressed together, proliferation levels increase. The difference in proliferation when PreB^{mycER} cells were induced for ICT1 and/or MYC expression were compared to the average for all the negative control conditions (untransfected, non-induced, and transfection control). When both *c-MYC* and *Ict1* were induced, proliferation levels increased by 15-20 % from 36 hours to 72 hours, with the greatest difference of 19.8 % at 36 hours. When *Ict1* alone was induced, proliferation levels increased up to 12 % at 72 hours ($\sigma = 8.27$). *c-MYC* induction resulted in 9 % higher proliferation levels compared to negative controls ($\sigma = 4.83$).

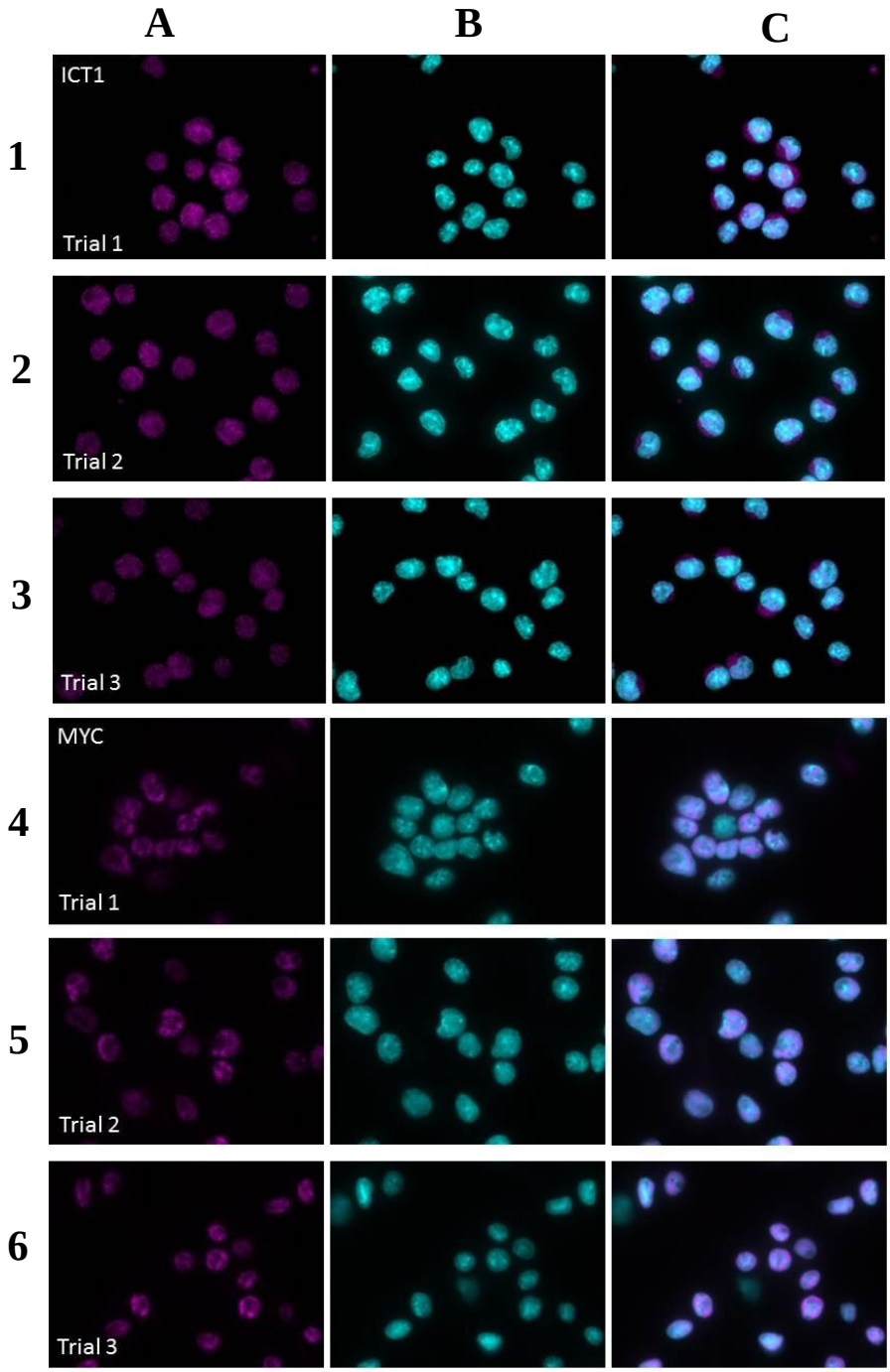

Figure 5 Immunofluorescence confirmed induction of *Ict1* and *c-MYC* at 24 hours.

ICT1 (magenta) is shown in panels A1-3, MYC (magenta) is shown in panels A4-6), nuclear DNA is counterstained with DAPI (cyan) in B1-6 and merged images are shown in panels C1-3 (ICT1) and C4-6 (MYC). At 24 hours post-Ponasterone A induction, transfected PreB^{mycER} cells showed ICT1 (magenta) expression (Panels A1-3, C1-3). At 24 hours post-

Ponasterone A induction, and 6 hours post-4HT induction PreB^{mycER} cells showed nuclear expression of MYC (magenta) (Panels A4-6, C4-6).

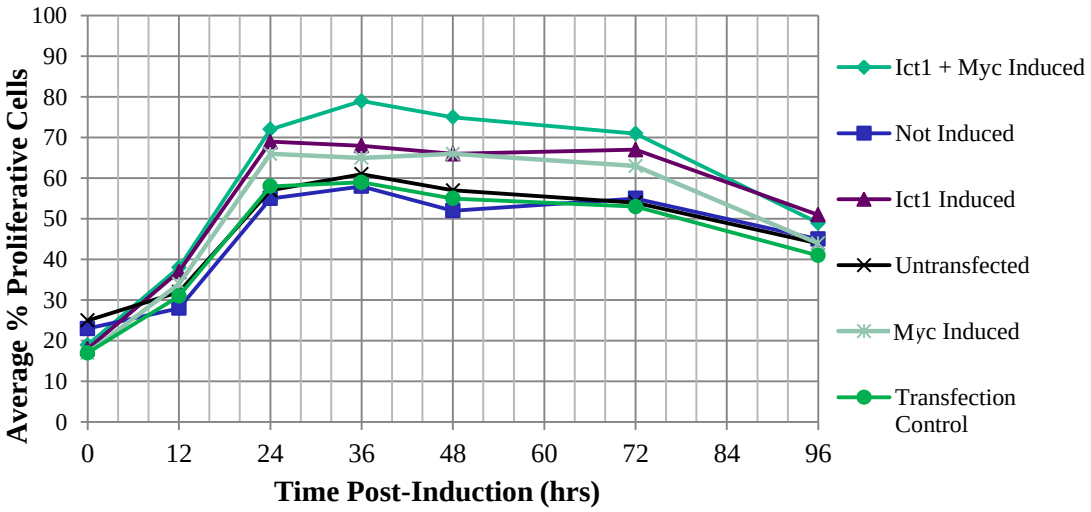

Figure 6 Mean proliferation levels during increased ICT1 and/or MYC levels in transfected PreB^{mycER} cells.

The number of cells that showed EdU incorporation were counted when both *Ict1 + c-MYC* induced, neither gene was induced (Not Induced), only *Ict1* induced, untransfected, only *c-MYC* induced, and for the Transfection Control. Three independent experiments were performed.

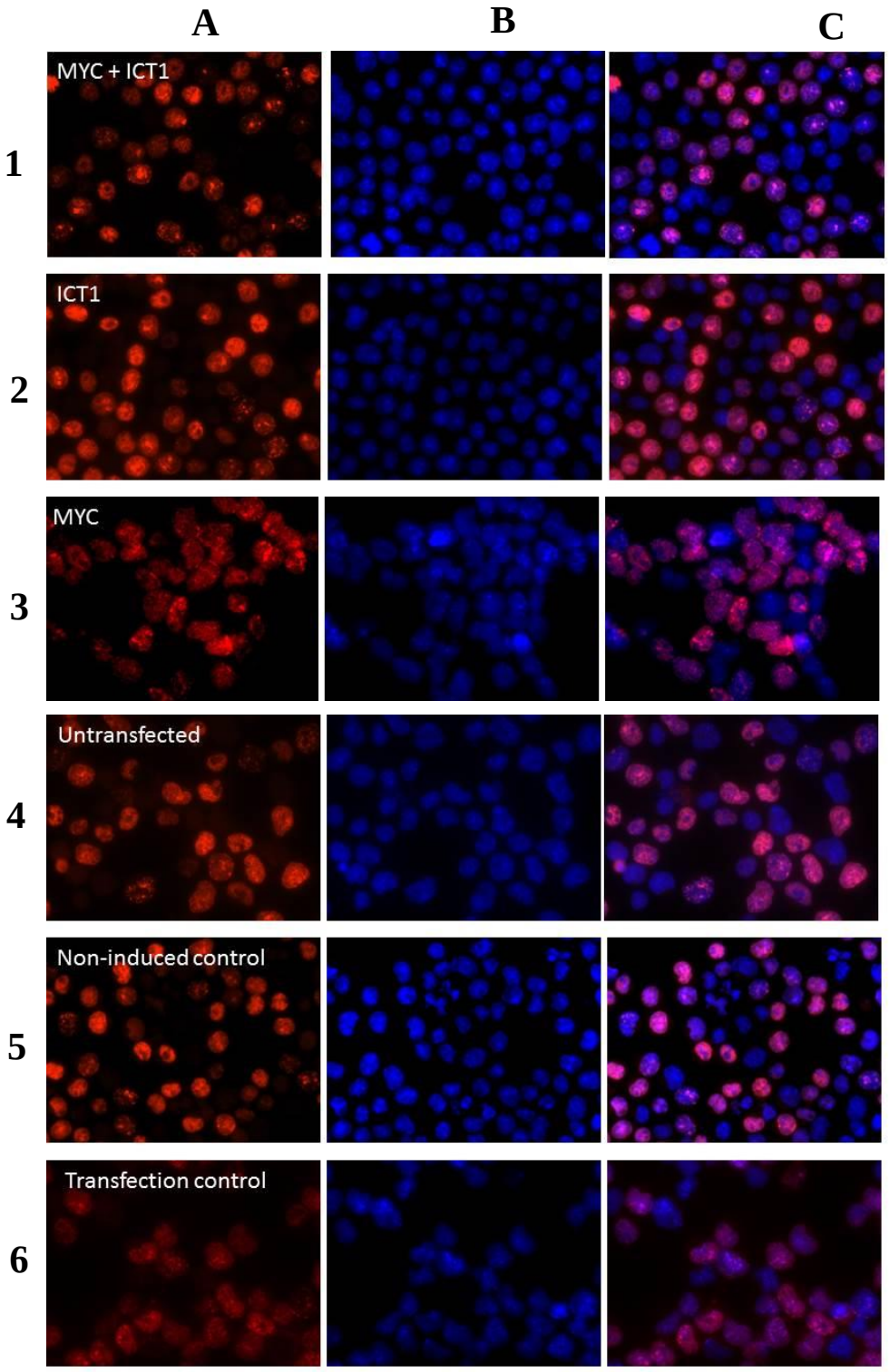

Figure 7 Proliferative cells in S-phase measured by Edu incorporation.

The proliferative cells found in the S-phase shown after induction with Ponasterone A for ICT1 expression or 4-Hydroxytamoxifen for MYC expression. Panels A1-A6 shows cells in

the S-phase (red), Panels B1-B6 show counterstained DNA in the nucleus (blue), and Panels C1-6 show the merged images.

To examine if proliferation levels were increased and not just more cells found in the S-phase for longer duration, cell doubling times and growth rates were calculated for each condition of induced ICT1 and/or MYC overexpression (

Table 4). Doubling time, t_d was calculated as follows:

$$t_d = t \ln 2/\ln(X_e/X_b)$$

where t is the incubation time in hours. X_b is the cell number at the beginning of the incubation time. X_e is the cell number at the end of the incubation time. From the doubling time, the rate of growth was calculated as below:

$$k = \ln(2)/t_d$$

Table 4 Average doubling time, t_d, and rate of growth, *k*, when ICT1 and/or MYC is overexpressed in transfected PreB^{mycER} cells.

	Trial 1		**Trial 2**		**Trial 3**		**Average**		**Std Dev**	
Condition	**t_d**	***k***	**t_d**	***k***	**t_d**	***k***	**t_d**	***k***	**t_d**	***k***
Untransfected	11.2	0.0617	11.6	0.0599	11.6	0.0599	11.46	0.0605	0.199	1.06E-03
Transfection Control	12.0	0.0577	11.9	0.0583	11.5	0.0601	11.82	0.0586	0.250	1.25E-03
Not Induced	11.4	0.0607	11.7	0.0591	11.5	0.0605	11.53	0.0601	0.165	8.58E-04
c-MYC Induced	10.5	0.0661	10.1	0.0688	10.1	0.0688	10.21	0.0679	0.234	1.53E-03
Ict1 Induced	10.2	0.0679	10.7	0.0645	10.4	0.0668	10.44	0.0664	0.272	1.71E-03
Ict1+c-MYC Induced	9.67	0.0717	10.0	0.0690	9.95	0.0697	9.89	0.0701	0.193	1.38E-03

Fluorescent detection of EdU incorporation is a common approach to look at changes in DNA synthesis in populations of suspension cells (146). Increased levels of DNA synthesis, as measured in this way, show increased numbers of cells in the S-phase, and this is directly related to a change in the proportion of cells dividing actively (146). It could be argued that the cells are spending a longer time in the S-phase, but this would only be true if the doubling time increased, but instead the doubling time has decreased.

4.4 Apoptosis Levels During ICT1 and/or MYC Overexpression in PreB^{mycER} Cells

Apoptosis levels were measured for the same time-points as proliferation assays, by fluorescein incorporation into apoptotic nuclei. The levels of apoptosis for each condition showed no significant difference, all had an average of less than 10 % apoptotic cells (mean 7.43, $\sigma = 1.04$) (Figure 8).

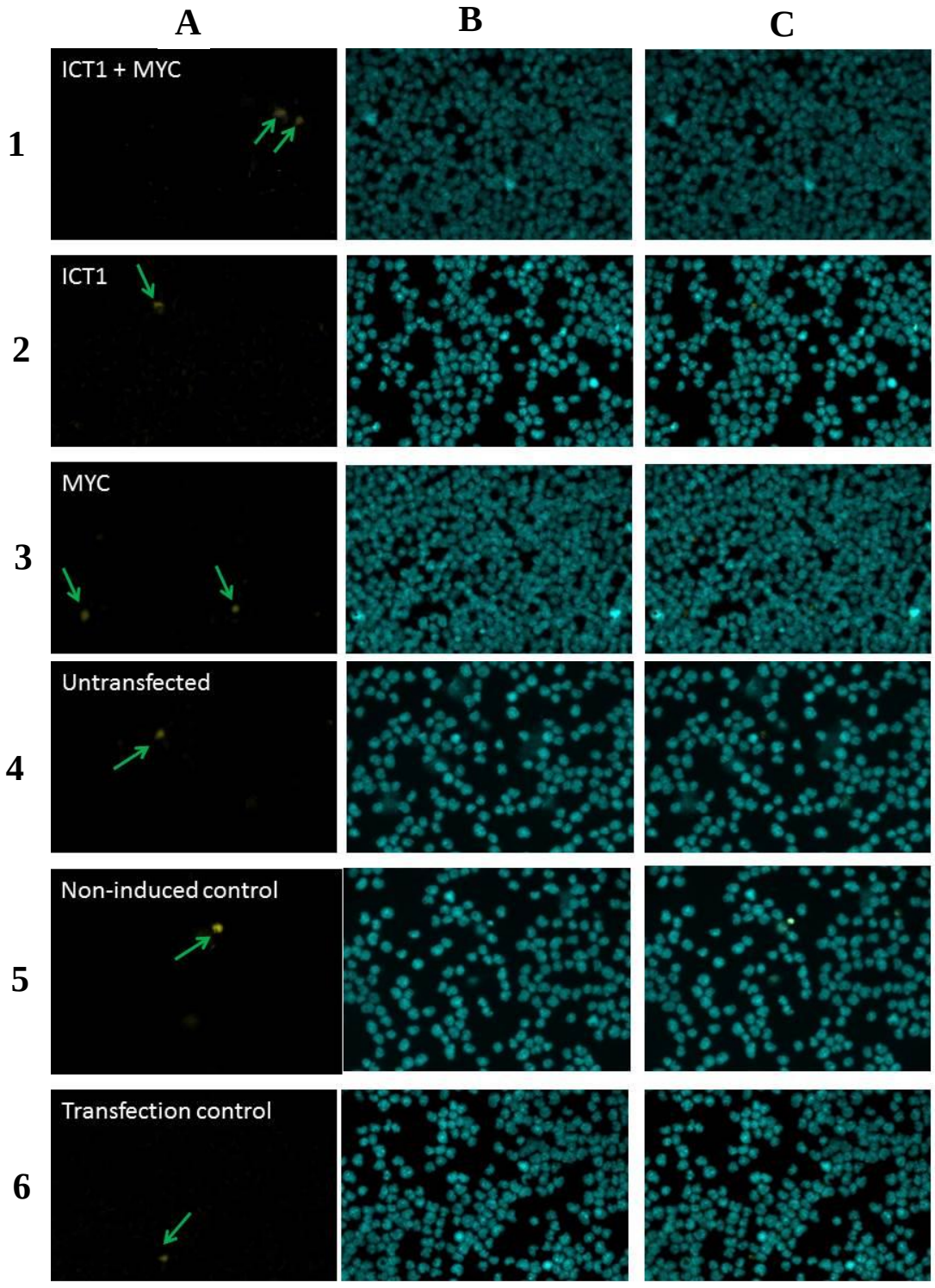

Figure 8 Representative images from fluorescent detection of apoptotic cells.

Apoptotic cells are shown in yellow Panel A1-6, with a green arrow to help point them out. Apoptosis levels were similar between all conditions (< 10 %) with no emerging trend. *Ict1*

and *c-MYC* induced (Panel 1A-C), *Ict1* induced (Panel 2A-C), *c-MYC* induced (Panel 3A-C), and untransfected cells (Panel 4A-C), non-induced control (Panel 5A-C), and the transfection control (Panel 6A-C). Panels A1-6 show FITC filtered images (shown in yellow for enhanced visualization), Panels B1-6 show DAPI filtered images of the DNA counterstained nucleus (shown in cyan for enhanced visualization), and Panels C1-6 show merged FITC and DAPI images.

4.5 SKY Analysis After ICT1 and/or MYC overexpression in PreB^{mycER} cells

To address the question of whether ICT1 overexpression contributes to genomic instability, SKY analysis was performed on metaphase spreads of cells for each condition collected at 48 hours post peak expression (Figure 9 - Figure 14). Conditional *c-MYC* deregulation demonstrated genomic instability in the form of various genetic alterations, including Robertsonian fusions, EEs, translocations, anaphase bridges, aneuploidy and potential gains and/or deletions (76). When *Ict1* was induced alone, no genomic alterations were observable by SKY analysis (Figure 9). When *Ict1* and *c-MYC* were induced, altered karyotypes were observed in the form of fusions, deletions, translocations, as well as broken and stretched out chromosomes (Figure 10). Again when *c-MYC* alone was induced, the same alterations to karyotypes were observed (Figure 11). No chromosomal alterations were observed with non-induced (Figure 12), untransfected cells (Figure 13), and transfection control cells (Figure 14), except for a few smaller EEs.

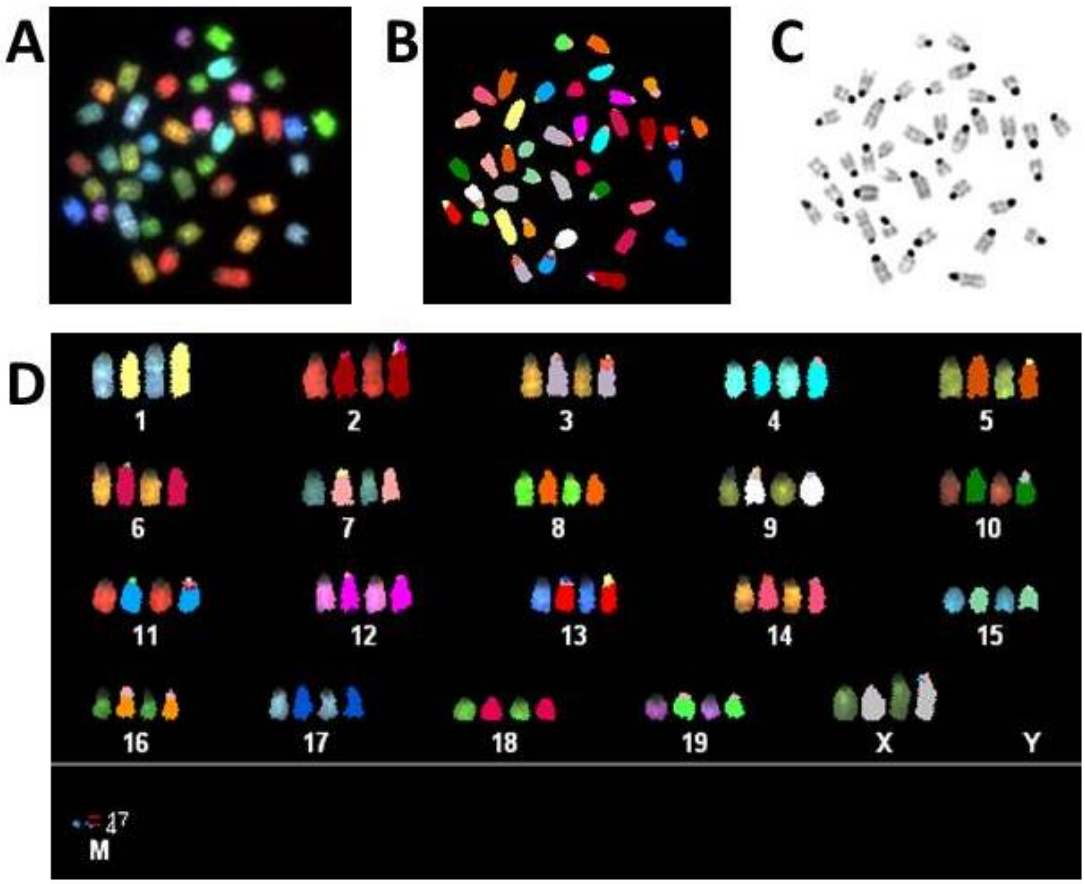

Figure 9 SKY of metaphase derived at 48 hours post-peak ICT1 overexpression.

Representative images from SKY analyses are shown: the raw image of a metaphase **A,** classified image **B**, inverted DAPI image **C**, and the spectral karyotype of the metaphase **D**.

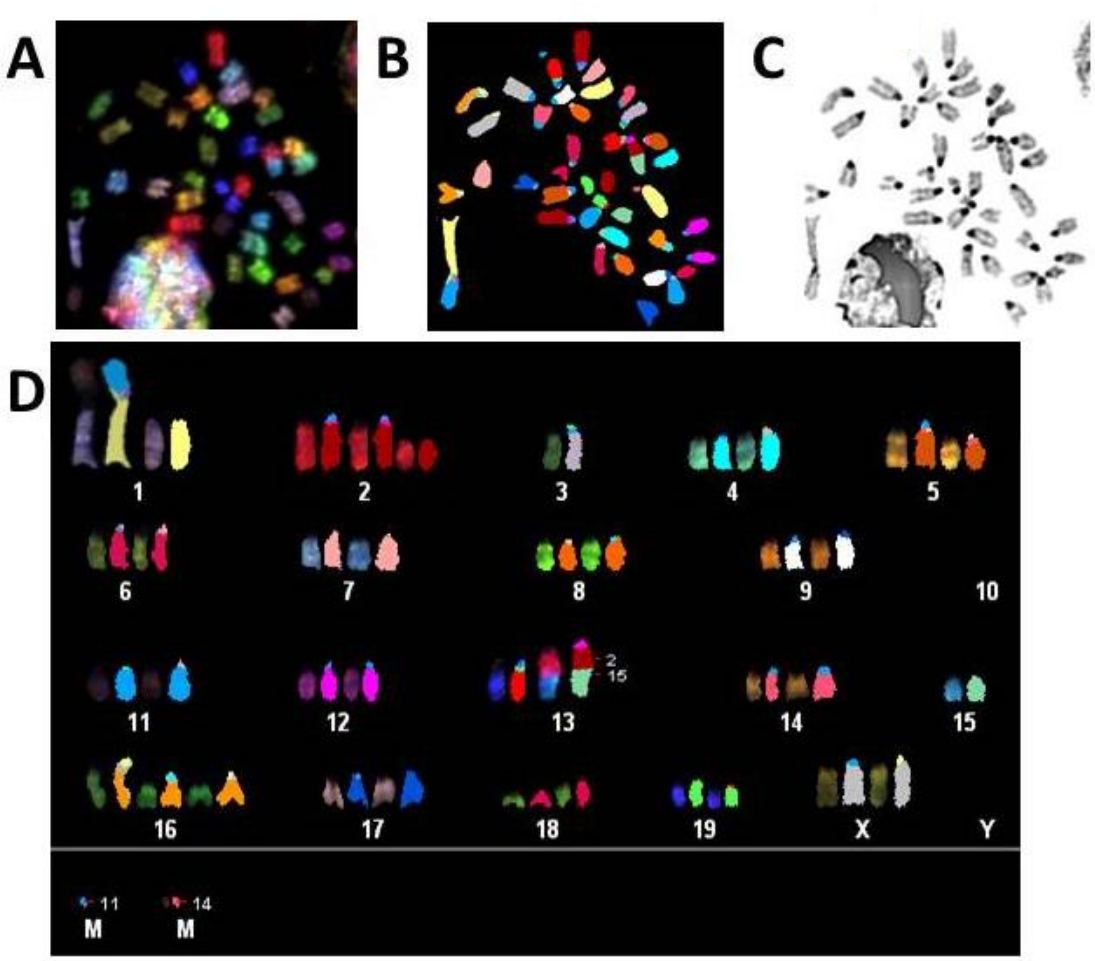

Figure 10 SKY of metaphase derived at 48 hours post-peak ICT1 + MYC overexpression.

Representative images from SKY analyses are shown: the raw image of a metaphase **A,** classified image **B**, inverted DAPI image **C**, and the spectral karyotype of the metaphase **D**.

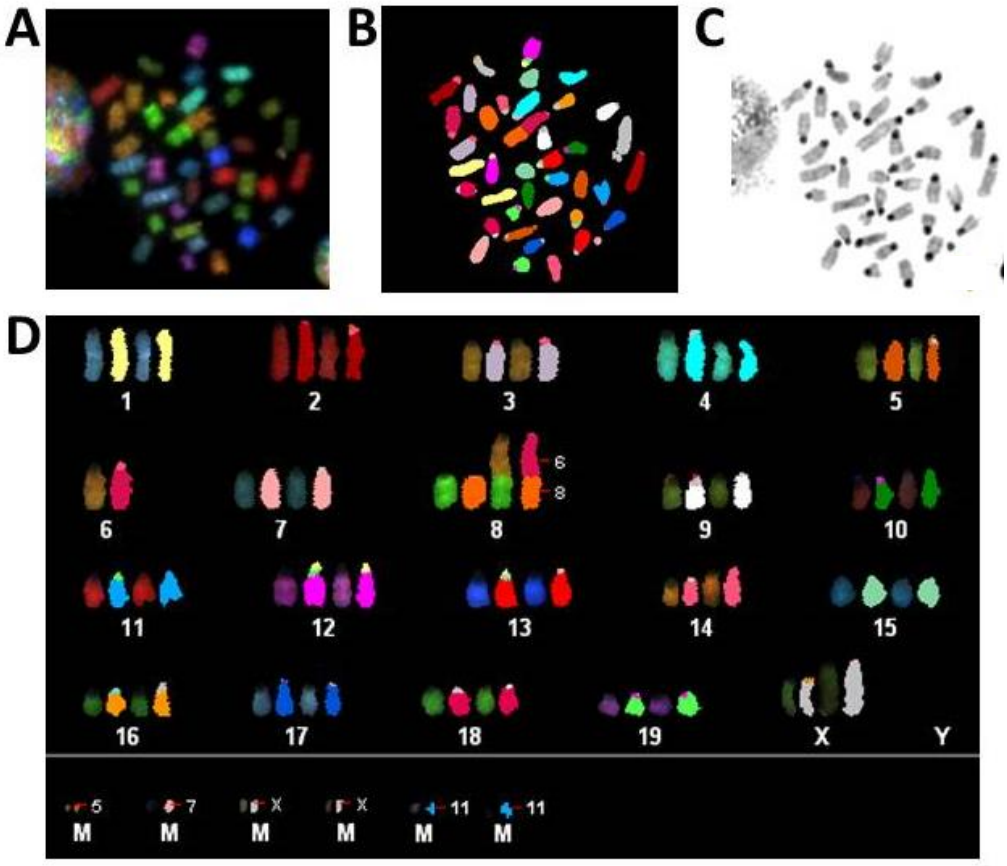

Figure 11 SKY of metaphase derived at 48 hours post-peak MYC overexpression.

Representative images from SKY analyses are shown: the raw image of a metaphase **A,** classified image **B**, inverted DAPI image **C**, and the spectral karyotype of the metaphase **D**.

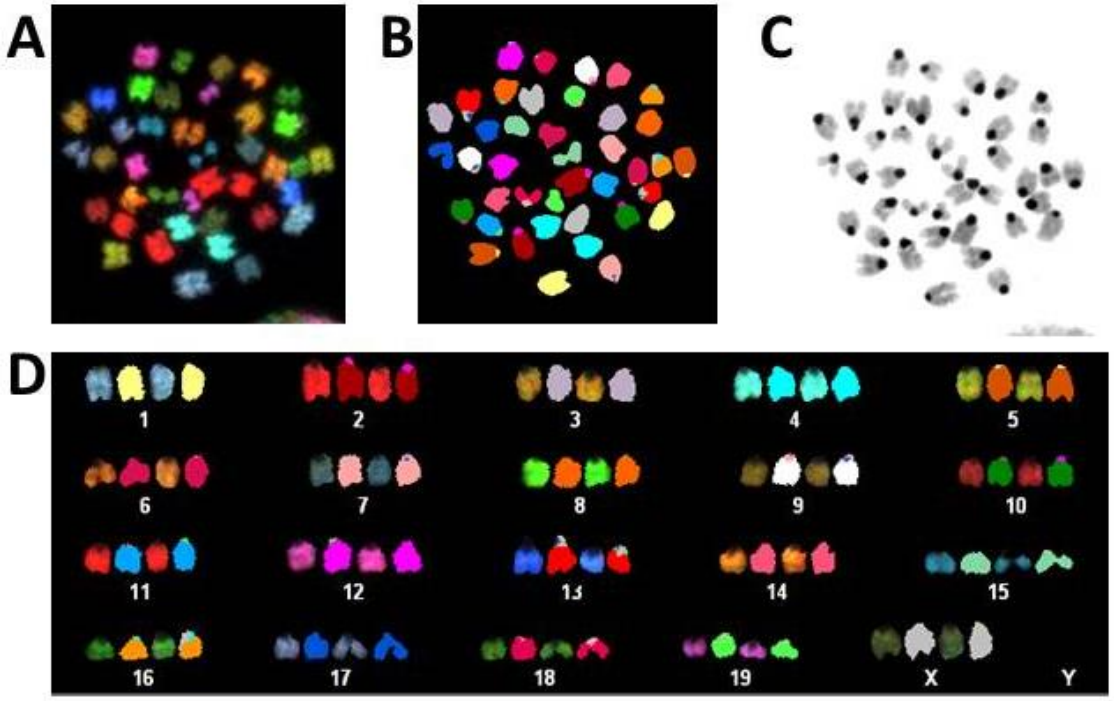

Figure 12 SKY of metaphase derived at 48 hours with no overexpression induced (Non Induced Control).

Representative images from SKY analyses are shown: the raw image of a metaphase **A,** classified image **B**, inverted DAPI image **C**, and the spectral karyotype of the metaphase **D**.

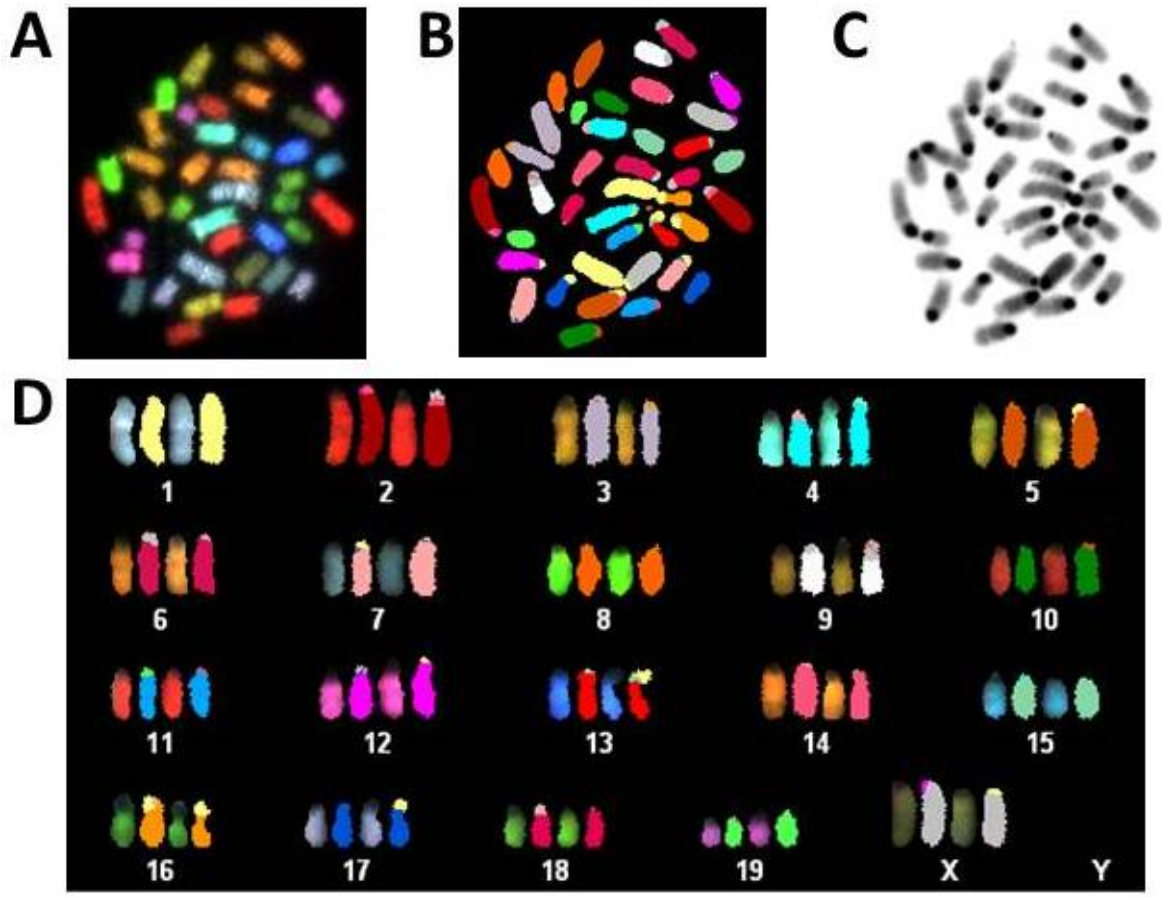

Figure 13 SKY of metaphase derived at 48 hours for untransfected PreB^{mycER} pVgRXR cells.

Representative images from SKY analyses are shown: the raw image of a metaphase **A,** classified image **B**, inverted DAPI image **C**, and the spectral karyotype of the metaphase **D**.

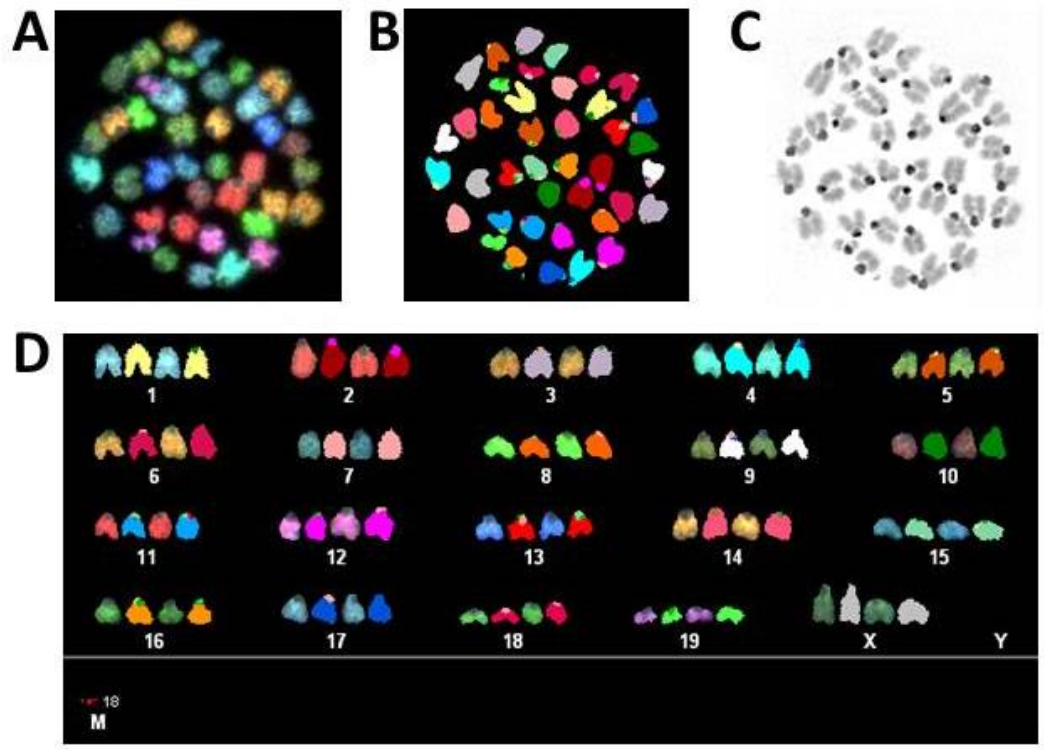

Figure 14 SKY of metaphase derived at 48 hours for PreB^{mycER} pVgRXR TC cells. Representative images from SKY analyses are shown: the raw image of a metaphase **A,** classified image **B**, inverted DAPI image **C**, and the spectral karyotype of the metaphase **D**.

Knowing that when *Ict1* and *c-MYC* were induced, altered karyotypes were observed in various forms, the spectral karyotype ploidy and aberrations were tabulated to see if any recurrent alterations were occurring. SKY abbreviation tables for all 3 experiments for *Ict1* and/or *c-MYC* induced conditions are shown in Table 5 - Table 10. Aneuploidy was found to be random when *c-MYC* was induced, with no recurrent aberration of statistical significance. The tables for control conditions are not shown, they had a normal diploid karyotype 2n = 20, with no large scale chromosomal abnormalities, or observable alterations other than the smaller EEs normally found in control cell lines (149).

Table 5 Experiment 1 SKY abbreviation table for *c-MYC* + *Ict1* induced PreB^{mycER} cells.

Green blocks represent chromosome gain (polysomy) and red blocks represent chromosome loss (monosomy and nullisomy). Notes describe characteristics of the chromosomes that were unusual, including obvious deletions, translocations and fusions.

Trial 1	1	2	3	4	5	6	7	8	9	10	11	12	13	14	15	16	17	18	19	X	Ch #	Notes
S01 1	2	2	2	2	1	2	2	1	2	1	2	2	2	2	1	2	0	2	2	2	34	Chr 14 unwound end
2	2	2	2	2	2	2	2	2	2	2	2	2	2	2	2	2	2	2	2	2	40	Both Chr 8 stretched
3	2	2	2	2	2	2	2	2	2	2	2	2	2	2	2	2	2	2	2	2	40	
4	2	2	2	2	2	2	2	2	2	2	2	2	2	2	2	2	2	2	2	2	40	Chr 8 stretched
5	2	2	2	2	2	2	2	2	2	2	2	2	2	2	2	2	2	2	2	2	40	Rb18;3
6	2	2	2	2	2	2	2	2	2	2	2	2	2	2	2	2	2	2	2	2	40	
7	2	2	2	2	2	2	2	2	2	2	2	2	2	2	2	2	2	2	2	2	40	Chr 9 centromere stretched
8	2	2	2	2	2	2	2	2	2	2	2	2	2	2	2	2	2	1	2	2	39	Chr 18 broken
S02 9	1	3	2	2	2	2	2	2	2	0	3	2	2	2	2	2	2	2	2	3	40	Chr 11 chromatid separation
10	2	2	2	2	2	2	2	2	2	2	2	2	2	2	2	2	2	2	2	2	40	
11	2	2	2	2	2	2	2	2	2	2	2	2	2	2	2	2	0	2	1	2	37	
12	2	2	2	2	2	2	2	2	2	2	2	2	3	2	2	2	2	2	2	2	41	
13	2	2	2	2	2	2	2	2	2	2	2	2	2	2	2	2	2	2	2	2	40	
14	1	2	2	2	2	2	2	2	2	2	2	2	2	2	2	2	2	2	2	2	40	
15	2	2	2	2	2	2	2	2	2	2	2	2	2	2	2	2	2	2	2	2	40	del2
16	2	2	2	2	2	2	2	2	2	2	2	2	2	2	2	2	2	2	2	2	40	
17	2	2	2	3	2	2	2	2	2	2	2	2	2	2	2	2	2	2	2	2	41	
18	2	2	2	2	2	2	2	2	2	2	2	2	2	2	2	2	2	2	2	2	40	
19	2	2	2	2	2	2	2	2	2	2	2	2	2	2	2	2	2	2	2	2	40	
20	2	2	2	2	2	2	2	2	2	2	2	2	2	2	2	2	2	2	2	2	40	del5, del16

Table 6 Experiment 2 SKY abbreviation table for c-*MYC* + *Ict1* induced PreB^{mycER} cells.

Green blocks represent chromosome gain (polysomy) and red blocks represent chromosome loss (monosomy and nullisomy). Notes describe characteristics of the chromosomes that were unusual, including obvious deletions, translocations and fusions.

Trial 2	1	2	3	4	5	6	7	8	9	10	11	12	13	14	15	16	17	18	19	X	#	Notes
S03 1	0	2	2	2	2	2	2	2	2	2	2	2	2	4	2	2	2	2	2	2	40	
2	2	2	2	2	2	2	2	2	2	2	2	2	2	2	2	2	2	2	2	2	40	
3	2	2	2	2	2	2	2	2	2	2	2	2	2	2	2	2	2	2	2	2	40	Chr 8 unwound
4	2	2	2	2	2	2	2	2	2	2	2	2	2	2	2	2	2	2	2	2	40	
5	2	2	2	2	2	2	2	2	2	2	2	2	2	2	2	2	2	2	2	2	40	F14;5
6	2	2	2	2	2	2	2	2	2	2	2	2	2	2	2	2	2	2	2	2	40	
7	2	2	2	2	2	2	2	2	2	2	2	2	2	2	2	2	2	2	2	2	40	
8	2	2	2	2	1	1	1	1	2	1	1	1	2	2	1	2	2	2	1	0	29	
9	2	4	2	2	2	2	2	2	2	0	2	2	2	2	2	2	2	2	2	2	40	T13;2
10	2	2	2	2	3	2	2	2	1	2	1	1	1	2	1	2	2	2	2	1	35	
11	2	2	2	2	2	2	2	2	2	2	2	2	2	2	2	2	2	2	2	2	40	
12	2	2	2	2	4	2	2	1	2	2	2	2	2	2	2	2	2	2	2	1	40	TX;4
13	2	2	2	2	2	2	2	2	2	2	2	2	2	2	2	2	2	2	2	2	40	delX
14	1	2	1	1	4	2	2	3	3	2	3	2	2	2	4	1	2	1	1	1	40	
15	2	2	2	2	2	2	2	2	2	2	2	2	2	2	2	2	2	2	2	2	40	
16	2	2	2	2	2	2	2	2	2	2	2	2	2	2	2	2	2	2	2	2	40	T12;2, del2, del7
17	2	2	2	2	2	2	2	2	2	2	2	3	3	2	2	2	2	2	1	2	41	
18	2	2	2	2	2	2	2	2	2	2	2	2	2	2	2	2	2	2	2	2	40	F8;5
19	2	2	2	1	2	2	1	2	1	2	2	2	2	2	1	2	2	1	2	2	35	T11;3
20	2	2	2	2	2	2	2	2	2	2	2	2	2	3	2	2	2	2	2	2	41	T10;14, F2;10

Table 7 Experiment 3 SKY abbreviation table for c-*MYC* + *Ict1* induced PreB^{mycER} cells.

Green blocks represent chromosome gain (polysomy) and red blocks represent chromosome loss (monosomy and nullisomy). Notes describe characteristics of the chromosomes that were unusual, including obvious deletions, translocations and fusions. This table includes the mean and standard deviations (St Dev) for each chromosome ploidy as well as overall chromosome number for all Experiments 1-3.

Trial 3	1	2	3	4	5	6	7	8	9	10	11	12	13	14	15	16	17	18	19	X	#	Notes
S04 1	2	3	2	2	2	2	2	2	2	1	2	2	2	2	1	2	2	2	2	2	49	F2;4
2	2	1	2	2	2	2	2	2	1	2	2	2	2	3	2	2	2	2	1	1	44	F14;X
3	2	2	3	2	2	2	1	2	2	2	2	1	2	2	1	2	2	1	2	2	44	
4	2	2	2	2	2	2	2	2	2	2	2	2	2	2	2	2	2	2	1	2	47	
5	2	2	2	2	2	2	2	2	2	2	2	2	2	2	2	2	2	2	2	2	46	Chr 14 unwound
6	2	2	2	2	3	2	2	2	2	2	2	2	2	2	2	2	2	2	2	1	44	
7	2	2	2	2	2	2	2	2	2	2	2	2	2	2	2	2	2	2	2	2	50	
8	2	2	2	2	2	2	2	2	2	2	2	2	2	2	2	2	2	2	2	2	36	
9	3	2	2	2	2	2	2	2	2	2	2	2	2	2	2	2	2	2	2	2	40	
10	2	2	2	2	2	2	2	2	2	2	2	2	2	2	2	2	2	2	2	2	42	F19;2, Chr 14 broken
11	2	2	2	2	2	2	2	2	2	2	1	2	2	2	2	2	2	2	2	2	45	
12	2	2	2	2	2	2	2	2	2	2	2	2	2	2	2	2	2	2	2	2	47	del19
13	2	4	1	2	2	2	2	2	2	0	3	2	2	2	1	3	2	2	2	2	40	Rb11;1, T15;2
14	2	2	2	2	2	2	2	2	2	2	2	2	2	2	2	2	1	2	2	2	41	
15	2	2	2	2	2	2	2	2	2	2	2	2	2	2	2	2	2	2	2	2	42	
16	2	2	2	2	2	2	2	2	2	2	2	2	2	2	2	2	2	2	2	2	47	
17	2	1	2	2	1	2	2	2	2	2	2	2	2	2	2	1	2	1	2	2	48	
18	2	1	1	2	2	2	2	2	2	2	2	2	2	1	2	2	1	2	2	1	47	del10
19	2	2	2	2	2	2	2	2	2	2	2	2	2	2	2	2	2	2	2	2	46	del2, del11, del12
20	2	2	2	1	2	2	2	1	2	2	2	2	2	2	2	2	2	2	2	1	47	F14;6
Mean	2	2	2	2	2	2	2	2	2	1.9	2	2	2	2	1.9	2	1.9	1.9	1.9	1.9	39.591	
St Dev	0.3	0.4	0.2	0.2	0.5	0.3	0.2	0.3	0.3	0.4	0.3	0.3	0.2	0.3	0.4	0.2	0.4	0.3	0.3	0.4	1.5011	
Mono	2	4	2	3	3	1	3	4	4	3	4	3	1	1	6	2	3	5	6	8		
Dip	58	55	59	59	54	60	59	57	57	57	56	58	60	58	55	60	57	57	56	52		
Trip	1	2	1	0	2	0	0	1	1	0	2	1	1	2	0	0	0	0	0	1		
Tet	0	1	0	0	2	1	0	0	0	0	0	0	0	1	1	0	0	0	0	0		

Table 8 Experiment 1 SKY abbreviation table for *c-MYC* induced PreB^{mycER} cells.

Green blocks represent chromosome gain (polysomy) and red blocks represent chromosome loss (monosomy and nullisomy). Notes describe characteristics of the chromosomes that were unusual, including obvious deletions, translocations and fusions.

Trial 1	1	2	3	4	5	6	7	8	9	10	11	12	13	14	15	16	17	18	19	X	Ch #	Notes
S01 1	2	2	2	2	2	2	2	2	2	2	0	2	2	4	2	2	2	2	2	2	40	
2	2	2	2	2	2	2	2	2	2	2	2	2	2	2	2	2	2	2	2	2	40	
3	2	2	2	2	1	2	2	3	2	2	2	2	2	2	2	2	2	2	2	2	40	Chr 9 stretched
4	1	2	2	2	2	2	2	2	2	2	2	2	2	3	2	2	1	2	2	2	38	R11;1
5	2	2	2	2	2	2	2	2	2	2	2	2	2	2	2	2	2	2	2	2	40	
6	2	1	2	2	3	1	2	2	2	3	2	2	2	1	2	2	2	3	2	2	38	Chr 12 stretched
7	2	2	2	2	2	2	2	2	2	3	2	2	2	2	2	2	2	2	2	2	41	T17;2
8	2	2	2	2	3	2	2	2	2	2	2	2	2	2	2	2	2	2	2	1	39	
9	2	3	2	2	2	2	2	1	2	2	2	2	2	2	2	2	2	2	2	2	40	Chr 2 stretched
10	2	2	2	2	2	2	2	2	2	2	2	2	2	2	2	2	2	2	2	2	40	
11	2	2	2	2	2	2	2	2	2	2	2	2	2	2	2	2	2	2	2	2	40	T18;3
12	2	2	1	2	2	2	2	2	2	2	2	2	2	2	2	3	2	2	2	0	40	
13	2	2	1	2	1	2	2	2	2	2	2	2	2	4	2	3	2	2	2	1	40	F9;10;2 traradial
14	2	2	2	2	2	2	2	2	2	2	1	2	2	3	2	2	2	2	2	0	38	
15	2	2	2	2	2	2	2	2	1	2	2	2	2	2	2	2	2	2	2	1	38	
16	2	2	2	2	2	2	2	2	2	2	2	2	2	2	2	2	2	2	2	2	40	
17	2	2	2	2	2	2	2	2	2	2	2	2	2	2	2	2	2	2	2	2	40	Chr 21 stretched
18	2	2	2	2	2	2	2	2	2	2	2	2	2	2	2	2	2	2	2	2	40	F5;1
19	2	2	2	2	2	2	2	2	2	2	2	2	2	2	2	2	2	2	2	2	40	
20	2	2	2	2	2	2	2	2	2	2	2	2	2	2	1	2	2	2	2	2	39	F7;11

Table 9 Experiment 2 SKY abbreviation table for *c-MYC* induced PreB^{mycER} cells.

Green blocks represent chromosome gain (polysomy) and red blocks represent chromosome loss (monosomy and nullisomy). Notes describe characteristics of the chromosomes that were unusual, including obvious deletions, translocations and fusions.

Trial 2	1	2	3	4	5	6	7	8	9	10	11	12	13	14	15	16	17	18	19	X	#	Notes
S02 1	2	2	2	2	2	2	2	2	2	2	2	2	2	2	2	2	2	2	2	2	40	
2	2	2	2	2	2	2	2	2	2	2	2	2	2	2	2	2	2	2	2	2	40	
3	2	2	2	2	2	3	2	2	2	2	2	2	2	2	2	2	2	2	2	2	41	F16;5
4	2	2	2	2	2	2	2	2	2	2	2	2	2	2	2	2	2	2	2	2	40	
5	2	2	2	2	2	2	2	2	2	2	2	2	2	2	2	2	2	2	2	1	39	TX;12
6	2	2	2	2	2	2	2	2	2	2	2	2	2	2	2	2	2	2	2	2	40	
7	2	2	2	2	2	2	2	2	2	2	2	2	2	2	1	2	2	2	2	2	39	Chr 5 stretched
8	1	2	2	2	2	1	2	2	2	2	1	2	2	2	2	2	1	2	2	2	36	F9;X, del4, chr 2 unwound
9	2	2	2	2	2	2	2	2	2	2	2	2	2	2	2	2	2	2	2	2	40	
10	2	2	2	2	2	2	2	2	2	2	2	2	2	2	2	2	2	2	2	2	40	
11	2	2	2	2	2	2	2	2	2	2	2	2	2	2	2	2	2	2	2	2	40	
12	2	2	2	2	2	2	2	2	2	2	2	2	2	2	2	2	2	2	2	2	40	
13	2	2	2	2	1	2	2	2	2	2	2	1	2	2	2	2	2	2	2	2	38	
14	2	2	2	2	2	2	2	2	2	2	2	2	2	2	2	2	2	2	2	2	40	
15	2	2	2	2	2	2	2	2	2	2	2	2	2	2	2	2	2	2	2	2	40	
16	2	2	2	2	2	2	2	2	2	2	2	2	2	2	2	2	2	2	2	2	40	Chr 1 stretched
17	2	2	2	2	4	2	2	2	2	2	2	2	2	2	2	2	2	2	2	1	41	T15;16, T15;16
18	2	2	2	2	2	2	2	2	2	2	2	2	2	2	2	2	2	2	2	2	40	
19	2	2	2	2	2	2	2	2	2	2	2	2	2	2	2	2	2	2	2	2	40	
20	2	2	2	2	2	2	2	2	2	2	2	2	2	2	2	2	2	2	2	2	40	

Table 10 Experiment 3 SKY abbreviation table for *c-MYC* induced PreB^{mycER} cells.

Green blocks represent chromosome gain (polysomy) and red blocks represent chromosome loss (monosomy and nullisomy). Notes describe characteristics of the chromosomes that were unusual, including obvious deletions, translocations and fusions. This table includes the mean and standard deviations (St Dev) for each chromosome ploidy as well as overall chromosome number for all experiments 1-3.

Trial 3	1	2	3	4	5	6	7	8	9	10	11	12	13	14	15	16	17	18	19	X	#	Notes
S03 1	2	2	2	2	2	2	2	2	2	2	2	2	2	2	2	2	2	2	2	2	40	
2	2	2	2	2	2	2	2	2	2	2	2	2	2	2	2	2	2	2	2	2	40	
3	2	2	2	2	2	1	2	2	2	2	2	2	2	2	2	2	2	2	2	2	40	T8;6
4	2	2	2	2	2	2	2	2	2	2	2	2	2	2	2	2	2	2	2	2	40	F13;6
5	2	2	2	2	1	2	2	2	2	2	2	2	2	2	2	2	2	3	2	2	39	
6	2	2	2	2	2	2	2	2	2	2	2	2	2	2	2	2	2	2	2	2	40	
7	2	2	1	2	2	2	2	2	2	2	2	2	2	2	2	3	2	2	2	2	40	Chr 11 centromere detached
8	2	2	2	2	2	2	2	2	2	2	1	2	2	2	2	2	2	2	2	2	35	
9	2	2	2	2	2	2	2	2	2	2	2	2	2	4	2	2	2	2	2	0	40	
10	2	2	1	2	2	2	3	2	2	2	2	2	1	2	2	2	2	2	2	2	40	
11	2	2	2	2	2	2	2	2	2	2	2	2	2	2	2	2	2	2	2	1	40	
12	2	2	2	2	2	2	2	1	2	2	2	2	2	2	2	2	1	2	2	2	40	F8;2
13	2	2	0	2	2	2	2	2	2	2	2	2	2	2	2	3	1	2	2	2	40	
14	2	2	2	2	2	2	2	2	2	2	2	2	2	2	2	2	1	2	2	2	40	Chr 8 stretched
15	2	2	2	2	2	2	2	1	2	2	2	2	1	2	2	2	2	2	2	2	40	
16	2	2	2	2	2	2	2	2	2	2	2	2	2	2	2	2	2	2	2	2	40	
17	2	2	2	2	2	2	2	2	2	2	2	2	2	2	2	2	2	2	2	2	41	
18	2	2	2	2	2	2	2	2	2	1	2	2	2	2	2	1	2	2	2	1	40	R16;15
19	2	2	2	2	2	2	2	2	2	2	2	2	2	2	2	2	2	2	2	2	40	R10;5
20	2	2	2	2	2	2	2	2	2	2	2	2	2	4	2	2	2	2	2	0	40	
Mean	1.9	2.4	1.9	2	1.9	1.9	2	2	2	2	1.6	2	2	2.3	2	2.1	1.9	2.1	2	1.7	**40.2**	
St Dev	0.2	0.9	0.3	0	0.5	0.2	0	0.3	0	0.3	0.7	0	0	0.7	0	0.3	0.2	0.2	0	0.7	**0.7**	
Mono	1	1	2	0	3	1	0	1	0	1	3	0	0	1	0	0	1	0	0	3		
Dip	18	14	17	19	14	18	19	17	19	17	14	19	19	14	19	17	18	18	19	14		
Trip	0	0	0	0	2	0	0	1	0	1	0	0	0	2	0	2	0	1	0	0		
Tetra	0	4	0	0	0	0	0	0	0	0	0	0	0	2	0	0	0	0	0	0		

It is noteworthy that MYC overexpressing conditions displayed a much greater number EE generation, and these EEs were larger in size compared to control conditions (Figure 15). Most of these EEs classified to Chr 11 of varying number, the highest being 14 EEs (mean = 4.25 per cell, $\sigma = 5.5$) (Figure 16). For conditions without *c-MYC* induction, Chr 11 EE occurrence was much less likely (mean 0.15 per cell, $\sigma = 0.96$). Although other conditions with no *c-MYC* induction showed EEs, they tended to be smaller, more difficult to classify and there was fewer of them (mean = 0.104 per cell, $\sigma = 0.11$).

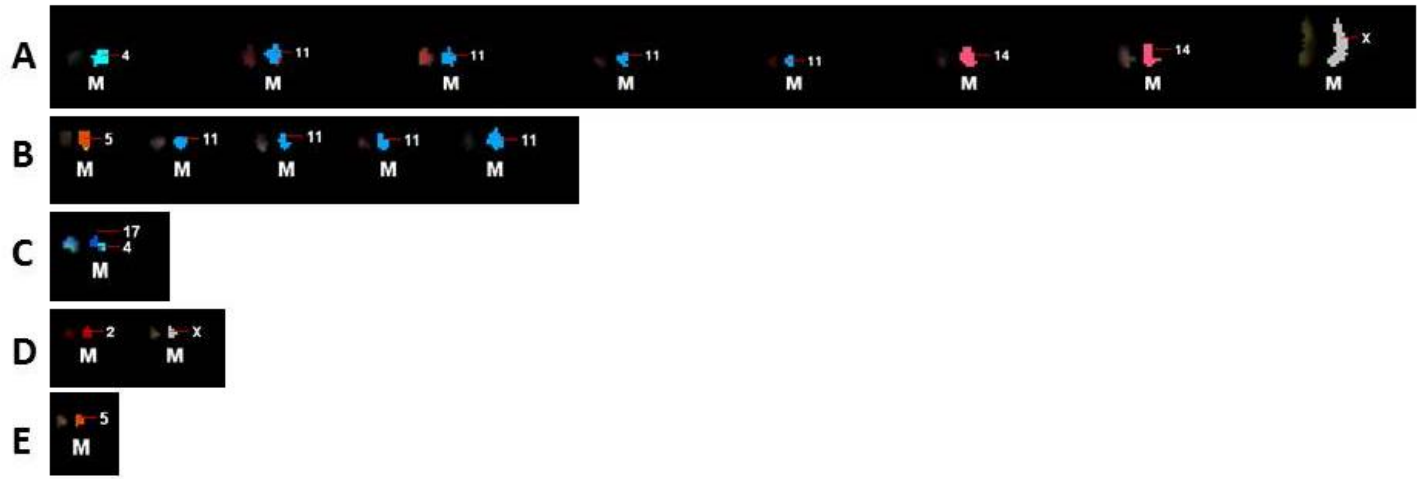

Figure 15 Comparison of EEs and number when MYC and/or ICT1 are overexpressed.

Many more EEs appear, especially for Chr 11 when *Myc* is induced **A**, or when *Myc* and *Ict1* are induced together **B**, but for not induced **C**, untransfected **D** and transfection control cells **E** less EEs are observed, and are smaller in size and harder to classify.

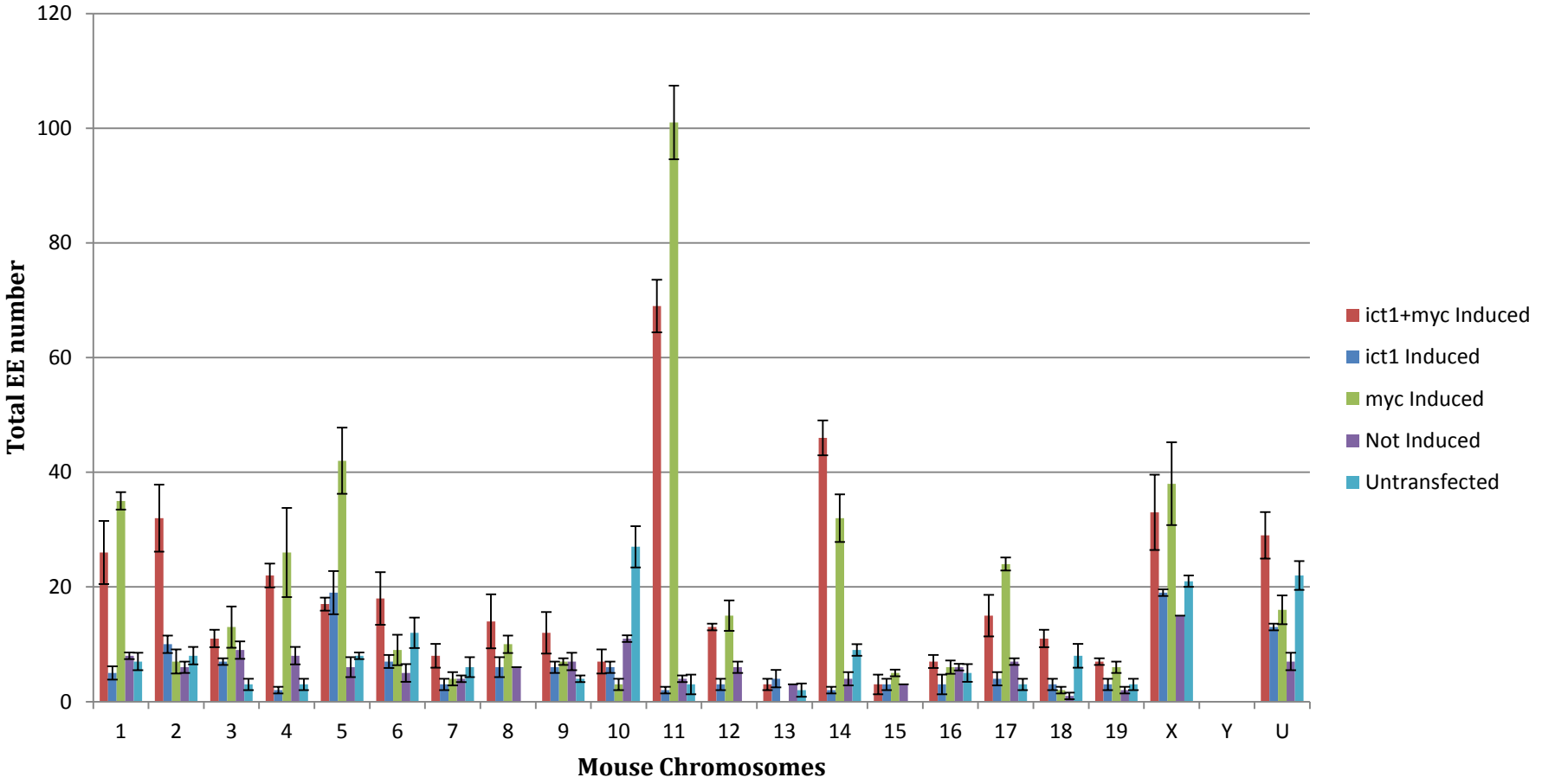

Figure 16 Occurrence of EEs for each mouse chromosome compared between experimental conditions.

Total number of EEs that classified to mouse chromosomes are displayed, including EEs that did not classify (U: Unclassified). Error bars show one standard deviation of uncertainty. 20 cells per condition were analyzed in three independent experiments.

5 DISCUSSION

These studies provide new insight into the role Ict1 may have during mPCT development. Increased ICT1 showed the potential to raise proliferation levels by increasing the number of cells in the S-phase. This impact was strengthened when both MYC and ICT1 were overexpressed in PreB^{mycER} cells. Consistent with previous literature, more EEs appeared when *c-Myc* was induced (168). Importantly, this study showed that a larger number of EEs mapped to Chr 11 than to any other chromosome.

In order to study ICT1 overexpression during MYC deregulation, a mouse cell line with conditional MYC deregulation was used. The Mai group generated the PreB^{mycER} cell line used in this study from of BALB/c bone marrow-derived diploid PreB lymphocytes (149). These cells were immortalized with the retroviral transforming oncogene *v-abl* and they remain stable with a diploid karyotype for over 70 passages (149). These cells were then transfected with the MycER^{TM} vector that encodes the MYC protein fused to the hormone binding domain of the mutated estrogen receptor responsive to activation not by estrogen, but 4HT (150). When these PreB^{mycER} cells had *c-Myc* induced, they became genomically unstable and able to form tumors with intraperitoneal injections into SCID mice (151, 152). This cell line models fast-onset mouse plasmactyoma mechanism. The Mai lab has successfully used the PreB^{mycER} cell line to study genomic instability events such as telomeric aggregate formation (9) that also occurs in fast-onset mouse plasmacytoma (76). The PreB^{mycER} cell line is ideal to study the effects of ICT1 overexpression alone, or paired with conditional *c-Myc* induction and acts as an *in vitro* model of fast-onset mPCT.

Initially, a non-random duplication of mouse Chr 11 was found in all cases of fast-onset mPCT (22). In order to narrow in on what region of Chr 11 was functionally important in mPCT disease progression, a mouse congenic strain was developed, T38HxBALB/c (23). These mice carry a reciprocal translocation between Chr 11 and X where the Chr X portion distal to band A moves onto the D band of Chr 11 (23). With *v-abl/c-MYC* induction, PCTs that developed acquired non-random duplication of Chr 11. Either the whole Chr 11 or T(X;11) duplication, or alternatively, an intrachromosomal duplication of the 11E2 band occurred in either 11E2 containing Chr, but never did the T(11;X) duplicate that does not harbor the 11E2 region. This highlighted the 11E2 region distal to cytoband D of Chr 11 as the region of interest involved in a non-random duplication, and was a candidate for further investigation in fast-onset mPCT.

To examine which 11E2 genes are consistently duplicated and overexpressed, array comparative genomic hybridization and expression analysis in *v-abl/c-Myc* induced primary PCT tumors were performed. Six candidate genes were identified as consistently amplified with 9 to 11-fold of higher mRNA levels, *Aspscr1, Foxk2, Ict1, Kcnj2, Sec14l1* and *Tbcd* (S. Mai, University of Manitoba, Winnipeg; unpublished results). The investigation of this thesis focused on *Ict1*, as the *Ict1* containing vectors were prepared and validated by sequencing analysis by the Mai group. The results of these studies do not consider Ict1 overexpression in the context of 11E2 duplication, with contributions from the remaining 5 genes found overexpressed in fast-onset mPCT. Further studies, using the experimental design described in this thesis could uncover increased ICT1 contribution to the aggressiveness of the disease.

Ict1 was named during its discovery in differentiation of colon carcinoma cells as *immature colon carcinoma transcript 1* (141). It is also named 39S mitoribosomal protein L58 (MRP-L58), and digestion substraction-1 (DS-1). Richter *et al.* (2010) demonstrated that the *Ict1* protein product, ICT1, is associated with the mitochondrial ribosome, where immunoprecipitation showed ICT1 to co-sediment with both the 39S and 55S subunits (153). They further showed ICT1 to be an essential mitoribosomal protein when knockdown of *Ict1* inhibited ribosome assembly, and altered mitochondrially encoded protein synthesis, specifically protein steady state levels for Complex I (COX2) and IV (NDUFB8) were reduced. The effect of ICT1 depletion in fibroblasts also caused a substantial decrease in oxidative phosphorylation complexes (154). Sequence alignment analysis suggested the ICT1 protein belongs to the release factor family (155). It has peptidyl-transfer RNA hydrolysis activity via a conserved GGQ motif, but has lost codon specificity (152). It is proposed that ICT1 functions to hydrolyze peptidyl-transfer RNAs that have been prematurely terminated in order to rescue stalled ribosomes like its bacterial homolog YaeJ (156). There are two transcript variants of *Ict1* that encode three different isoforms.

There is emerging research that supports a role for *Ict1* in tumorigenesis. There has been increasing evidence for participation of translation release factors in cancer development, especially ones that have lost codon specificity, such as ICT1 (143). These general translation release factors can rescue stalled ribosomes and allow release of truncated proteins in a case where mutations have propagated into the mRNA sequence (143). Mitoribosomal protein recruitment in tumor progression would provide an advantage when the altered cellular metabolism cancer hallmark is considered. The increased energy demand

of the developing cancer cell would require recruitment of machinery, specifically mitochondria, to support the increased metabolism (6, 7). Also, the role *c-MYC* plays in cellular processes that would require recruitment of mitoribosomal proteins, such as translation (48), and ribosome biogenesis (51). It is well established that *c-MYC* deregulation is involved in early initiating events, but that additional genomic alterations are necessary for the full progression of fast-onset mPCT (23). These events would likely include recruitment of a partner able to help with increased metabolic demand such as *Ict1*. In addition, recent studies have found connections between increased *Ict1* in human cancers, such as lung (24), glioblastoma (25), and prostate cancer (26), where *c-MYC* also is involved in the mechanism of tumorigenesis (27-29).

ICT1 Protein Levels Matched Levels Expressed in the Plasmacytoma Cell Line MOPC 460D

The level of ICT1 expression that peaked at 24 hours was comparable to ICT1 expression levels in MOPC 460D positive control cells. This is consistent with ICT1 expression at physiologically relevant levels in the disease under investigation, mPCT. The Ecdysone-Inducible Mammalian Expression Vector system uses promoters that allow for expression at physiologically relevant levels (157). The amount of Ponasterone A to induce the $PreB^{mycER}$ cells was titrated previously in the Mai group to determine the final Ponasterone A concentration of 10 μM. The hybrid receptor utilized by the Ecdysone inducible mammalian expression system, reduces any potential endogenous effects that could activate gene expression. This is also confirmed by the immunofluorescent experiments that did not show increased ICT1 levels in the absence of Ponasterone A induction.

Transfection Efficiency in PreB^{mycER} Cells

Transfection efficiency was first measured with green fluorescent protein (GFP), and found to be 98 % efficient at 48 hours when GFP expression peaks. During determination of peak ICT1 expression levels, transfection efficiency was 96 % at 24 hours. Electroporation is an invasive method for transfection, acting by electroporation where the cells may not efficiently recover. However, electroporation was determined to be the most efficient way to transfect the PreB cells, and confirmed in a set of preliminary experiments that looked at alternative methods for transfection. Although the cells remained alive and healthy with lipid-mediated, and cationic polymer-mediated transfection, compared to electroporation, transfection efficiency was very low, and hardly detectable in some cases.

Proliferation Increases with Ict1 and/or c-MYC Overexpression in PreB^{mycER} Cells

The ability to sustain unlimited proliferation is a fundamental trait of cancer cells (6, 7). Homeostasis of cell number is normally controlled by mitogenic signals that instruct entry and exit within the cell cycle, and these mitogenic signaling pathways are deregulated in cancer cells. Compared to controls, ICT1 overexpressing cell conditions had increased proliferation levels. When performing cell counts and experiments, cells that were not induced for *Ict1* and/or *c-MYC* had low cell counts during harvesting of cells, which indicated that proliferation levels may be higher in *c-MYC* and/or *Ict1* induced conditions. Here, replication levels were measured by looking at EdU incorporation into newly synthesized DNA. When both *Ict1* and *c-MYC* were induced proliferation levels increased by 15-20 % relative to controls (Figure 6). Considering EdU incorporation tells how many cells

are in the S-phase, and they just may be spending more time in S-phase, cell counts were re-examined from each experiment. The quantification of doubling time and rate of growth were used to confirm the difference between proliferation levels (Table 4). Doubling time shortened to 10.21 from the calculated negative control average of 11.6 hours when *Ict1* was induced, and was reduced even more to 9.67 hours when paired with *c-MYC* induction. When considering the function of ICT1, overexpression may lead to increase in the translation efficiency of specific oncogenic transcripts.

MYC regulates a large number of genes, and affects multiple cellular processes. The metabolic demand increases when quiescent cells enter into S-phase, which would increase reactive oxygen species (ROS) that either act as mediators of proliferative signals, or at high enough levels would create an oxidative burden (158). Interestingly, the Evan group found that Rat-1 fibroblasts with constitutive MYC expression show increased apoptosis levels under apoptotic-inducing conditions such as serum starvation (159). This was further demonstrated in subsequent studies by Vafa *et al.* who found that conditional deregulation of MYC increases levels of apoptosis in serum-deprived human fibroblasts, and the same fate was true for serum-deprived mouse ProB cells (150, 158). Increased MYC levels lead to the unregulated expression of many genes, some of which may support proliferation and cell growth, and others that may enable the cell to evade apoptosis.

Apoptotic Levels Unchanged During Ict1 and/or c-MYC Overexpression in PreB^{mycER} Cells

Another key hallmark for cancer cells is when they gain the ability to bypass apoptosis, an organized program for cell death when accumulated damage is deemed irrecoverable (6, 7). During apoptosis, DNA fragmentation occurs by the activity of cellular endonucleases. Detection of endonucleolysis specific to apoptosis is achieved with the TUNEL assay. Here, the nicked DNA free 3'OH terminus is modified to incorporate fluorescein labeled nucleotide polymers catalyzed by Terminal deoxynuclotidyl transferase (160). Typically, deregulated MYC is paired with anti-apoptotic partner alterations in cancer so that both cell growth and survival advantages are obtained (44). Genomic destabilization normally activates apoptotic mechanisms, and in order for the cell to survive, the apoptotic pathway needs to be altered to allow anygenomic alterations that increase tumorigenic potential to be carried to daughter cells. The MYC oncoprotein activities naturally target the cell to activate control apoptotic pathways. In order to overcome the apoptotic driving effects of MYC, overexpression of BCL2 or loss of p53 tumor suppressor often occurs along with *Myc* amplifications (44). Even in mice that are not susceptible to mPCT development, p53 deficient mice (161)

The potential for ICT1 to have an anti-apoptotic role was explored with the TUNEL assay. Apoptosis levels appeared unchanged, but perhaps with only transient overexpression apoptotic or related pathways were not affected under these conditions. Fluorescein incorporation into the nucleus detects DNA fragmentation characteristic of late stage apoptosis, and recent studies have detected an increase in late stage apoptosis as a result of ICT1 knockdown (25, 26). Knockdown of ICT1 in DU145 prostate cells resulted in a

significant level of proteolytic cleavage of poly(ADP-ribose) polymerase (PARP), which indicates a pro-apoptotic role for ICT1 knockdown, but not necessarily an anti-apoptotic role for ICT1 normal levels. These results match the previous findings of ICT1 knockdown in HeLa cells where increased levels of apoptosis were reported (143).

Another way to explore altered apoptotic potential would have been to examine the effects of apoptotic-inducing conditions on ICT1 and/or MYC overexpressing PreB^{mycER} cells, such as serum starvation, or apoptotic inducing drugs like staurosporine. The apoptosis-inducing drug staurosporine works through both caspase-dependent and caspase-independent mechanisms. It is important to consider both methods of apoptosis induction because ICT1 knockdown has been shown to affect PARP levels, and PARP can induce apoptosis on its own, in a caspase-independent mechanism (162). The design of these experiments had cells harvested for both proliferation and apoptosis assays from the same pool. The goal during this experiment was to see if any changes to normal apoptosis levels occurred as a result of ICT1 overexpression, and no changes were perceived under the conditions explored with either ICT1 and/or MYC overexpressed.

Genomic Instability Occurs When c-MYC is Induced in PreB^{mycER} Cells

It has been shown in mouse PreB cells that MYC deregulation causes the formation of Robertsonian fusion chromosomes (82). Conditional expression of MYC remodeled centromere positions in interphase nuclei and resulted in telomeric fusions at the telocentric mouse chromosome ends. These Robsertsonian fusions occurred in 33 % of metaphases (6 out of 20) within 30 hours. I wanted to look at the effect of *Ict1* on genomic instability while

MYC was dysregulated. Although it seemed unlikely for increased ICT1 protein levels to play a role in genomic instability, perhaps a change in *c-MYC*-induced genomic instability was possible.

c-MYC Induced Conditions had Increased Chromosome 11 EEs

When *c-MYC* was induced, an increase in the number and size of EEs occurred, specifically, an increase in EEs that classified as belonging to Chr 11. EEs could be further analyzed with mBAND experiments to show if those from Chr 11 contain the 11E2 fragment (152). Although an increased source for *Ict1* was provided, *c-MYC* induction demonstrates that MYC interacts with Chr 11 preferentially, and that *c-MYC* deregulation precedes the11E2 duplication event. For full tumorigenic potential to be achieved, *c-MYC* recruits the other 11E2 genes in order for development of tumorigenic potential. Billings *et al.* (2010) identified patterns of recombination on mouse Chr 11 with high resolution genetic mapping (163). They found elevated recombination rates in the proximal end of the chromosome that contains the 11E2 region. This suggests hot spot sites for topoisomerase generation of double-strand breaks that could lead to chromosomal aberrations.

Generation of extrachromosomal DNA was observed in a variety of tumor types as a common product of DNA amplification (15). Specifically, generation of EEs has been associated with disease progression in hematological cancers such as acute myelogenous leukemia, myelodysplastic syndrome, and acute lymphoblastic leukemia (164, 165). Studies have shown these EEs to carry oncogenes and able to contribute to cellular transformation (144, 167). Mouse PreB^{mycER} lymphocytes with induced *c-MYC* have shown generation of a

new class of EEs that are larger in structure compared to control EEs (168). These *c-MYC* induced EEs were shown to carry competent chromatin able to propagate into daughter cells by self-replication. In plasmacytomas that do not carry the hallmark *c-MYC* translocation, the *IgH* and *c-MYC* genes were found on EEs (22).

The observation from SKY analysis in this study was that during *c-MYC* deregulation in PreB^{mycER} cells generated a significant number of EEs that classified with Chr 11 more so than with any other chromosome. This provides a strong association that MYC may interact in some way with Chr 11 to induce gene amplification events. With transient *c-MYC* induction, and no subsequent G-banding or cytogenetic analysis performed, it is hard to tell if 11E2 duplication also occurred intra-chromosomally. Multi-coloured banding could have shown larger 11E2 bands within the intact Chr 11 and also, if the Chr 11 EEs were also from the 11E2 region. However, if it were shown that the Chr 11 EEs generated contain specifically the subcytoband 11E2, it would argue strongly for direct or indirect interaction of MYC with this region. This would be in agreement with the proposed model for acceleration of mPCT (23). This may be directly by repositioning Chr 11 (103), or indirectly increasing cellular metabolism which would increase the risk of reactive oxygen species damage to the DNA and induce DNA repair that could lead to the 11E2 duplication or EE generation. The Chr 11 EEs generated suggest that this model of transient *c-MYC* deregulation may be sufficient to foster an environment to selectively access 11E2 genes required for progression to mPCT.

The larger size of the *c-MYC* generated EEs were qualitative observations during SKY analysis. The SKY experimental set up did not allow quantitative measurements as was done previously (156). Although the different experimental slides were treated with pepsin

for the same amount of time, there is no guarantee the chromosomes were condensed or unwound to the same extent to allow quantitative measurements.

MYC Interaction with Chr 11

The positioning of genes in nuclear space has been functionally linked to gene activation (169). The nuclear periphery has been shown to contain genes that are transcriptionally repressed, and genes on chromosomes in the central nuclear space are transcriptionally active (99, 100). MYC is a known driver of genomic instability, with the ability to remodel nuclear organization of the interphase nucleus (74, 75). A single MYC conditional deregulation event can lead to multiple changes to 3 dimensional (3D) nuclear space, with altered positions of telomeres and chromosomes (9, 76). Chr 11 was shown to occupy non-random orientation patterns in the nuclear space in control PreB cells (103). When plasmacytoma cells were studied, the tumorigenic cells showed changes in nuclear positioning of Chr 11 compared to non-neoplastic PreB cells (103). MYC deregulation has been shown to initiate telomeric aggregate formation, and chromosomal fusions that initiate ongoing breakage-fusion bridge cycles as early as 12 hours post-*c-MYC* induction (73, 76). It is well established that nuclear organization of chromosomes is non-random, and that chromosomes occupy distinct territories within the 3D nuclear space (170), and the changes to these chromosome positions must have some functional consequence. If *c-MYC* deregulation in PreB cells results in altered Chr 11 position within the 3D nuclear space, this may position Chr 11, specifically 11E2 genes next to transcriptional machinery which could increase the chance of amplification of 11E2 genes. Alternatively, MYC may activate transcription of the genes within 11E2, and instead the altered transcriptional activity may change Chr 11 position within the nucleus (104).

Investigating the Chromosome 11 Extrachromosomal Elements

In an effort to understand what region of Chr 11 the EEs mapped to, preliminary multi-colour banding (mBAND) experiments were performed. Multi-colour banding provides an opportunity to characterize intra-chromosomal regions, and so if applied to EEs, you can tell what region of the chromosome the EE belongs to. I attempted to mBAND untransfected control slides that were already used in SKY experiments that contained the smaller EEs. Although I had a good hybridisation, in order to complete analysis, the software required strong DAPI stain, which my re-hybridized slides lacked. SKY analysis does not solely depend on DAPI intensity, and so the low DAPI signal did not affect SKY data. It would have been of great value to examine if the EEs generated were in fact belonging to 11E2. This would help to demonstrate that deregulated MYC protein recruits 11E2 genes in this *in vitro* model consistent with previous studies that never looked to map EEs that were generated (23). However, these experiments did show a substantial number of EEs when MYC levels were increased, and many of them (25 %, $p < 0.05$) mapped to Chr 11 during SKY analysis (Figure 16). When increased MYC levels were paired with ICT1 overexpression, a substantial amount of EEs still mapped to Chr 11 (17 %, $p < 0.05$), which is reduced from when MYC alone was induced. If the EEs generated do in fact contain 11E2 genes, perhaps the need to generate as many EEs were negated with this experimental model that provided the increased ICT1 by introduction of the pIND/Hygro vector. This requires further investigation, looking at mBANDing experiments to see if the EEs do in fact map to 11E2, and if the other 11E2 candidate genes when transfected show similar results.

Mouse Plasmacytoma Models B Cell Malignancies

The canonical *c-MYC*/*Ig* translocation is the primary event in BL and mPCT development. However, this translocation also occurs in subsets of other B cell malignancies that include diffuse large B-cell lymphoma, high-grade unclassifiable lymphomas, double-hit lymphomas, TDT-positive blastic tumors, plasmablastic lymphomas, and rare cyclin D1-positive lymphomas (31). For these additional lymphomas, the *c-MYC* translocating event occurs mostly as a secondary event. MM shares tumor biology and phenotype characteristics with mPCT also (112). Although MM does not carry the *c-MYC* translocation regularly (<5 %), there is evidence for overexpression of *c-MYC* in MM (171).

11E2 Human Synteny Region is 17q25 Also Implicated in Cancer

The focus on mouse 11E2 cytoband is relevant for the respective synteny regions in human (17q25) and rat (10q32) (33, 34). The 11E2, 17q25, and 10q32 regions are evolutionarily conserved and found rearranged in tumors of lymphoid and non-lymphoid origin which supports a role these regions may play in tumorigenesis (35-40, 172). A gain in Chromosome 17 at the 17q region was discovered in early studies (173-175). Recently, a frequent gain of 17q25 was identified in neuroblastoma cell lines, and a strong correlation between 17q25 gain and MYCN protein levels in neuroblastoma tissue which suggests that the 17q25 gain and MYCN levels are strong correlative biomarkers. Park *et al.* describe a role isochromosome 17q plays in myelodysplastic syndrome-leukemic transformation (176). A frequent gain in 17q25 is common in prostate and breast cancer (172, 177). Bermudo *et al.* (2010) showed with FISH experiments the presence of a copy number gain in 17q25.3 in pre-neoplastic lesions, primary tumors and metastatic samples which suggests involvement of

this gain in prostate cancer onset and progression. A gain in this region was also recurrent in breast cancer (177). Differentiating driver from bystander genomic events remains a challenge. The growing evidence of cross-species tumor associated copy number alteration synteny is promising, and shows promise for mouse models to bridge knowledge gaps for complex human oncogenomes (144). Therefore, information gained for the role 11E2 genes, such as *Ict1*, play in tumorigenesis in mouse models has a strong potential to translate into identification of putative driver genes for human cancers that involve gains in 17q25.

6 CONCLUSIONS

Gene amplification events are common genetic alterations in tumorigenesis, and here 11E2 duplication that included *Ict1* amplification and overexpression was explored. Deregulation of *c-MYC* is necessary for development of mouse plasmacytoma, however, *c-MYC* deregulation alone is insufficient for accelerated development of the disease. Infection with the retroviral vector *v-abl*/*c-MYC* induces plasmacytomagenesis in 100 % of plasmacytomas isolated from mice that were examined along with trisomy of 11E2. The genes that are overexpressed as a result of 11E2 duplication along with *Ict1* are likely drivers for accelerated plasmacytomagenesis, and contribute to a more aggressive mechanism for mPCT development. Altered MYC regulation recruits cellular capabilities that favour the development of mouse plasmacytoma. When 11E2 is duplicated, those capabilities seem to be accelerated, as the latency period decreases. We expected *Ict1*, an 11E2 gene, to enable hallmark cancer capability to help explain the aggressive onset for accelerated mPCT. *Ict1* overexpression was found to increase proliferation by 15-20 %, with decreased doubling time

by 2 hours. Apoptosis levels remained uniform whether *Ict1* and/or *c-MYC* was overexpressed when late stage apoptosis levels were measured. However, only natural levels of apoptosis were explored, and not how the cells behaved under apoptotic inducing conditions. Increased genomic instability occurred as a result of *c-MYC* deregulation, which was expected. MYC induction resulted in the formation of more and larger EEs. It was exciting to see such a strong association of MYC deregulation with generation of Chr 11 EEs, where 20 % of MYC induced EEs and 17 % of MYC and ICT1 induced EEs mapped to Chr 11. These EEs were larger in size, and reminiscent of functional self-replicating EEs, which warrants a future independent study. These results help to demonstrate that the cell model we have used to uncover the role of *Ict1*in mPCT development, is physiologically relevant and the experimental design will help to look at the other 11E2 genes.

7 FUTURE OUTLOOK

The cytoband 11E2 human synteny region is on Chr 17q25 commonly involved in human chromosome aberrations found within tumors. These 17q25 aberrations are common and associated with poor prognosis in human cancers such as acute myeloid leukemia, breast, ovarian and thyroid cancers (18, 20, 34, 41, 42). The characterization of gene(s) within the chromosome 11E2 region will provide new mechanistic insights into many tumor types and may lead to the development of new therapeutic targets and concepts that can be applied to human cancers. Once the mechanisms of accelerated versus slow onset mPCTs have been elucidated, a more accurate determination of tumor progression will become possible, improving therapeutic approaches. Understanding the mechanism of disease progression that results from *c-MYC* deregulation may uncover insights into human cancers that harbor aberrant *c-MYC* activity.

8 LITERATURE CITED

1. Fest T, Guffei A, Williams G, Silva S, Mai S. Uncoupling of genomic instability and tumorigenesis in a mouse model of Burkitt's lymphoma expressing a conditional box II-deleted Myc protein. Oncogene. 2005;24:2944-53.
2. Holland AJ, Cleveland DW. Boveri revisited: chromosomal instability, aneuploidy and tumorigenesis. Nature Reviews Molecular Cell Biology. 2009;10:478–87.
3. Weaver BA, Cleveland DW. The role of aneuploidy in promoting and suppressing tumors. The Journal of Cell Biology. 2009;185,:935–7.
4. Vogelstein B, Kinzler KW. Cancer genes and the pathways they control. Nature Medicine. 2004;10:789-99.
5. Stratton MR, Camplbell PJ, Futreal PA. The cancer genome. Nature. 2009;458:719-24
6. Hanahan D, Weinberg RA. Hallmarks of Cancer. Cell 2001;100:57-70.
7. Hanahan, D, Weinberg RA. Hallmarks of Cancer: The Next Generation. Cell. 2011;144:646-71.
8. Jones PA, Liang G. Rethinking how DNA methylation patterns are maintained. Nature Reviews Genetics. 2009;10 805-11.
9. Louis SF, Vermolen BJ, Garini Y, Young IT, Guffei A, Lichtenstejn Z, Kuttler F, Chuang TC, Moshir S, Mougey V, Chuang AY, Kerr PD, Fest T, Boukamp P, Mai S. c-Myc induces chromosomal rearrangements through remodeling in the interphase nucleus.

Proceedings of the National Academy of Sciences of the United States of America. 2005;102:9613-8.

10. Rockwood LD, Torrey TA, Kim JS, Coleman AW, Kovalcuk AL, Xiang S, Ried T, Morse HC 3rd, Janz S.Genomic instability in mouse Burkitt lymphoma is dominated by illegitimate genetic recombinations, not point mutations. Oncogene. 2002; 21:7235-40.

11. Mai S. Overexpression of c-Myc precedes amplification of the gene encoding dihydrofolate reductase. Gene. 1994;148:253-60.

12. Mai S, Fluri M, Siwarski D, and Huppi K. Genomic instability in MYCER-activated Rat1A-MycER cells. Chromosome Research. 1994;4:365-371.

13. Mai S, Hanley-Hyde J, Fluri M. c-Myc overexpression associated DHFR gene amplification in hamster, rat, mouse and human cell lines. Oncogene. 1996;12:277-88.

14. Kuschak TI, Kuschak BC, Taylor CL, Wright JA, Wiener F, Mai S. c-Myc initiates illegitimate replication of the ribonucleotide reductase R2 gene. Oncogene. 2002;21:909-20.

15. Benner SE, Wahl GM, Von Hoff DD. Double minute chromosomes and homogeneously staining regions in tumors taken directly from patients versus in human tumor cell lines. Anti-Cancer Drugs. 1991;2:11-25.

16. Windle B, Draper BW, Yin YX, O'Gorman S, Wahl GM. A central role for chromosome breakage in gene amplification, deletion formation, and amplicon integration. Genes & development. 1991;5:10-74.

17. Felsher DW, Bishop JM. Transient excess of Myc activity can elicit genomic instability and tumorigenesis. Proceedings of the National Academy of Sciences of the United States of America. 1999;96:3940-4.

18. Nesbit CE, Tersak JM, Prochownik EV. MYC oncogenes and human neoplastic disease. Oncogene. 1999;18:3004-16.

19. van Es JH Barker N, Clevers H. You Wnt some H, you lose some: oncogenes in the Wnt signaling pathway. Current Opinions in Genetics & Development. 2003;13:28-33.

20. Popescu NC and Zimonjic DB. Chromosome-mediated alterations of the MYC gene in human cancer. Journal of Cellular and Molecular Medicine. 2002;6:151-9.

21. Bahram F, von der Lehr N, Cetinkaya C, Larsson LG. c-Myc hot spot mutations in lymphomas result in inefficient ubiquination and decreased proteasome-mediated turnover. Blood. 2000;95:2104-10.

22. Potter M, Wiener F. Plasmacytomagenesis in mice: model of neoplastic development dependent upon chromosomal translocations. Carcinogenesis. 1992;13:787-9.

23. Wiener F, Schmälter AK, Mowat MR, Mai S. Duplication of subcytonand 11E2 of chromosome 11 is regularly associated with accelerated tumor development in v-abl/myc induced mouse plasmacytomas. Genes Cancer. 2010;1:847-58.

24. Huang P, Cao K, Zhao H. Screening of critical genes in lung adenocarcinoma via network analysis of gene expression profile. Pathology and Oncology Research. 2014;20:853-8.

25. Xie R, Zhang Y, Shen C, Cao X, Gu S, Che X. Knockdown of immature colon carcinoma transcript-1 inhibits proliferation of glioblastoma multiforme cells through Gap 2/mitotic phase arrest. Journal of OncoTargets and Therapy. 2015;19:1119-1127.

26. Wang Z, Xu D, Gao Y, Liu Y, Ren J, Yao Y, Yin L, Chen J, Gan S, Cui X. Immature colon carcinoma transcript 1 is essential for prostate cancer cell viability and proliferation. Cancer Biotherapy and Radiopharmaceuticals. 2015;30:278-84.

27. Chen S, Xu Y, Chen Y, Li X, Mou W, Wang L, Liu Y, Reisfeld RA, Xiang R, Lv D, Li N. SOX2 gene regulates the transcriptional network of oncogenes and affects tumorigenesis of human lung cancer cells. PLoS ONE. 2012;7:e36326. doi:10.1371/journal.pone.0036236.

28. Herms JW, von Loewenich FD, Behnke J, Markakis E, Kretzschmar HA. c-Myc oncogene family expression in glioblastoma and survival. Surgical Neurology. 1999;51:536–42.

29. Quinn DI, Henshall SM, Sutherland RL. Molecular markers of prostate cancer outcome. European Journal of Cancer. 2005;41:858–87.

30. Turhan N, Yurur-Kutlay N, Topcuoglu P, Sayki M, Yuksel M, Gurman G, Tukun A. Translocation (13;17)(q14;q25) as a novel chromosomal abnormality in acute myeloid leukemia-M4. Leukemia Research. 2006;30:903-5.

31. Said J, Lones M, Yea S. Burkitt Lymphoma and MYC: What Else Is New? Advances in Anatomic Pathology. 2014;21:160-5.

32. Adams JM, Gerondakis S, Webb E, Corcoran LM, Cory S. Cellular myc oncogene is altered by chromosome translocation to an immunoglobulin locus in murine

plasmacytomas and is rearranged similarly in human Burkitt lymphomas. Proceedings of the National Academy of Sciences of the United States of America. 1983;80:1982-6.

33. Koelsch BU, Rajewsky MF, Kindler-Rohrborn A. A 6-Mb contig-based comparative gene and linkage map of the rat schwannoma tumor suppressor region at 10q32.3. Genomics. 2005;85:322-9."

34. Montagna C, Lyu MS, Hunter K, Lukes L, Lowther W, Reppert T, Hissong B, Weaver Z, Ried T. The Septin 9 (MSF) gene is amplified and overexpressed in mouse mammary gland adenocarcinomas and human breast cancer cell lines. Cancer Research. 2003;63:2179-87.

35. Helou K, Walentinsson A, Beckmann B, Johansson A, Hedrich HJ, Szpirer C, Klinga-Levan K, Levan G. Analysis of genetic changes in rat endometrial carcinomas by means of comparative genomic hybridization. Cancer Genetics and Cytogenetics. 2001;127:118-27.

36. Bermudo R, Abia D, Ferrer B, Nayach I, Benguria A, Zaballos A, del Rey J, Miro R, Campo E, Martinez-A C, Ortiz AR, Fernandez PL, Thomson TM. Coregulation analysis of closely linked genes identifies a highly recurrent gain on chromosome 17q25.3 in prostate cancer. BMC Cancer. 2008;8:315.

37. Zou H, Kang X, Pang LJ, Hu W, Zhao J, Qi Y, Hu J, Liu C, Li H, Liang W, Yuan X, Li F. Xp11 translocation renal cell carcinoma in adults: a clinicopathological and comparative genomic hybridization study. International Journal of Clinical and Experimental Pathology. 2014;7:236-45.

38. Rice KL, Lin X, Wolniak K, Ebert BL, Berkofsky-Fessler W, Buzzai M, Sun Y, Xi C, Elkin P, Levine R, Golub T, Gilliland DG, Crispino JD, Licht JD, Zhang W. Analysis of

genomic aberrations and gene expression profiling identifies novel lesions and pathways in myeloproliferative neoplasms. Blood Cancer Journal. 2011;1:e40.

39. Kawasaki H, Altieri DC, Lu CD, Toyoda M, Tenjo T, Tanigawa N. Inhibition of apoptosis by survivin predicts shorter survival rates in colorectal cancer. Cancer Research. 1998;58:5071-4.

40. Sarela AI, Macadam RC, Farmery SM, Markham AF, Guillou PJ. Expression of the antiapoptosis gene, survivin, predicts death from recurrent colorectal carcinoma. Gut. 2000;46:645-50.

41. Langan JE, Cole CG, Huckle EJ, Byrne S, McRonald FE, Rowbottom L, Ellis A, Shaw JM, Leigh IM, Kelsell DP, Dunham I, Field JK, Risk JM. Novel microsatellite markers and single nucleotide polymorphisms refine the tylosis with oesophageal cancer (TOC) minimal region on 17q25 to 42.5 kb: sequencing does not identify the causative gene. Human Genetics. 2004;114:534-40.

42. Arvanitis C and Felsher DW. Conditional transgenic models define how MYC initiates and maintains tumorigenesis. Seminars in Cancer Biology. 2006;6:313-7.

43. Matsui A, Ihara T, Suda H, Mikami H, Semba K. Gene amplification: mechanisms and involvement in cancer. Biomolecular Concepts. 2013;4:567-82.

44. Pelengaris S, and Khan M. The many faces of c-MYC. Archives of Biochemistry and Biophysics. 2003;416:129-36.

45. Kitanaka C, Sugiyama A, Kanazy S, Miyagi Y, Mishima K, Asai A, Kuchino Y. S-Myc acts as a transcriptional activator and its sequence-specific DNA binding is required for induction of programmed cell death in glioma cells. Cell Death and Differentiation. 1995;2:123-131.

46. Dang CV. c-Myc target genes involved in cell growth, apoptosis, and metabolism. Molecular and Cellular Biology. 1999;19:1-11.

47. Henriksson M, Luscher B. Proteins of the Myc network: essential regulators of cell growth and differentiation. Advances in Cancer Research. 1996;68:109-82.

48. Cole MD, Cowling VH. Transcriptotion-independent functions of MYC: regulation of translation and DNA replication. Nature Reviews Molecular Cell Biology. 2008;9:810-5.

49. Grandiori C, Gomez-Roman N, Felton-Edkins ZA, Ngouenet C, Galloway DA, Eisenman RN, White RJ. c-Myc binds to human ribosomal DNA and stimulates transcription of rRNA genes by RNA polymerase I. Nature Cell Biology. 2005;7:311-8.

50. Frank SR, Schroeder M, Fernande P, Taubert S, Amati B. Binding of c-Myc to chromatin mediates mitogen-induced acetylation of histone H4 and gene activation. Genes & Development. 2001;15:2069-82.

51. van Riggelen J, Yetil A, Felsher DW. MYC as a regulator of ribosome biogenesis and protein synthesis. Nature Reviews Cancer. 2010;10:301-9.

52. Gandarillas A, Davies D, Blanchard JM. Normal and c-Myc-promoted human keratinocyte differentiation both occur via a novel cell cycle involving cellular growth and endoreplication. Oncogene. 2000;19:3278-89.

53. Weber A, Kristiansen I, Johannsen M, Oelrich B, Scholmann K, Guinia S, May M, Meyer H, Behnke S, Moch H, Kristiansen G. The FUSE binding proteins FBP1 and FBP3 are potential c-myc regulators in renal, but not in prostate and bladder cancer. BMC Cancer 2008;8:369.

54. Lutz W, Leon J, Eilers M. Contributions of Myc to tumorigenesis. Biochimica et Biophysica Acta. 2002;1602:61-71.

55. Kuttler F, Mai S. C-Myc, genomic instability and disease. Genome Dynamics. Genome and Disease. J-N Volff (Ed). Karger Publishers, Würzburg, Germany, 20061;:171-191.

56. Tansey WP. Mammalian MYC Proteins and Cancer. New Journal of Science. 2014;2014:27.

57. Oster SK, Mao DY, Kennedy J, Penn LZ. Functional analysis of the N-terminal domain of the Myc oncoprotein. Oncogene. 2003;22:1998-2010.

58. Cole MD, Cowling VH. Transcription-independent functions of MYC: regulation of translation and DNA replication.

59. Manolov G, Manolova Y. Marker band in one chromosome 14 from Burkitt lymphomas. Nature. 1972;237:33-4.

60. Zech L, Haglund U, Nilsson K, Klein G. Characteristic chromosomal abnormalities in biopsies and lymphoid-cell lines from patients with Burkitt and non-Burkitt lymphomas. International journal of cancer Journal International du Cancer. 1976;17:47-56.

61. Vennstrom B, Sheiness D, Zabieslski J, and Bishop JM. Isolation and characterization of c-myc, a cellular homolog of the oncogene (v-myc) of avvian myelocytomatosis virus strain 29. Journal of Virology. 1982;42:773-9.

62. Ellerman VB, O. Experimentelle Leukamie bei Huhnern. Zentralbl Bakteriol Parasitenkd Infectionskr Hyg Abt I. 1908;46:595-609.

63. Chiswell DJ, Ramsay G, Hayman MJ. Two virus-specific rna species are present in cells transformed by defective leukemia virus OK10. Journal of Virology. 1981;40:301-4.

64. Bunte T, Greiser-Wilke I, Moelling K. The transforming protein of the MC29-related virus CMII is a nuclear DNA-binding protein whereas MH2 codes for a cytoplasmic RNA-DNA binding polyprotein. The EMBO Journal. 1983;2:1087-92.

65. Hann SR, Abrams HD, Rohrschneider LR, Eisenman RN. Proteins encoded by v-myc and c-myc oncogenes: identification and localization in acute leukemia virus transformants and bursal lymphoma cell lines. Cell. 1983;34:789-98.

66. Kan NC, Flordellis CS, Garon CF, Duesberg PH, Papas TS. Avian carcinoma virus MH2 contains a transformation-specific sequence, mht, and shares the myc sequence with MC29, CMII, and OK10 viruses. Proceedings of the National Academy of Sciences of the United States of America. 1983;80:6566-70.

67. Thompson CB, Humphries EH, Carlson LM, Chen CL, Neiman PE. The effect of alterations in myc gene expression on B cell development in the bursa of Fabricius. Cell. 1987;51:371-81.

68. Fernandez PC, Frank SR, Wang L, Shroeder M, Liu S, Greene J, Cocito A, Amati B. Genomic targets of the human c-Myc protein. Genes & Development. 2003;17;1115-29.

69. Hulf T, Bellosta P, Furrer M, Steiger D, Svensson D, Barbour A, Gallant P. Whole genome analysis reveals a strong positional bias of conserved Myc-dependent E-boxes. Molecular and Cellular Biology. 2005;25:3401-10.

70. Orian A, van Steensel B, Delrow J, Buessemaker HK, Li L, Sawado T, Williams E, Loo LWM, Cowley SM, Yost C, Pierce S, Edgar BA, Parkhurst SM, Eisenman RN. Genomic ninding by the Drosophilia Myc, Max, Ma/Mnt transcription factor netowrk. Genes & Development. 2003;17:1101-14.

71. Weaver BA, Silk AD, Montagna C, Verdier-Pinard P, Cleveland DW. Aneuploidy acts both oncogenetically and as a tumor suppressor. Cancer Cell. 2007;1:25-36.

72. Rowley JD. Chromosome translocations: dangerous liasons revisited. Nature Reviews Cancer. 2001;1:245-250.

73. Guffei A, Sarkar R, Klewes L, Righolt C, Knecht H, Mai S. Dynamic chromosomal rearrangements in Hodgkin's lymphoma are due to ongoing three dimensional nuclear remodeling and breakage-bridge-fusion cycles. Haematologica. 2010;95:2038-46.

74. Gadji M, Vallente R, Klewes L, Righolt C, Wark L, Kongruttanachok N, Knecht H, Mai S. Nuclear remodeling as a mechanism for genomic instability in cancer. Advances in Cancer Research. 2011;112:77-126.

75. Mai S. Initiation of telomere-mediated chromosomal rearrangements in cancer. Journal of Cellular Biochemistry. 2010;109:1095-102.

76. Mai S, Garini Y. Oncogenic remodeling of the three-dimensional organization of the interphase nucleus: c-Myc induces telomeric aggregates whose formation precedes chromosomal rearrangements. Cell Cycle. 2005;4:1327-31.

77. Hartwell L, Hood L, Goldberg M, Reynolgs A, Silver L. Genetics from Genes to Genomes 4e. New York: McGraw-Hill. 2011;443-54.

78. de Lange T. How telomeres solve the end-protection problem. Science. 2009;326:948-52.

79. Murnane JP. Telomeres and chromosome instability. DNA Repair. 2006;5:1082-92.

80. Silva AG, Graves HA, Guffei A, Ricca TI, Mortara RA, Jasiulionis MG, Mai S. Telomere-centromere-driven genomic instability contributes to karyotype evolution in a mouse model of melanoma. Neoplasia. 2010;12:11-19.

81. Mai S, Hanley-Hyde J, Fluri M. Genomic instability in MycER-activated Rat1A-MycER cells. Chromosome Research: an International Journal on the Molecular, Supramolecular and Evolutionary Aspects of Chromosome Biology. 1996;4:365-71.

82. Guffei A, Lichtensztejn Z, Goncalves Dos Santos Silva A, Louis SF, Caporali A, Mai S. c-Myc-dependent formation of Robertsonian translocation chromosomes in mouse cells. Neoplasia. 2007;9:578-88.

83. Caporali A, Wark L, Vermolen BJ, Garini Y, Mai S. Telomeric aggregates and end-to-end chromosomal fusions require myc box II. Oncogene. 2007;26:1398-406.

84. Kuschak TI, Taylor C, McMillan-Ward E, Israels S, Henderson DW, Mushinski JK, Wright JA, Mai S. The ribonucleotide reductase R2 gene is a non-transcribed target of c-Myc-induced genomic instability. Gene. 1999;238:351-65.

85. Chenova OB, Chnov MV, Ishizaka Y, Agrawal ML, Stark GR. MYC abrogates p2-mediated cell cycle arrest in N-(phosphonacetyl)-L-aspartate-treated cells, permitting CAD gene amplificationl Molecular and cellular biology. 1998;18:536-45.

86. Eberhardy SR, Farnham PJ. c-Myc mediates activation of the cad promoter via a post-RNA polymerase II recruitment mechanism. The Journal of Biological Chemistry. 2001;276:48562-71.

87. Fukasawa K, Wiener F, Vande Woude GF, Mai S. Genomic instability and apoptosis are frequient in p53 deficient young mice. Oncogene. 1997;15:1295-302.

88. Mitltenberger RJ, Sukow KA, Fanham PJ. An E-box-mediated increase in cad transcription at te G1/S-phase boundary is supressed by inhibitory c-Myc mutants. Molecular and Cellular Biology. 1995;15:2527-35.

89. George RE, Kenyon RM, McGukin Ag, Malcolm Ah, Pearson AD, Luenec J. Investigation of co-amplification of the candidate genes orhithine decarbxylase, ribonucleotide reducatse, syndecan-1 and a DEAD box gene, DDX1, with N-myc in neuroblastoma. Oncogene. 1996;12:1583-7.

90. Rounbehler RH, Li W, Hall MA, Yang C, Fllahi M, Ceveland JL. Targeting ornithine decarboxylase impairs development of MYCN-amplified neuroblastoma. Cancer Research. 2009;69:547-53.

91. Schnell JR, Dyson HJ, Wright PE. Structure, dynamics, and catalytic function of dihydrofolate reductase. Annual Review of Biophysics and Biomolecular Structure. 2004;33:119-40.

92. Li R, Sirawaraporn R, Chitnumsub P, Sirawaraporn W, Wooden J, Athappilly F, Turley S, Hol WG. Three-dimensional structure of M. tuberculosis dihydrofolate reductase reveals opportunities for the design of novel tuberculosis drugs. Journal of Molecular Biology. 2000;295:307–23.

93. Aye Y, Li M, Long MJ, Weiss RS. Ribonucleotide reductase and cancer: biological mechanisms and targeted therapies. Oncogene. 2015;34:2011-21.

94. Aoki T, Weber G. Carbamoyl phosphate synthetase (glutamine-hydrolyzing): increased activity in cancer cells. Science. 1981;212:463-5.

95. Bello-Fernandez, Packham G, Cleveland JL. The ornithine decarboxylase gene is a transcriptional target of c-Myc. Proceedings of the National Academy of Sciences of the United States of America. 1993;90:7804-8.

96. Casimiro MC, Crosariol M, Loro E, Li Z, Pestell RG. Cyclins and cell cycle control in cancer and disease. Genes and Cancer. 2012;3:649-57.

97. Cremer T, Kurz A, Zirbel R, Dietzel S, Rinke B, Schröck E, Speicher MR, Mathieu U, Jauch A, Emmerich P, Scherthan H, Ried T, Cremer C, Lichter P. Role of chromosome territories in the functional compartmentalization of the cell nucleus. Cold Spring Harbor Symposia on Quantitative Biology. 1993;58:777–92.

98. Foster HA, Bridger JM. The genome and the nucleus: a marriage made by evolution. Genome organisation and nuclear architecture. Chromosoma. 2005;114:212–29.

99. Finlan LE, Sproul D, Thomson I, Boyle S, Kerr E, Perry P, Ylstra B, Chubb JR, Bickmore WA. Recruitment to the nuclear periphery can alter expression of genes in human cells. PLoS genetics. 2008;4e1000039.

100. Kumaran RI, Spector DL. A genetic locus targeted to the nuclear periphery in living cells maintains its transcriptional competence. The Journal of Cell Biology. 2008;180:51-65.

101. Zink D, Fischer AH, Nickerson JA. Nuclear structure in cancer cells. Nature Reviews Cancer. 2004;4:677–87.

102. Cremer T, Cremer C. Chromosome territories, nuclear architecture and gene regulation in mammalian cells. Nature Reviews Genetics. 2001;2:292–301.

103. Schmälter AK, Righolt CH, Kuzyk A, Mai S. Changes in nuclear orientation patterns of chromosome 11 during mouse plasmacytoma development. Translational Oncology. 2015;8:417-23.

104. Schmälter AK, Kuzyk A, Righolt CH, Neusser M, Steinlein OK, Müller S, Mai S. Distinct nuclear orientation patterns for mouse chromosome 11 in normal B lymphocytes. BMC Cell Biology. 2014;12:15-22. Lanctot C, Cheutin T, Cremer M, Cavalli G, Cremer T. Dynamic genome architecture in the nuclear space: reuglation of gene expression in three dimensions. Nature Reviews Genetics. 2007;8:104-15.

105. Righolt CH, Wiener F, Taylor-Kashton C, Harizanova J, Vermolen BJ, Garini Y, Young IT, Mai S. Translocation frequencies and chromosomal proximities for selected mouse chromosomes in primary b lymphocytes. Cytometry. 2011;79A:276-283.

106. Cremer M, Kupper K, Wagler B, Wizelman L, von Hase J, Weiland Y, Kreja L, Diebold J, Speicher MR, Cremer T. Inheritance of gene density-related higher order chromatin arrangements in normal and tumor cell nuclei. The Journal of Cell Biology. 2003;162:809–20.

107. Ballabio E, Cantarella CD, Federico C, Di Mare P, Hall G. Ectopic expression of the HLXB9 gene is associated with an altered nuclear position in T(7;12) leukaemias. Leukemia. 2009;23:1179–82.

108. Hochberg J, Waxman I, Kelly K. Adolescent non-Hodgkin lymphoma and Hodgkin lymphoma: state of the science. British Journal of Haematology. 2009;114:24-40.

109. Miles RR, Arnold S, Cairo MS. Risk factors and treatment of childhood and adolescent Burkitt lymphoma/leukaemia. British Journal of Haematology. 2012;156:730-43.

110. Soutar R, Lucraft H, Jackson G, Reece A, Bird J, Low E, Samson D. Guidelines on the diagnosis and management of solitary plasmacytoma of bone and solitary extramedullary plasmacytoma. British Journal of Haematology. 2004;124:717–26

111. Dingli D, Kyle RA, Rajkumar SV, Nowakowski GS, Larson DR, Bida JP, Gertz MA, Therneau TM, Melton LJ III, Dispenzieri A, Katzmann JA. Immunoglobulin free light chains and solitary plasmacytoma of bone". Blood. 2006;108:1979–83.

112. Gado K, Silva S, Paloczi K, Domian G, Falus A. Mouse plasmacytoma: an experimental model of human multiple myeloma. Haematologica. 2001;86:227-36.

113. Walker BA, Wardell CP, Brioli A, Boyle E, Kaiser MF, Begum DB, Dahir NB, Johnson DC, Ross FM, Davies FE, Morgan GJ. Translocations at 8q24 juxtapose MYC with genes that harbor superenhanccers resulting in overexpression and poor prognosis in myeloma patients. Blood Cancer Journal. 2014;14;4:e191. doi: 10.1038/bcj.2014.13.

114. Rakoff-Nahoum S. Why cancer and inflammation? Yale Journal of Biology and Medicine. 2006;79:123-30.

115. Potter M. Indomethacin inhibition of pristane plasmacytomagenesis in genetically susceptible inbred mice. Advances in Experimental Medicine and Biology. 1999;469:151-6.

116. Suematsu S, Matsusaka T, Matsuda T, Ohno S, Miyazaki J, Yamamura K, Hirano T, Kishimoto T. Generation of plasmacytomas with the chromosomal translocation t(12;15) in the interleukin 6 transgenic mice. Proceedings of the National Academy of Sciences of the United States of America.1992;89:232-5.

117. Sellers RS, Clifford CB, Treuting PM, Brayton C. Immunological variation between inbred laboratory mouse strains: points to consider in phenotyping genetically immunomodified mice. 2012;49:32-43.

118. Morse III HC, Riblet R, Asfsky R, Weigert M. Plasmacytomas of the NZB mouse. The Journal of Immunology. 1978;121:1969-72.

119. Baron JA, Sandler RS. Nonsteroidal anti-inflammatory drugs and cancer prevention. Annual Review of Medicine. 2000;51:511-23.

120. Lattanzio G, Libert C, Aquilina M, Cappelletti M, Ciliberto G, Musiani P, Poli V. Defective development of pristane-oil-induced plasmacytomas in interleukin-6-deficient BALB/c mice. American Journal of Pathology. 1997;151:689-96.

121. Pattengale PK. Role of interleukin-6 in the pathogenesis of murine plasmacytoma and human multiple myeloma. American Journal of Pathology. 1997;151:647-9.

122. Potter M. History of the BALB/c family, pp 1-5. In: The BALB/c Mouse: Genetics and Immunology, Current Topics in Microbiology and Immunology, Vol. 122. Springer-Verlag, NY. 1985.

123. Potter M. Neoplastic development in plasma cells. Immunological Reviews. 2003;194:177-195.

124. Lindahl T. Instability and decay of the primary structure of DNA. Nature. 1993;362:709-714.

125. Liou G, Storz P. Reactive oxygen species in cancer. Free Radical Resolutions. 2010;5:479-96.

126. Degrassi A, Hilbert DM, Rudikoff S, Anderson AO, Potter M, Coon HG. In vitro culture of primary plasmacytomas requires stromal feeder layers. Proceedings of the National Academy of Sciences of the United States of America. 1992;90:2060-4.

127. Wong KK, Zou X, Merrell KT, Patel AJ, Marcu KB, Chellappan S, Calame K. v-Abl activates c-myc transcription through the EF2 site. Molecular and Cellular Biology. 1995;15:6535-44.

128. Largaespada DA, Kaehler DA, Mishak H, Weissinger E, Potter M, Mushinski JF, Risser R. A retrovirus that expresses v-abl and c-myc oncogenes rapidly induces plasmacytomas. Oncogene. 1992;7:811-9.

129. Ohno S, Hayakawa J, Hashimoto N, Wiener F. Murine plasmacytomas, carrier of the t(12;15) chromosomal translocation, develop from immature/mature B cells not from differentiated plasma cells. Carcinogenesis. 1999;20:529-38.

130. Silva S, Klein G. Plasmacytoma induction in specific pathogen-free (SPF) bcl-2 transgenic BALB/c mice. Current Topics in Microbiology and Immunology. 1999;246:379-385.

131. Potter M, Wax JS. Peritoneal plasmacytomagenesis in mice: comparison of different pristane dose regimens. Journal of the National Cancer Institute. 1983;71:391-5.

132. Kobos R, Nagai M, Tsuda M, Merl MY, Saito T, Laé M, Mo Q, Olshen A, Lianoglou S, Leslie C, Ostrovnaya I, Antczak C, Djaballah H, Ladanyi M. Combining integrated genomics and functional genomics to dissect the biology of a cancer-associated, aberrant transcription factor, the ASPSCR1-TFE3 fusion oncoprotein. The Journal of Pathology. 2013;229:743-54.

133. Heimann P, Devalck C, Debusscher C, Sariban E, Vamos E. Alveolar soft-part sarcoma: further evidence by FISH for the involvement of chromosome band 17q25. Genes Chromosomes Cancer. 1998;23:194-7.

134. Argani P, Olgac S, Tickoo SK, Goldfischer M, Moch H, Chan DY, Eble JN, Bonsib SM, Jimeno M, Lloreta J, Billis A, Hicks J, De Marzo AM, Reuter VE, Ladanyi M. Xp11 translocation renal cell carcinoma in adults: expanded clinical, pathologic, and genetic spectrum. The American Journal of Surgical Pathology. 2007;31:1149-60.

135. Marais A, Ji Z, Child ES, Krause E, Mann DJ, Sharrocks AD. Cell cycle-dependent regulation of the forkhead transcription factor FOXK2 by CDK.cyclin complexes. The Journal of Biological Chemistry. 2010;285:35728-39.

136. Fujii Y, Nakamura M. FOXK2 transcription factor is a novel G/T-mismatch DNA binding protein. The Journal of Biochemistry. 2010;147:705-9.

137. Collins A, Larson M. Differential sensitivity of inward rectifier K+ channels to metabolic inhibitors. Journal of Biological Chemistry. 2002;277: 35815-18.

138. Kalikin LM, Bugeaud EM, Palmbos PL, Lyons RH Jr, Petty EM. Genomic characterization of human SEC14L1 splice variants within a 17q25 candidate tumor suppressor gene region and identification of an unrelated embedded expressed sequence tag. Mammalian Genome, 2001;12:925-9.

139. Li X, Xie Z, Bankaitis VA. Phosphatidylinositol/phosphatidylcholine transfer proteins in yeast. Biochimica et Biophysica Acta (BBA). 2000;1486:55-71.

140. Walker RA, O'Brien ET, Pryer NK, Soboeiro MF, Voter WA, Erickson HP, Salmon ED. Dynamic instability of individual microtubules analyzed by video light microscopy: rate constants and transition frequencies. The Journal of Cell Biology. 1988;107:1437-48.

141. van Belzen N, Diesveld MP, van der Made AC, Nozawa Y, Dinjens WN, Vlietstra R, Trapman J, Bosman FT. Identification of mRNAs that show modulated expression during colon carcinoma cell differentiation. European Journal of Biochemistry. 1995;234:843–8.

142. van Belzen N, Dinjens WN, Eussen BH, Bosman FT. Expression of differentiation-related genes in colorectal cancer: possible implications for prognosis. Histology and Histopathology. 1998;13:1233–42.

143. Handa Y, Hikawa Y, Tochio N, Kogure H, Inoue M, Koshiba S, Guntert P< Inoue Y, Kigawa T, Yokoyama S, Nameki N. Solution structure of the catalytic domain of the mitochondrial protein ICT1 that is essential for cell vitality. Journal of Molecular

Biology. 2010;404:260–73.Ruggero D. Translation control in cancer etiology. Cold Spring Harbor Perspectives in Biology. 2013;2:a012336.

144. de Jong D, Janz S. Anaplastic plasmacytoma of mouse - establishing parallels between subtypes of mouse and human plasma cell neoplasia. The Journal of Pathology. 2010;221:242-7.

145. Mai S, Wiener E. Murine FISH. In: Beatty B, Mai S. Squire J. FISH – A Practical Approach. Oxford, UK: Oxford University Press; 2002.

146. Riss TL, Moravec RA, Niles AL, Duellman S, Benink HA, Worzella TJ, Minor L. Cell Viability Assays. 2016; NBK144065.

147. Harlow E, Lane D. Antibodies a Laboratory Manual. Cold Spring Harbor Press, NY. 1988:449.

148. Bickar D, Reid PD. A high-affinity protein stain for western blots, tissue prints, and electrophoretic gels. Analytical Biochemistry. 1992;203:109.

149. Mai S, Hanley-Hyde J, Rainey GJ, Kuschak TI, Paul JT, Littlewood TD. Chromosomal and extrachromosomal instability of the cyclin D2 gene is induced by Myc overexpression. Neoplasia. 1999;1:241-52.

150. Littlewood TD, Hancock DC, Danielian PS, Parker MG, Evan GI. A modified oestrogen receptor ligand-binding domain as an improved switch for the regulation of heterologous proteins. Nucleic Acids Research. 1995;23:1686-90.

151. Fest T, Mougey V, Dalstein V, Hagerty M, Milette D, Silva S, Mai S. c-Myc overexpression in Ba/F3 cells simultaneously elicits genomic instability and apoptosis. Oncogene. 2002;21:2981-90.

152. Benedek K, Chudoba I, Klein G, Wiener F, Mai S. Rearrangements of the telomeric region of mouse chromosome 11 in Pre-B ABL/MYC cells revealed by m-BANDing, spectral karyotyping, and fluorescence in-situ hybridization with a subtelomeric probe. Chromosome Research. 2004;12:777-85.

153. Richter R, Rorbach J, Pajak A, Smith PM, Wessels HJ, Huynen MA, Smeitink JA, Lightowlers RN, Chrzanowska-Lightowlers ZM. A functional peptidyl-tRNA hydrolase, ICT1, has been recruited into the human mitochondrial ribosome. EMBO Journal. 2010;29:1116-25.

154. Antonicka H, Ostergaard E, Sasarman F, Weraarpachai W, Wibrand F, Pedersen AM. Mutations in C12orf65 in patients with encephalomyopathy and a mitochondrial translation defect. The American Journal of Human Genetics. 2010;87:115-122.

155. Finn R D, Mistry J, Tate J, Coggill PC, Heger A, Pollington JE, Gavin OL, Gunasekaran P, Ceric G, Forslund K, Holm L, Sonnhammer EL, Eddy SR, Bateman A. The Pfam protein families database. Nucleic Acids Research. 2010;38:D211-D222.

156. Gagnon MG, Seetharaman SV, Bulkley D, Steitz TA. Structural basis for the rescue of stalled ribosomes: structure of YaeJ bound to the ribosome. 2012;335:1370-2.

157. No D, Yao TP, Evans RM. Ecdysone-inducible gene expression in mammalian cells and transgenic mice. Proceedings of the National Academy of Sciences of the United States of America. 1996;93:3346-51.

158. Vafa O, Wade M, Kern S, Beeche M, Pandita TK, Hampton GM, Wahl GM. c-Myc can induce DNA damage, increase reactive oxygen species, and mitigate p53 function: a mechanism for oncogene-induced genetic stability. Molecular Cell. 2002;9:1031-44.

159. Evan G, Wyllie A, Gilbert C, Littlewood T, Land H, Brooks M, Waters C, Penn L, Hancock D. Induction of apoptosis in fibroblasts by c-myc protein. Cell. 1992;63:119-25.

160. Gold R, Schmied M, Giegerich G, Breitschopf H, Hartung HP, Toyka KV, Lassmann H. Differentiation between cellular apoptosis and necrosis by the combined use of in situ tailing and nick translation techniques. Laboratory Investigation. 1994;71:219-25.

161. Mai S and Wiener F. The impact of p53 loss on murine plasmacytoma development. Chromosome Reseaerch. 2002;10:239-251.

162. Yu SW, Andrabi SA, Wang H, Kim NS, Poirier GG, Dawson TM, Dawson VL Apoptosis-inducing factor mediates poly(ADP-ribose) (PAR) polymer-induced cell death". Proceedings of the National Academy of Sciences of the United States of America. 2006;103:18314–9.

163. Billings T, Sargent EE, Szatkiewicz JP, Leahy N, Kwak IY, Bektassova N, Walker M, Hassold T, Graber JH, Broman KW, Petkov PM. Patterns of recombination activity on mouse chromosome 11 revealed by high resolution mapping. 2010;5:e15340.

164. Slovak ML, Ho JP, Pettanati MH, Khan A, Douer D, Lal S, Traweek ST. Localization of amplified MYC gene sequences to double minute chromosomes in acute myelogenous leukemia. Genes Chromosomes Cancer. 1994;9:62-7.

165. Keung YK, Cobos E, Morgan D, Whitehead RP, Tonk V. Double minute chromosomes and myelodysplastic syndrome: a case report and literature review. Cancer Genetics and Cytogenetics. 1997;97:94-6.

166. Von Hoff DD, Needham-Van Devanter DR, Yucel J, Windle BE, and Wahl GM. Amplified human MYC oncogenes localized to replicating submicroscopic circular DNA

molecules. Proceedings of the National Academy of Sciences of the United States of America. 1988;85:4804-4808.

167. Pauletti G, Lai E, Attardi. Early appearance and long term persistence of the submicroscopic extrachromosomal elements (amplisomes) containing the amplified DHFR genes in human cell lines. Proceedings of the National Academy of Sciences of the United States of America. 1990;87:2955-9.

168. Smith G, Taylor-Kashton C, Duschnicky L, Symons S, Wright J, Mai S. c-Myc-induced extrachromosomal elements carry active chromatin. Neoplasia. 2003;5:110-120.

169. Solovei I, Kreysing M, Lanctot C, Kosem S, Peichl L, Cremer T, Guck J, Joffe B. Nuclear architecture of rod photoreceptor cells adapts to vision in mammalian evolution. Cell. 2009;137:356-68.

170. Cremer T, Cremer M. Chromosome territories. Cold Spring Harbor Perspectives in Biology. 2010;2:a003889.

171. Kuehl WM, Brents LA, Chesi M, Bergsagel PL. Selective expression of one c-myc allele in two human myeloma cell lines. Cancer Resolutions. 1996;56:4370-3.

172. Bermudo R, Abia D, Benitez D, Carrio A, Vilella R, Ortiz AR, Thomson TM, and Fernandez PL. Discovery of genomic alterations through coregulation analysis of closely linked genes: a frequent gain in 17q25.3 in prostate cancer. Annals of the New York Academy of Sciences. 2010;1210:17-24.

173. Brinkschmidt C, Christiansen H, Terpe HJ, Simon R, Boecker W, Lampert F, Stoerkel S. Comparative genomic hybridization (CGH) analysis of neuroblastomas--an important methodological approach in paediatric tumour pathology. The Journal of pathology. 1997;181:394-400.

174. Lastowska M, Nacheva E, McGuckin A, Curtis A, Grace C, Pearson A, Bown N. Comparative genomic hybridization study of primary neuroblastoma tumors. United Kingdom Children's Cancer Study Group. Genes, chromosomes & cancer. 1997;18:162-9.

175. Plantaz D, Mohapatra G, Matthay KK, Pellarin M, Seeger RC, Feuerstein BG. Gain of chromosome 17 is the most frequent abnormality detected in neuroblastoma by comparative genomic hybridization. The American journal of pathology. 1997;150:81-9.

176. Park TS, Song J, Lee J, Kim JS, Yang WI, Choi JR. Concomitant Isochromosome 17q and trisomy 14 in a patient with myelodysplastic syndrome in leukemic transformation. Annals of Clinical and Laboratory Science. 2009;39:176-81.

177. Toffoli S, Bar I, Abdel-Sater F, Delree P, Hilbert P, Cavallin F, Moreau F, Van Criekinge W, Lacroix-Triki M, Campone M, Martin AL, Roche H, Machiels JP, Carrasco J, Canon JL. Identification by array comparative genomic hybridization of a new amplicon on chromosome 17q highly recurrent in BRCA1 mutated triple negative breast cancer. Breast Cancer Research. 2014;16:466.

9 APPENDIX

pIND F primer: **AAGAACTCACACACAGCTAG**

NCNNNNNNNGGNGACCGCCTGGGGCCTACGCTGGGGCCTGAGCCGAACTGGAACGTTGTTGCTCGCGCCGCCCGCGCGCT
GTGCTCGCCGGGCTCTGCACAGACAGGTAGACGGCACCACGTTCCAGAGCATCTACAGCCTGGACAAGCTGTACCCCGAG
TCCAAGGGCGCGGATACCGCCTGGAAGGTCCCGGAGCATGCAAAACAAGCCAGCAGTTACATCCCTCTGGATCGGTTAAG
CATATCTTACTGTCGGAGCAGCGGTCCTGGTGGGCAGAATGTGAACAAAGTGAATTCCAAGGCTGAAGTAAGGTTTCACT
TGGCCAGTGCAGACTGGATTGAGGAGCCCGTGCGCCAGAAGATTGCCCTCACGCATAAAAATAAGATCAACAAGGCAGGA
GAGCTGGTACTTACCTCTGAGAGCAGCCGGTATCAGTTCCGCAATCTGGCAGAATGCCTACAGAAAATTCGAGACATGAT
TGCCGAGGCCAGCCAGGTACCCAAAGAGCCATCCAAGGAAGATGCTCGGCTTCAGAGACTCAGGATTGAAAAGATGAATC
GGGAAAGGCTACGACAGAAAAGACTAAACTCTGCCCTAAAGACCAGCAGGAGGATGACTATGGACTGAAGTCGGCCTCTA
GAGGGCCCGTTTAAACCCGCTGATCAGCCTCGACTGTGCCTTCTAGTTGCCAGCCATCTGTTGTTTGCCCCTCCCCCGTG
CCTTCCTTGACCCTGGAAGGTGCCACTCCCACTGTCCTTTCCTAATAAAATGAGGAAATTGCATCGCATTGTCTGAGTAG
GTGTCATTCTATTCTGGGGGGGNGGGGGGNGGGGGCAGGACAGCAAGGGGGAGGATTNNGAAGACAATAGCAGGCATGCT
GGGGATGCGGTGNCTCTATGGCTTCTGAGGCGGAAAGAACCAGCTGGGCTCTAGGGGGTATCCCCACGCGNCCTGNAGCG
NGCATAAGCNNNGNNGGGNNNTGGNNGNNCGCGCAGCNNGACNCTACANNNNNGCGCCNAGCGCCNGNTCNTNNNNNNNC
TNNNNNNGCCNNNNNNCNNTTNCCGTNANNNNAAATCGGGNNNNNNNNNNCGATNN

pIND R for primer: **TAGAAGGCACAGTCGAGGCT**

NNNNNNTTNACGGNNNCTAGAGGCCGACTTCNGTCCATAGTCATCCTCCTGCTGGTCTTTAGGGCAGAGTTTAGTCTTTT
CTGTCGTAGCCTTTCCCGATTCATCTTTTCAATCCTGAGTCTCTGAAGCCGAGCATCTTCCTTGGATGGCTCTTTGGGTA
CCTGGCTGGCCTCGGCAATCATGTCTCGAATTTTCTGTAGGCATTCTGCCAGATTGCGGAACTGATACCGGCTGCTCTCA
GAGGTAAGTACCAGCTCTCCTGCCTTGTTGATCTTATTTTTATGCGTGAGGGCAATCTTCTGGCGCACGGGCTCCTCAAT
CCAGTCTGCACTGGCCAAGTGAAACCTTACTTCAGCCTTGGAATTCACTTTGTTCACATTCTGCCCACCAGGACCGCTGC
TCCGACAGTAAGATATGCTTAACCGATCCAGAGGGATGTAACTGCTGGCTTGTTTTGCATGCTCCGGGACCTTCCAGGCG
GTATCCGCGCCCTTGGACTCGGGGTACAGCTTGTCCAGGCTGTAGATGCTCTGGAACGTGGTGCCGTCTACCTGTCTGTG
CAGAGCCCGGCGAGCACAGCGCGCGGGCGGCGCGAGCAACAACGTTCCAGTTCGGCTCAGGCCCCAGCGTAGGCCCCAGG
CGGTCGCCATGTTCAAGCTTAAGTTTAAACGCTAGCTGTGTGTGAGTTCTTCTTTCTCGGTAACTTGTTGAAAGTATTCA
GAGTTCTCTTCTTGTATTCAATAATTACTTCTTGGCAGATTTCAGTAGTTGCAGTTGATTTACTTGGTTGCTGGTTACTT
TTAATTGATTCACTTTAACTTGCACTTTACTGCAGATTGTTTAGCTTGTTCAGCTGCGCTTGTTTATTTGCTTAGCTTTC
GCTTAGCGACGTGTTCACTTTGCTTGTTTGAATTGAATTGNCGCTCCGTAGACGAAGCGNNTCTATTTATACNCCGGCGG
TCGAGGGTACTCCCNGGTACTGANCTTCAGCAAGANAANANGCACTNGTCCATCNAGCNTTCAGCANNNNNNNNANGGNA
CTTGNNCNTCNNGNNNCAGCAANNNAANNNATNNNCNNNGTCNTNNNCTANNNAGN

Figure 17 Sequencing result for pIND/Hygro-Ict1 vector prepared as a cDNA clone from Ict1pT7T3D-PacI (Openbiosystems)